Electronic Supplementary Information

Binuclear platinum(II) complexes bearing various bridging 1,1'-diphosphinoferrocene ligands as potential anticancer agents: Synthesis and biological evaluations

*Jalalaldin Zangeneh,[a] Lotfollah Saghaie,[*a] Mahmoud Etebari,[b] Vahideh Dolatyari,[c] Zahra Farasat,[d] Masood Fereidoonnezhad,[e] and Hamid R. Shahsavari[*c]*

[a]Department of Medicinal Chemistry, School of Pharmacy and Pharmaceutical Sciences, Isfahan University of Medical Sciences, Isfahan, Iran. *E-mail: saghaie@pharm.mui.ac.ir. L.S. is the corresponding author of the biology section.

[b]Department of pharmacology and toxicology, School of Pharmacy and Pharmaceutical Sciences, Isfahan University of Medical Sciences, Isfahan, Iran.

[c]Department of Chemistry, Institute for Advanced Studies in Basic Sciences (IASBS), Zanjan 45137-66731, Iran. *E-mail: shahsavari@iasbs.ac.ir.

[d]Professor Rashidi Laboratory of Organometallic Chemistry, Department of Chemistry, College of Sciences, Shiraz University, Shiraz, 71467-13565, Iran.

[e]Department of Medicinal Chemistry, School of Pharmacy; Cancer, Environmental and Petroleum Pollutants Research Center, Ahvaz Jundishapur University of Medical Sciences, Ahvaz, Iran.

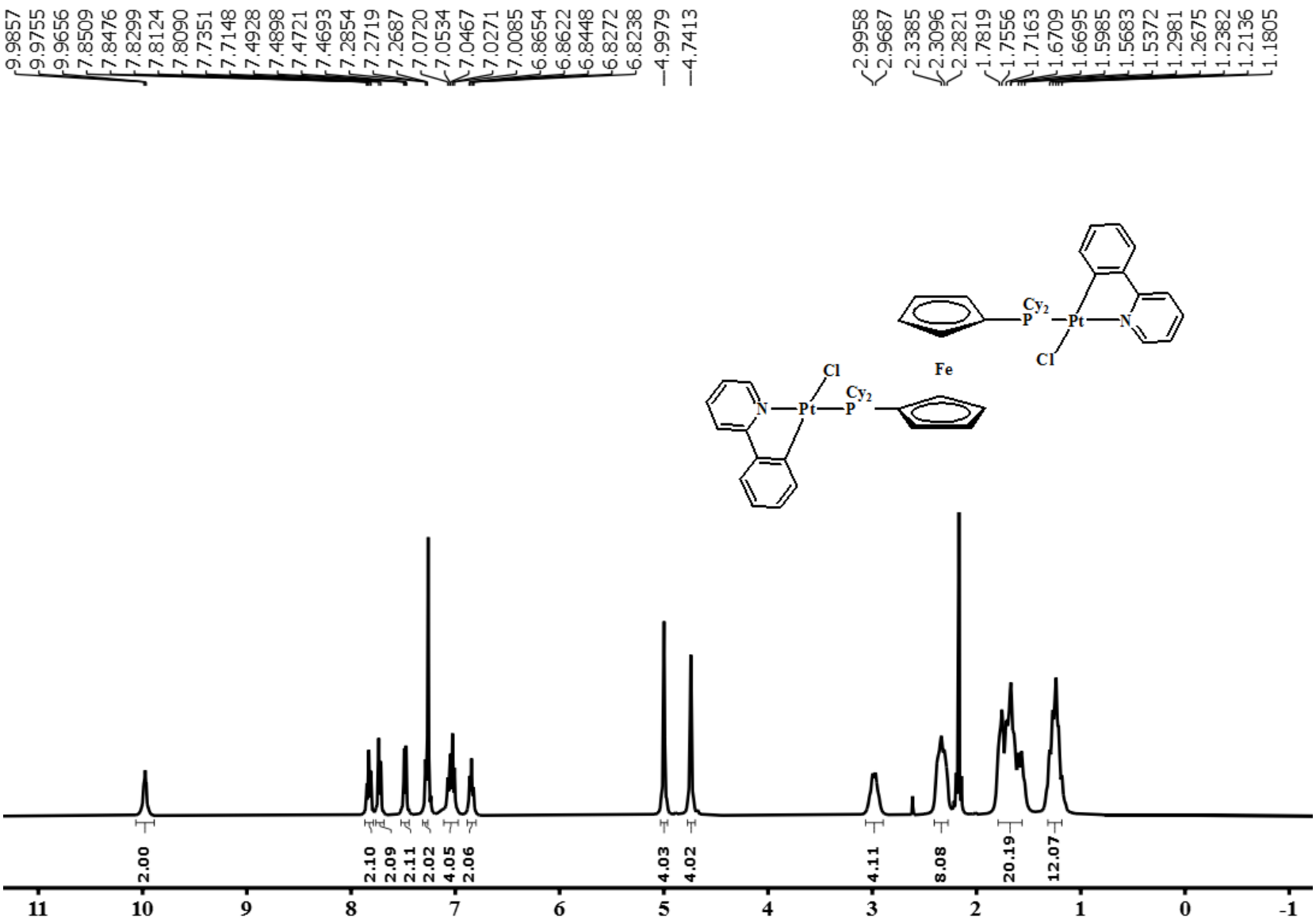

Figure S1. ^{1}H NMR spectrum of **2b** in $CDCl_3$.

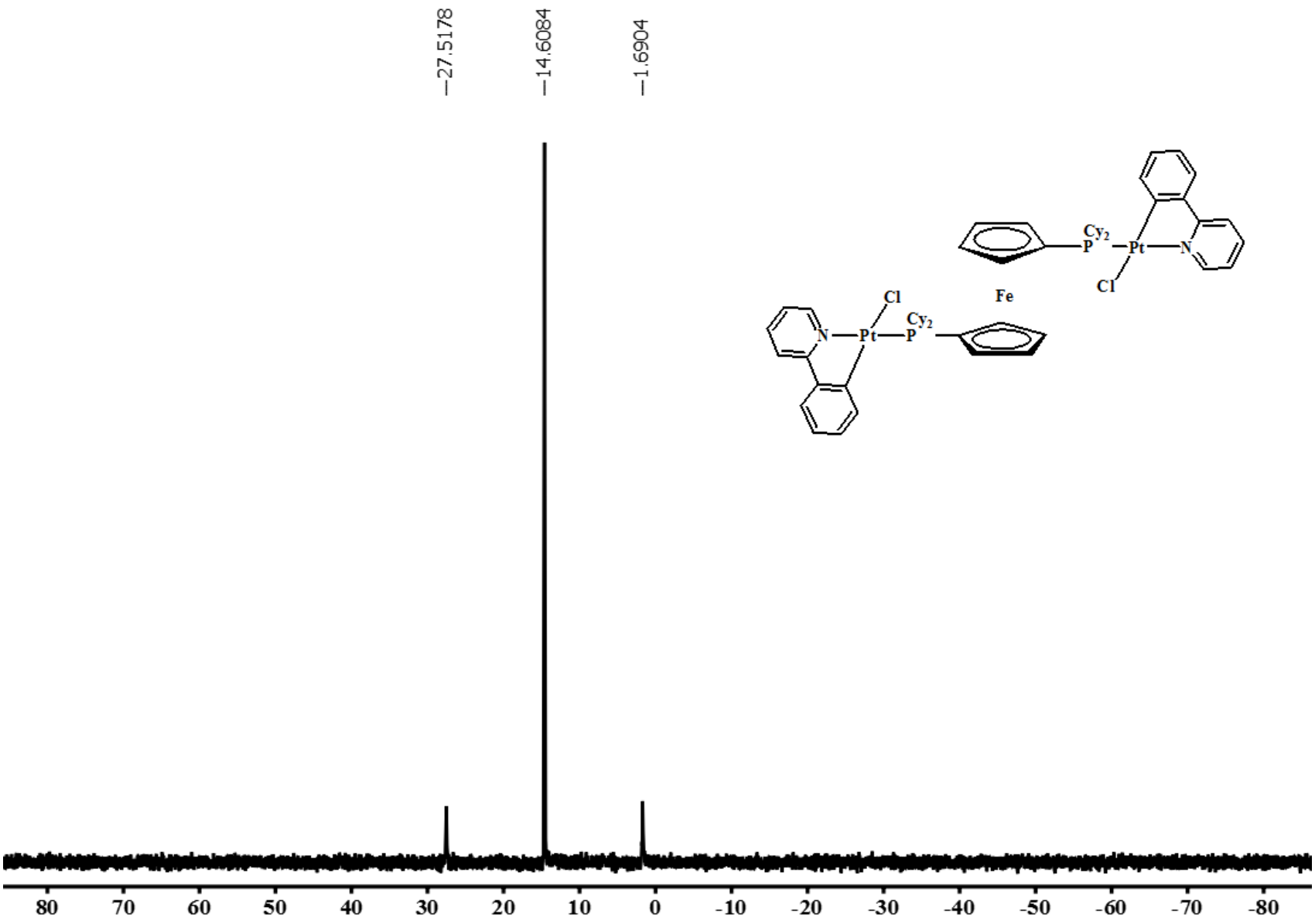

Figure S2. $^{31}P\{^{1}H\}$ NMR spectrum of **2b** in $CDCl_3$.

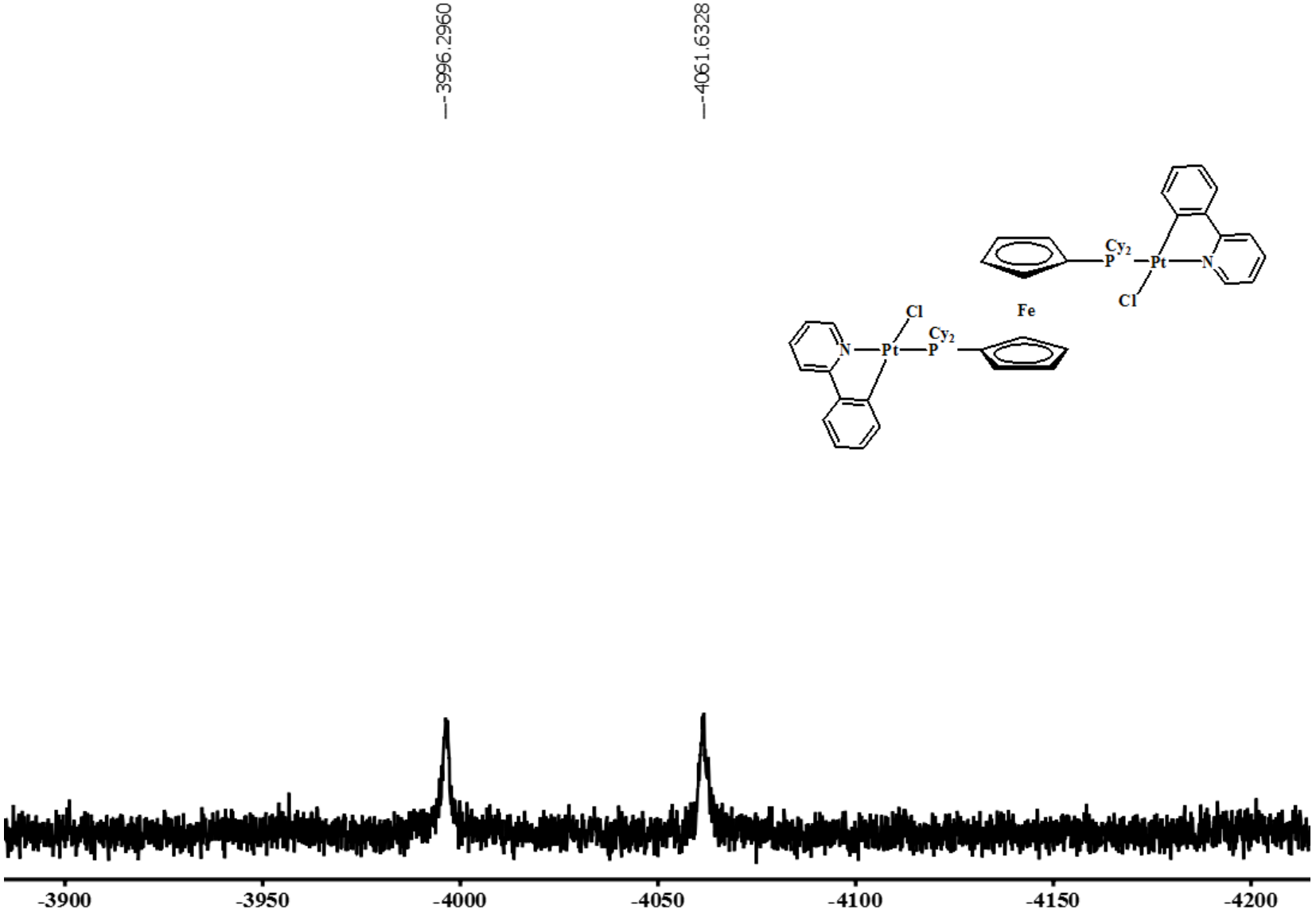

Figure S3. $^{195}Pt\{^{1}H\}$ NMR spectrum of **2b** in $CDCl_3$.

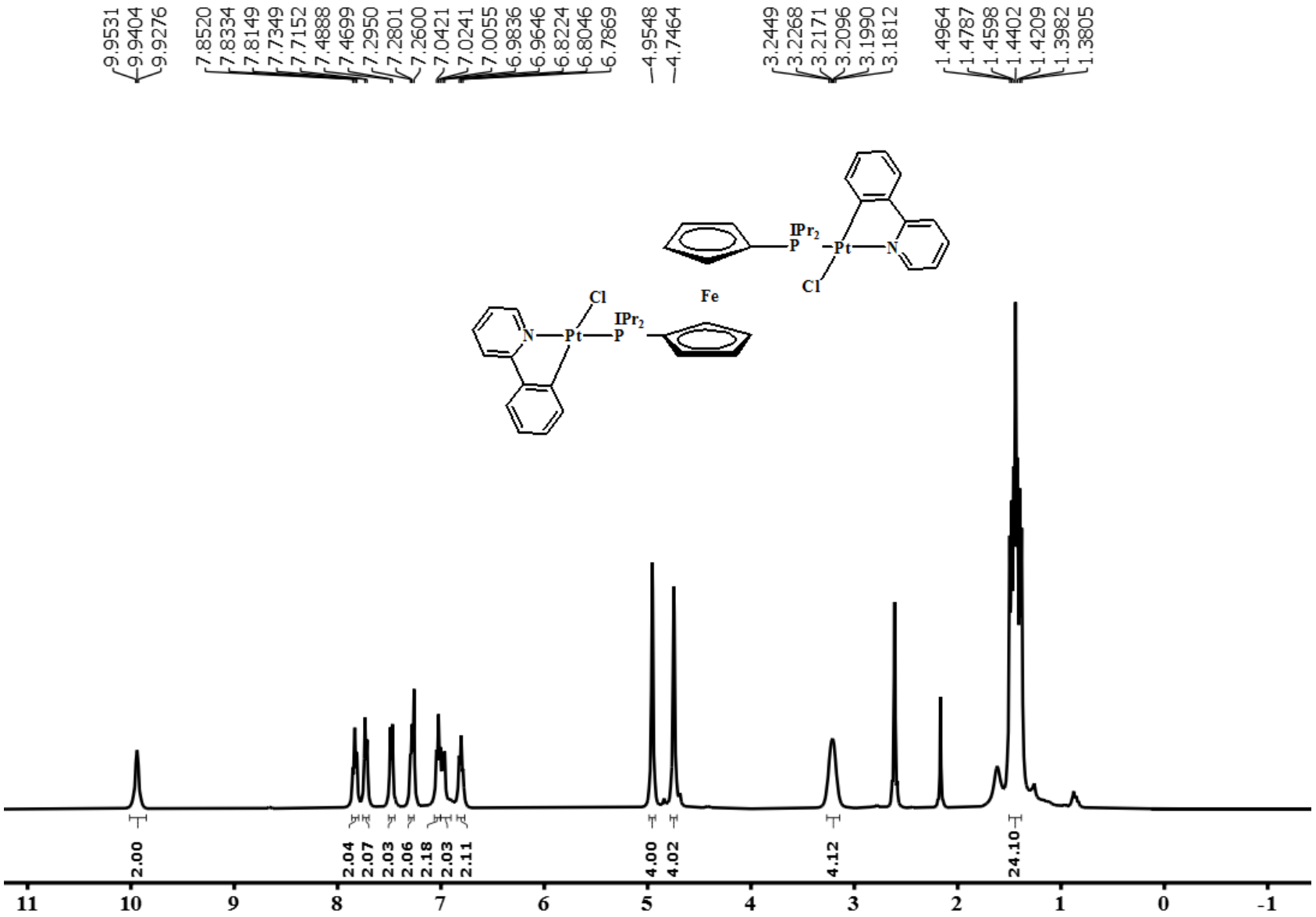

Figure S4. ^{1}H NMR spectrum of **2c** in $CDCl_3$.

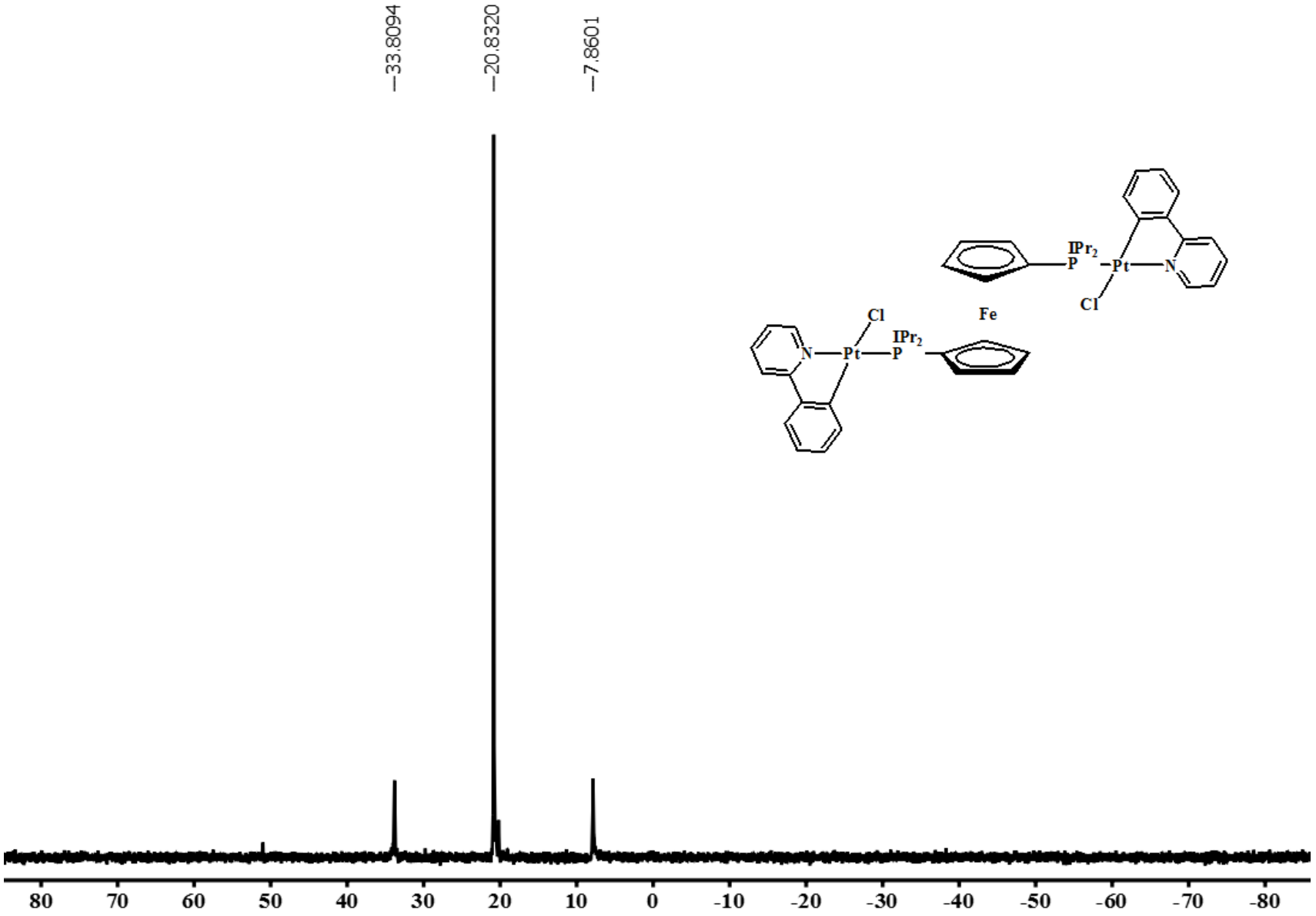

Figure S5. $^{31}P\{^{1}H\}$ NMR spectrum of **2c** in $CDCl_3$.

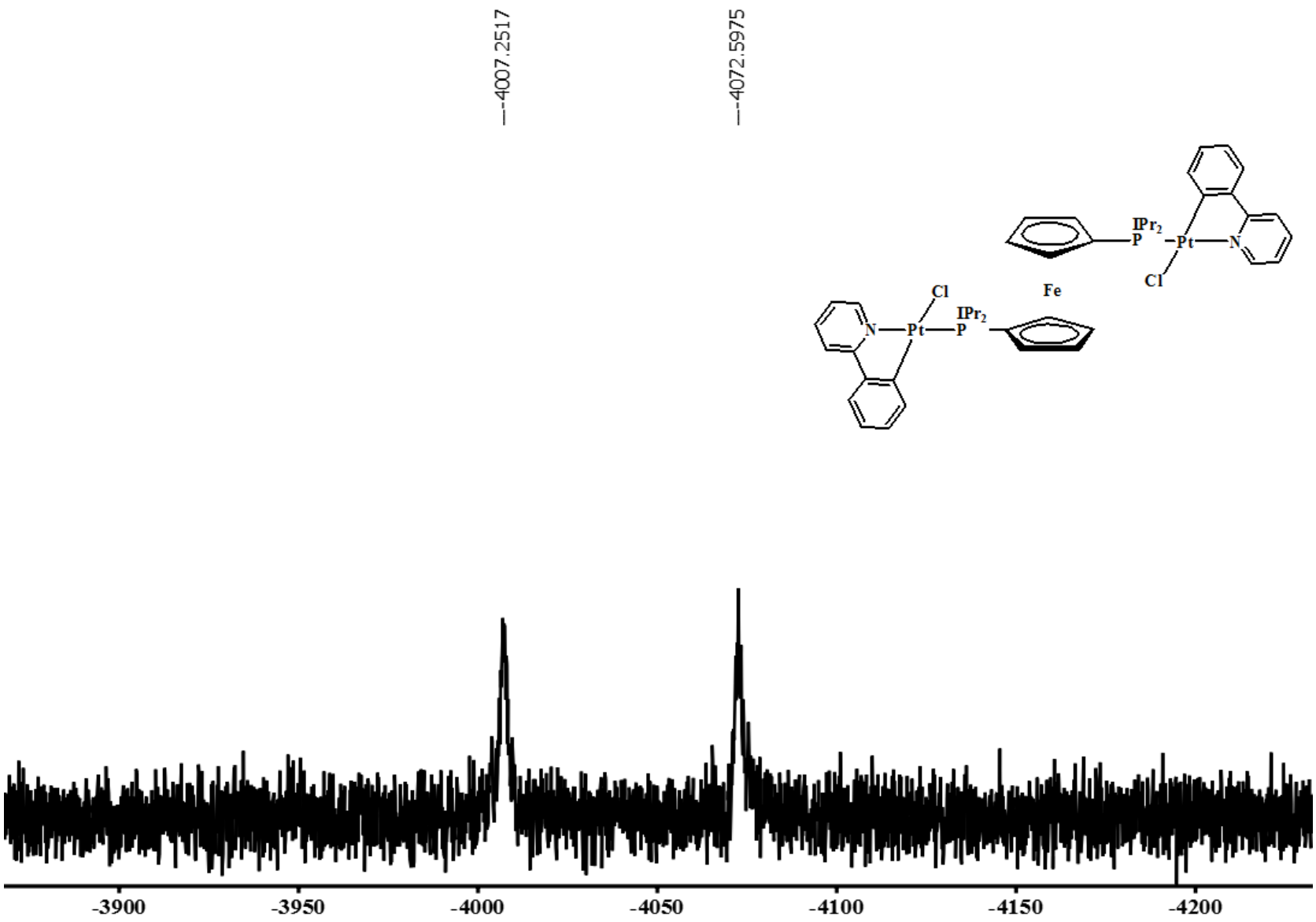

Figure S6. $^{195}Pt\{^{1}H\}$ NMR spectrum of **2c** in $CDCl_3$.

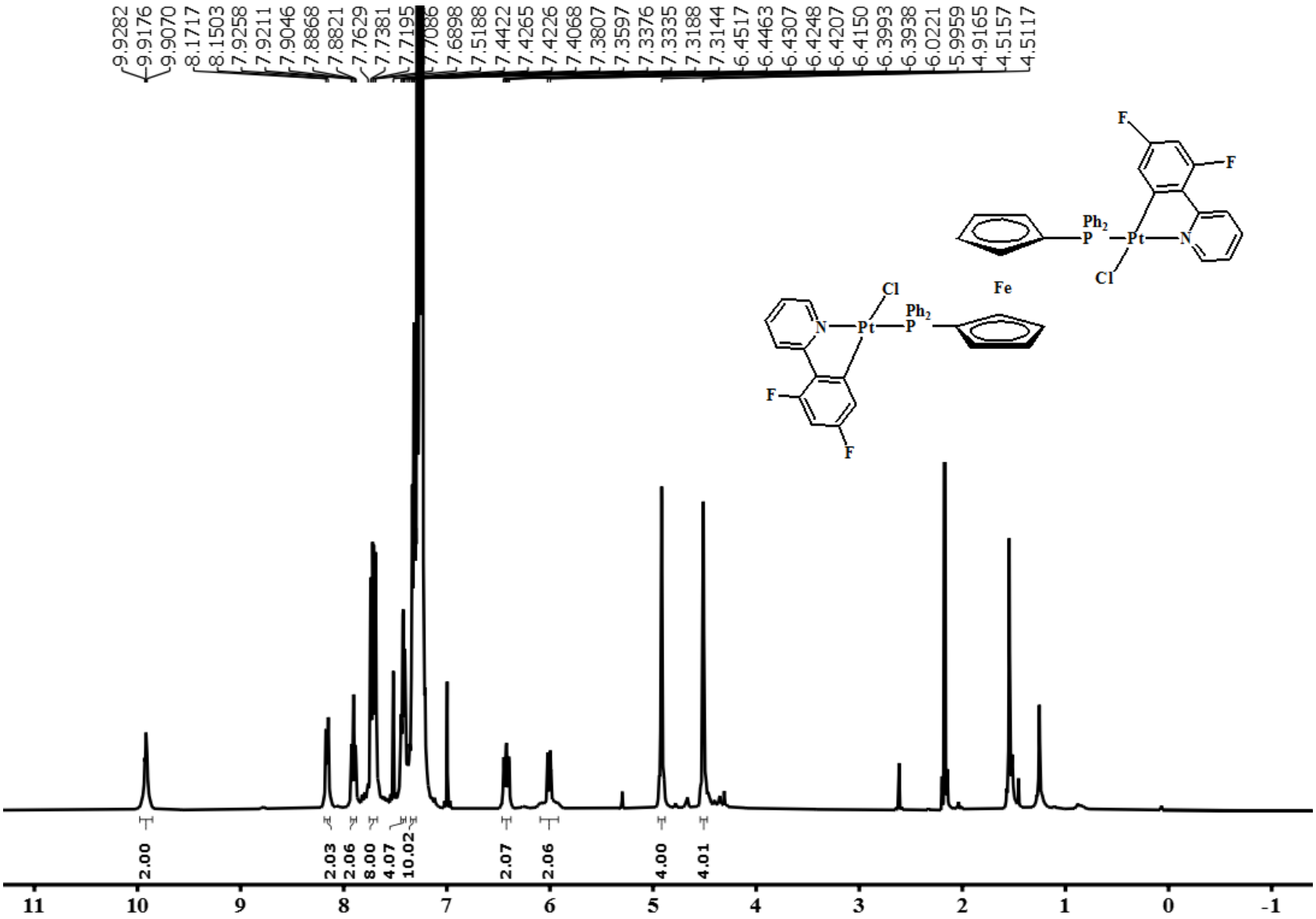

Figure S7. ^{1}H NMR spectrum of **3a** in $CDCl_3$.

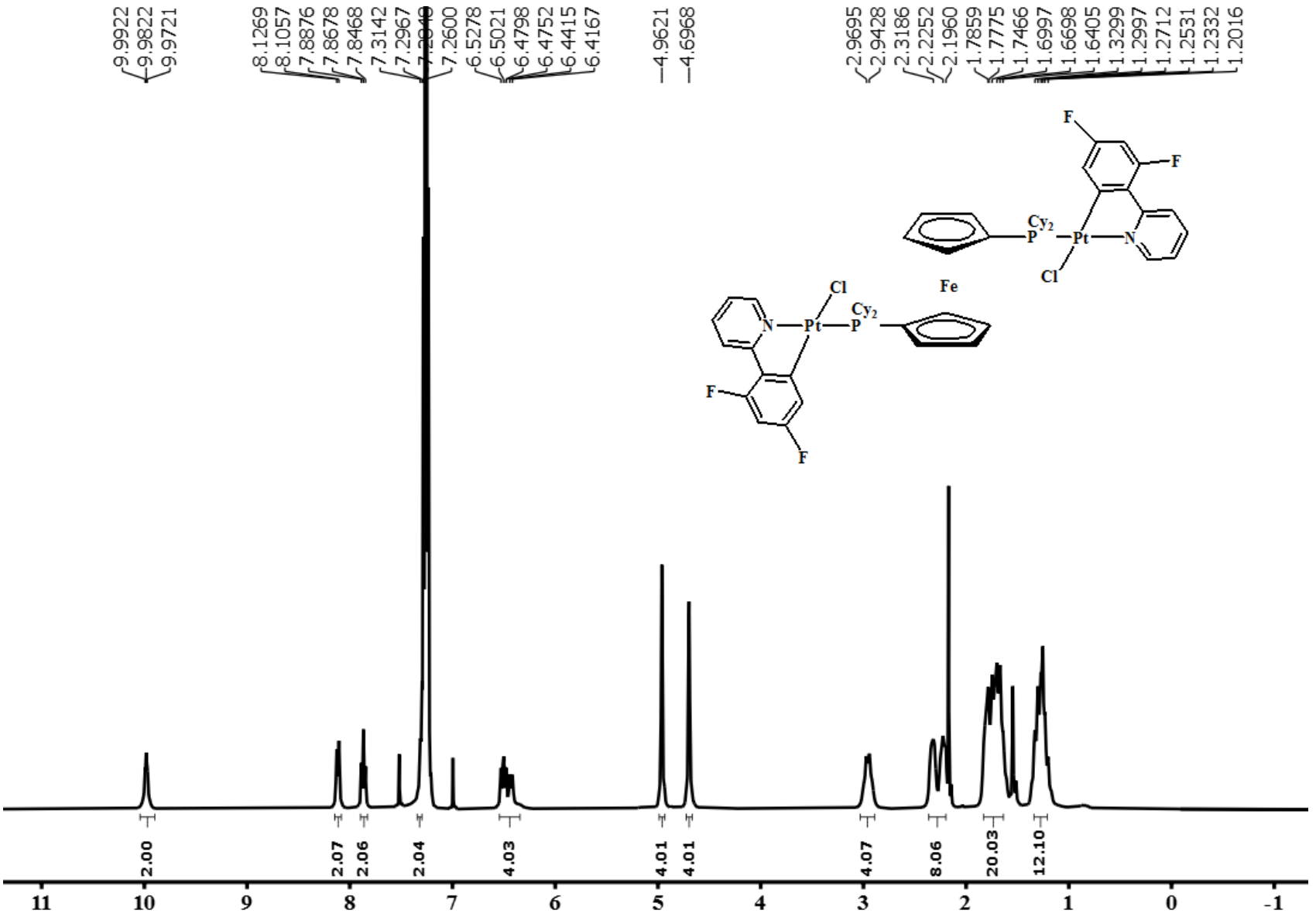

Figure S8. ^{1}H NMR spectrum of **3b** in $CDCl_3$.

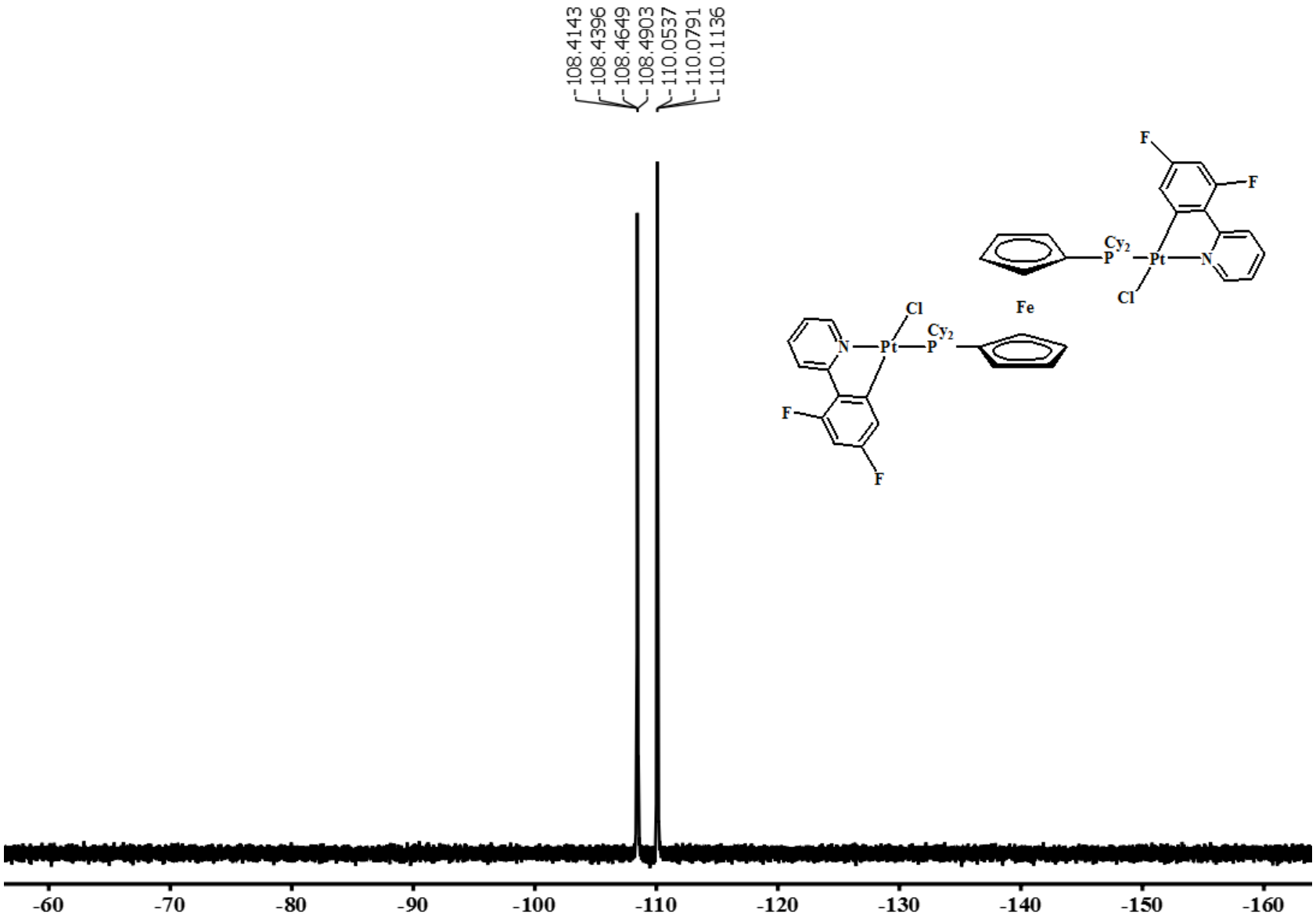

Figure S9. ^{19}F NMR spectrum of **3b** in $CDCl_3$.

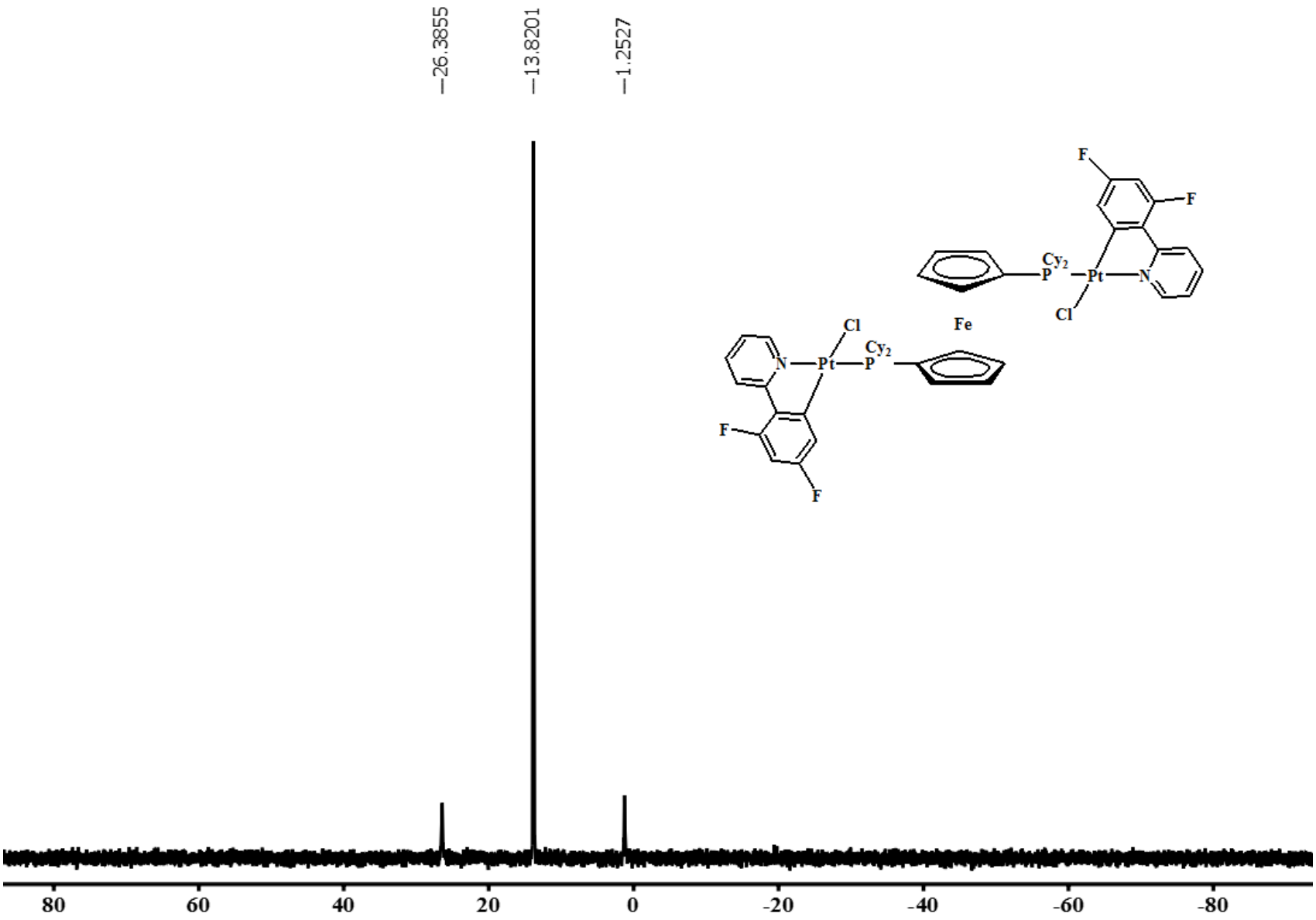

Figure S10. $^{31}P\{^{1}H\}$ NMR spectrum of **3b** in $CDCl_3$.

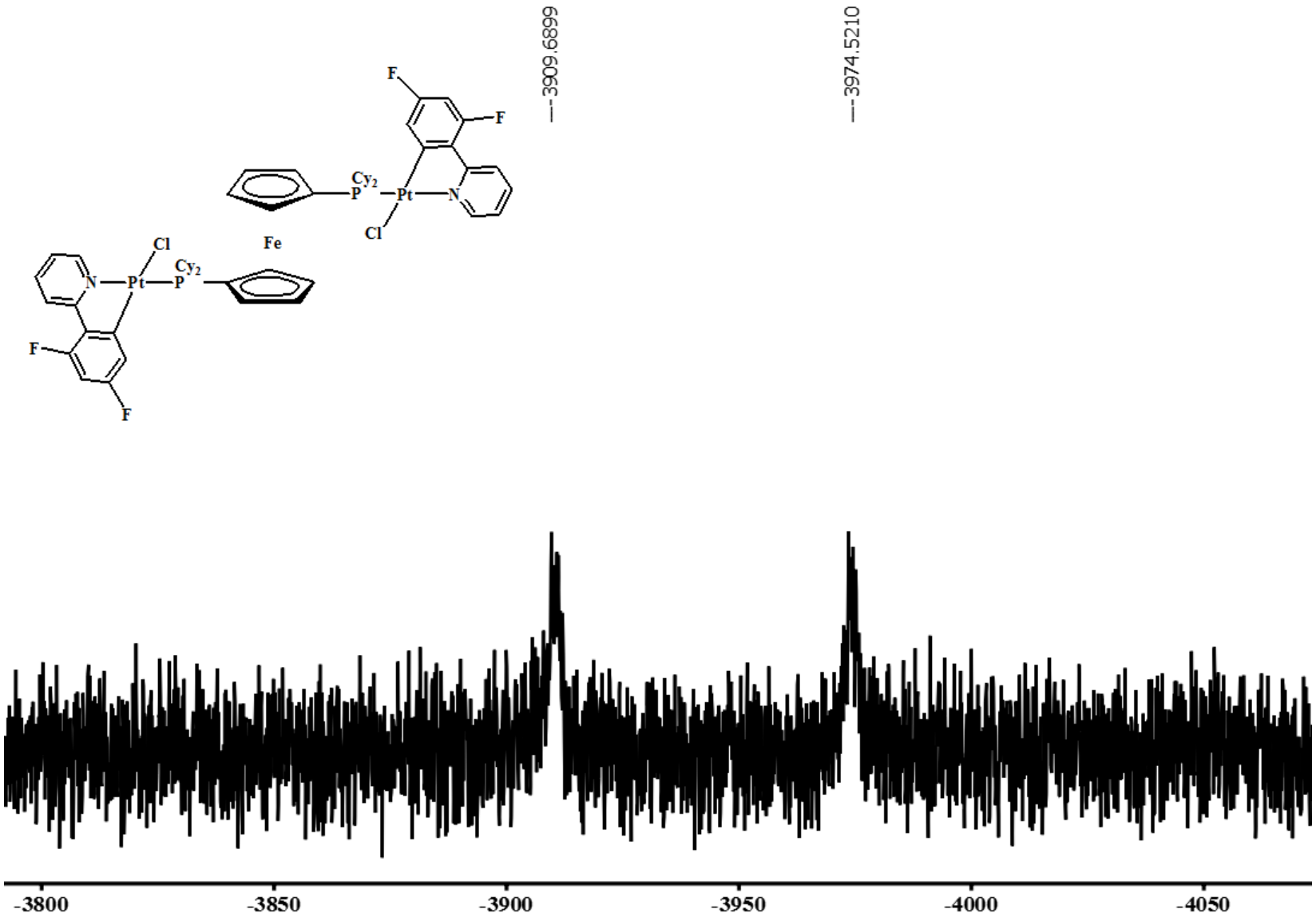

Figure S11. $^{195}Pt\{^{1}H\}$ NMR spectrum of **3b** in $CDCl_3$.

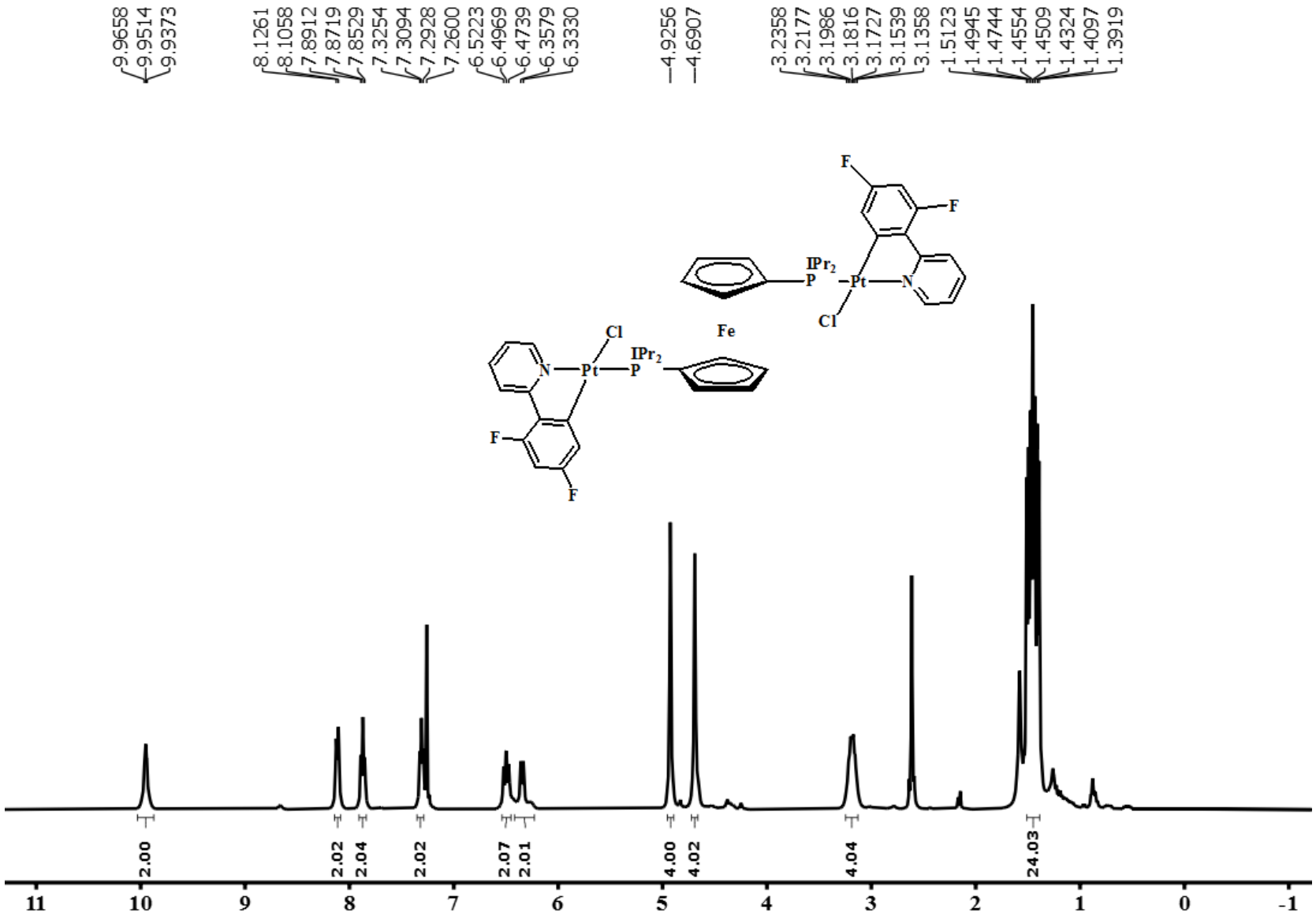

Figure S12. ^{1}H NMR spectrum of **3c** in $CDCl_3$.

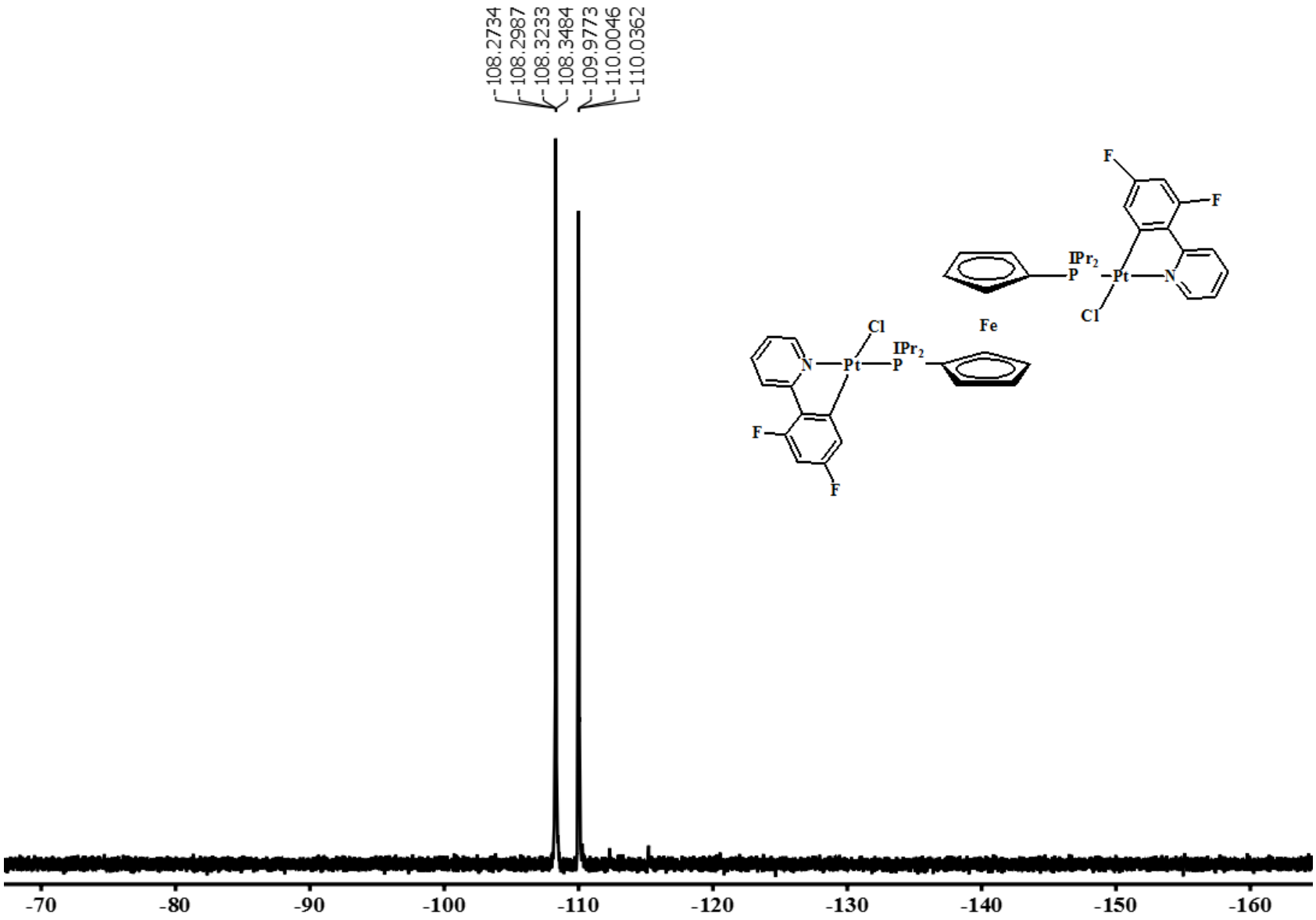

Figure S13. ^{19}F NMR spectrum of **3c** in $CDCl_3$.

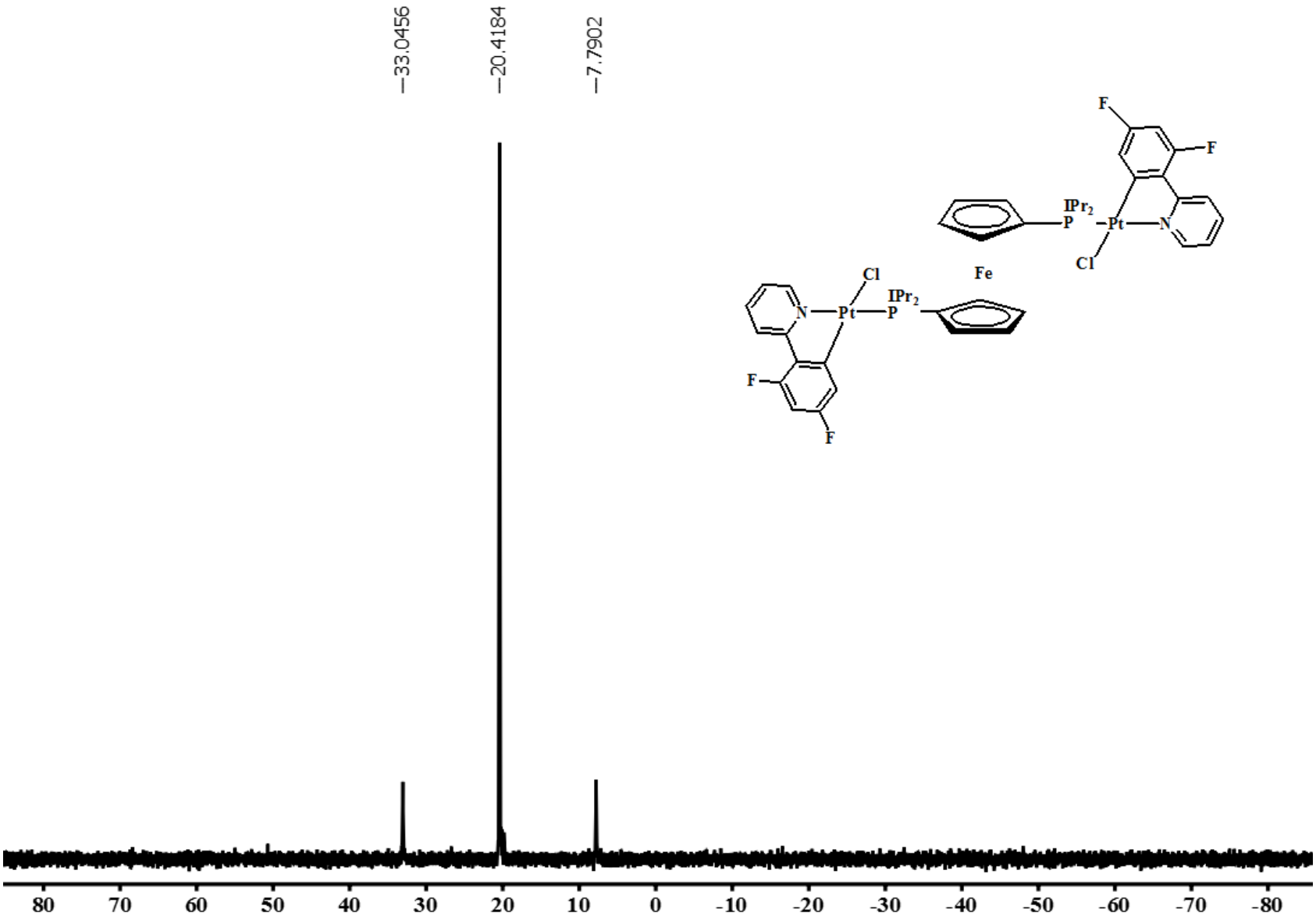

Figure S14. $^{31}P\{^{1}H\}$ NMR spectrum of **3c** in $CDCl_3$.

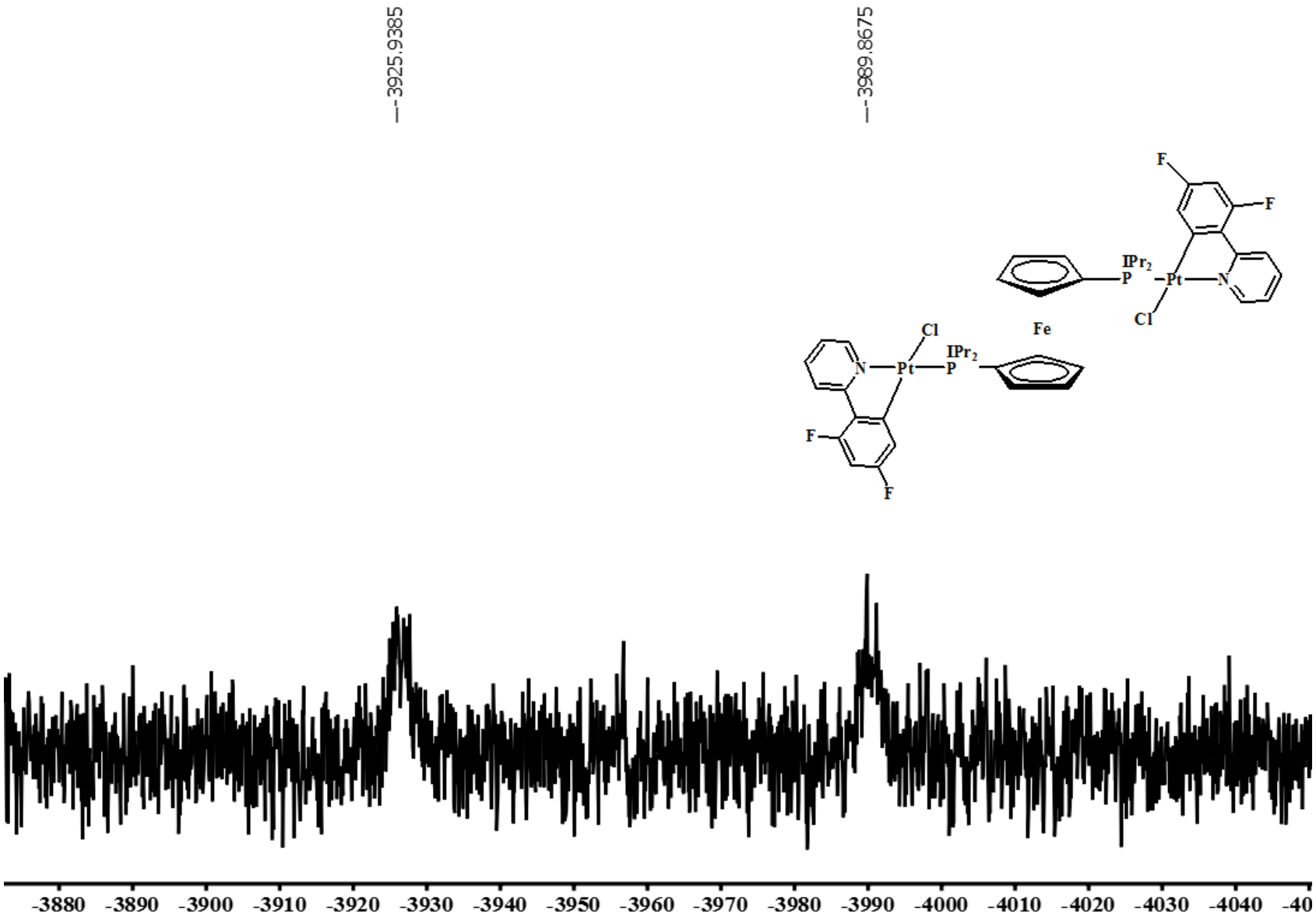

Figure S15. $^{195}Pt\{^{1}H\}$ NMR spectrum of **3c** in $CDCl_3$.

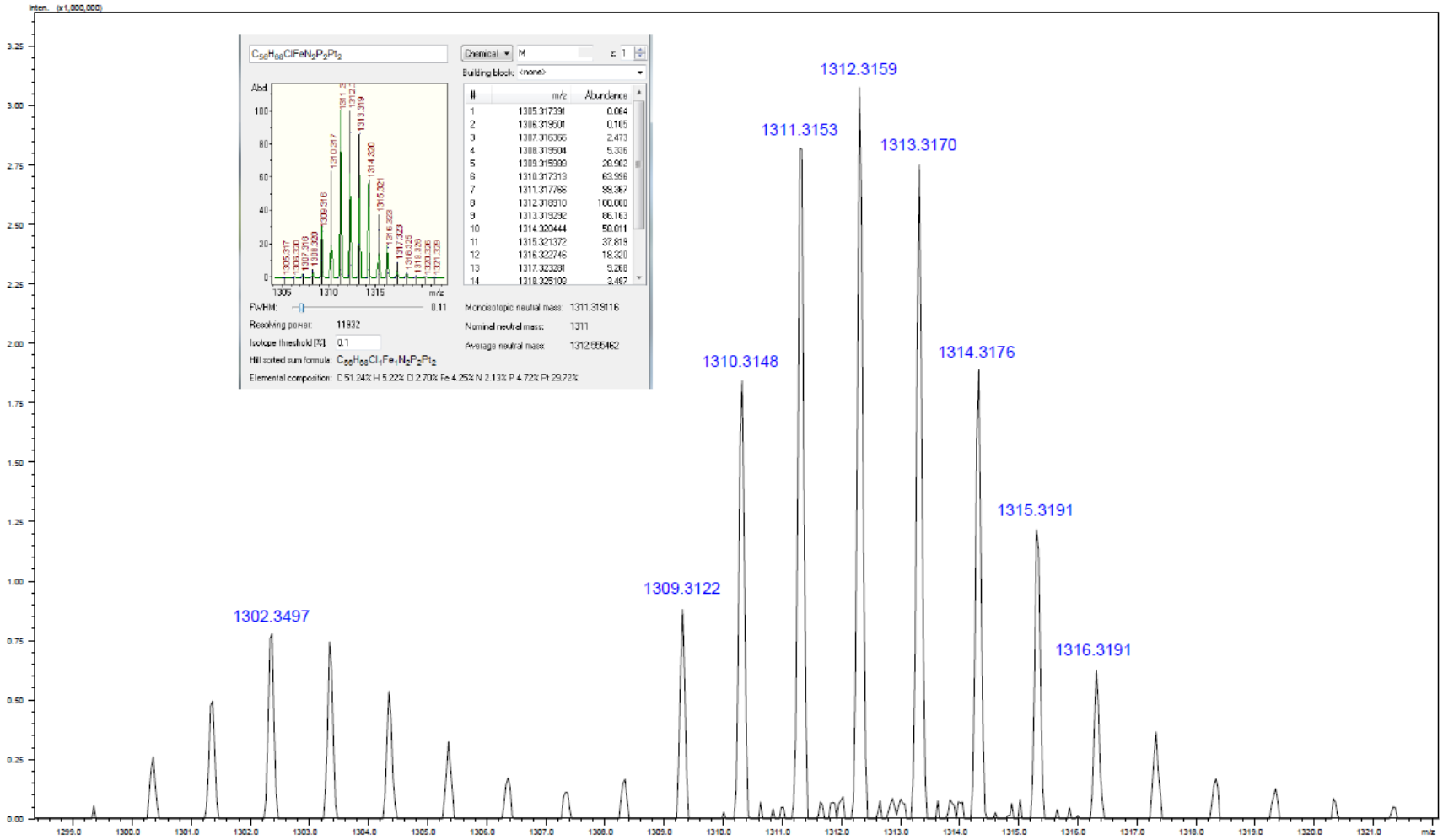

Figure S16. HR ESI Mass spectrum of **2b**. Inset shows the calculated pattern.

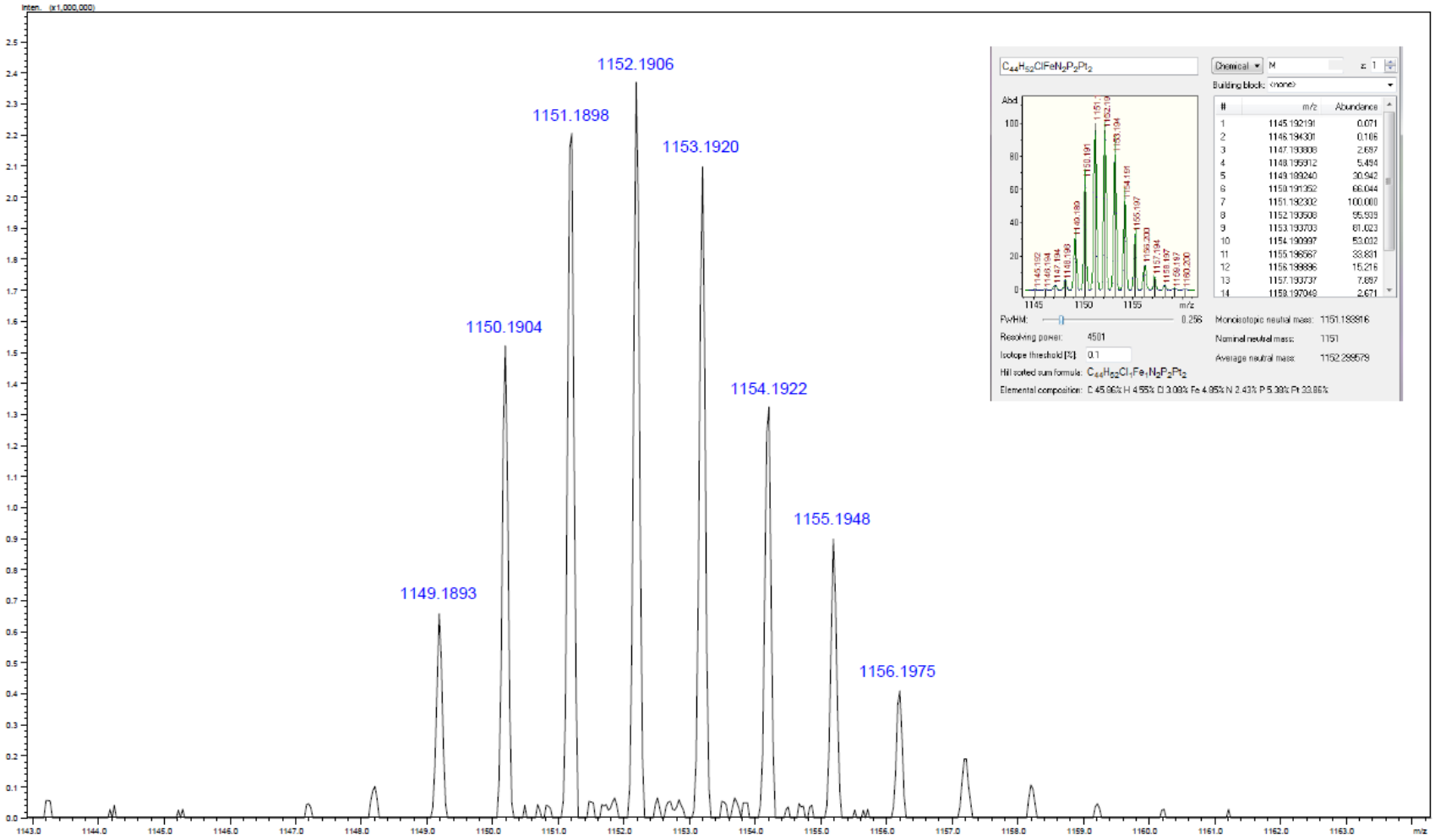

Figure S17. HR ESI Mass spectrum of **2c**. Inset shows the calculated pattern.

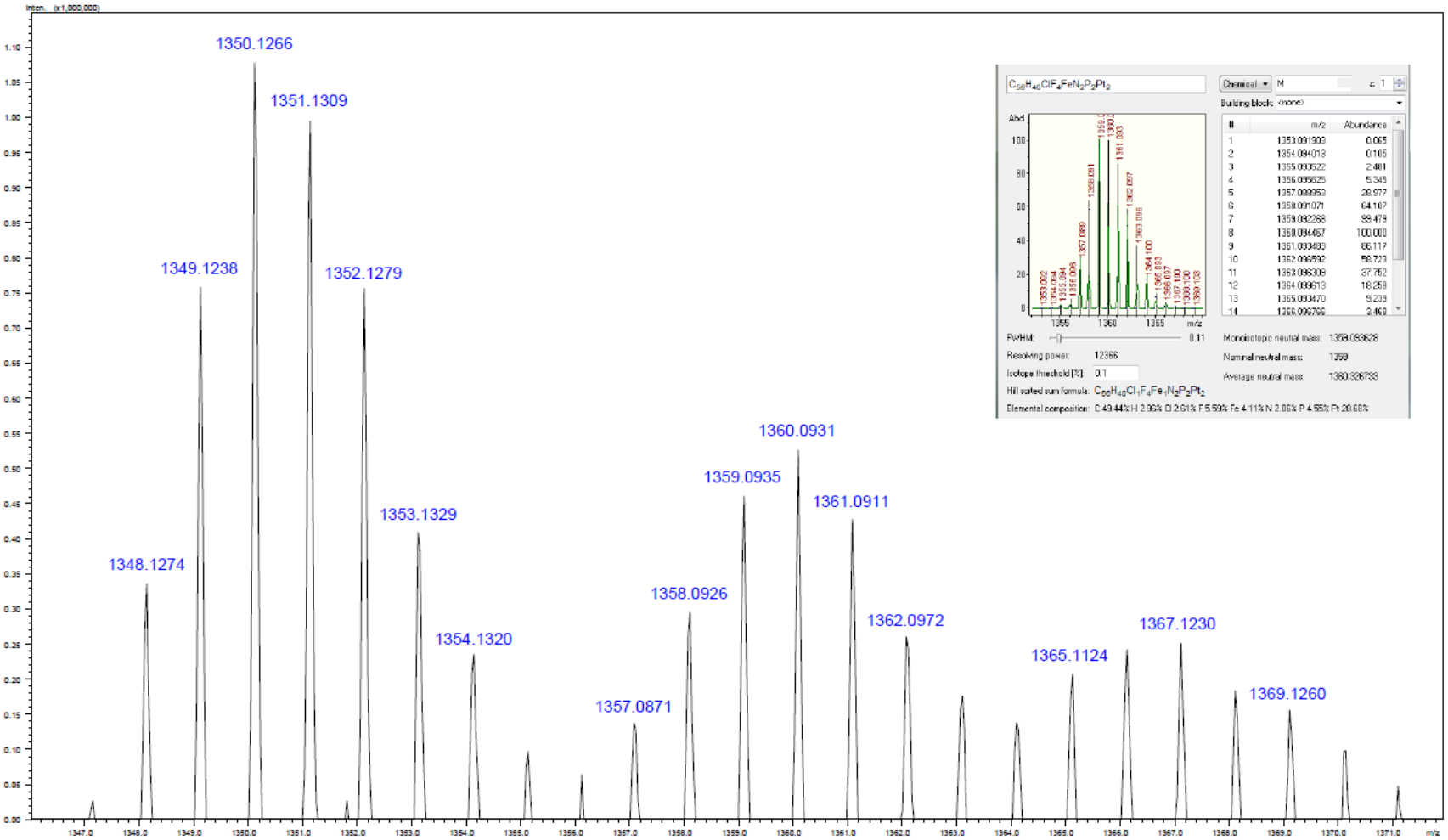

Figure S18. HR ESI Mass spectrum of **3a**. Inset shows the calculated pattern.

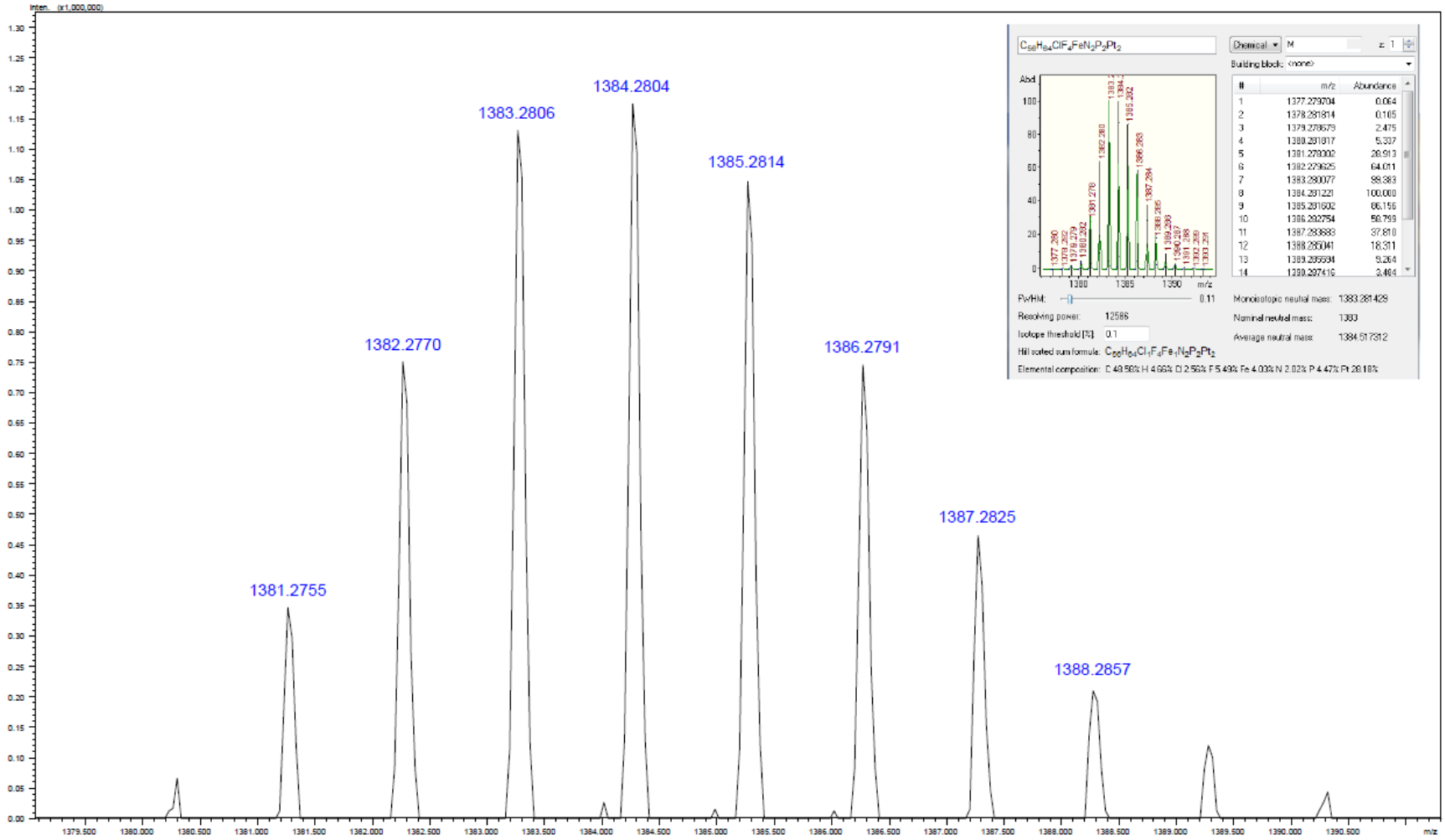

Figure S19. HR ESI Mass spectrum of **3b**. Inset shows the calculated pattern.

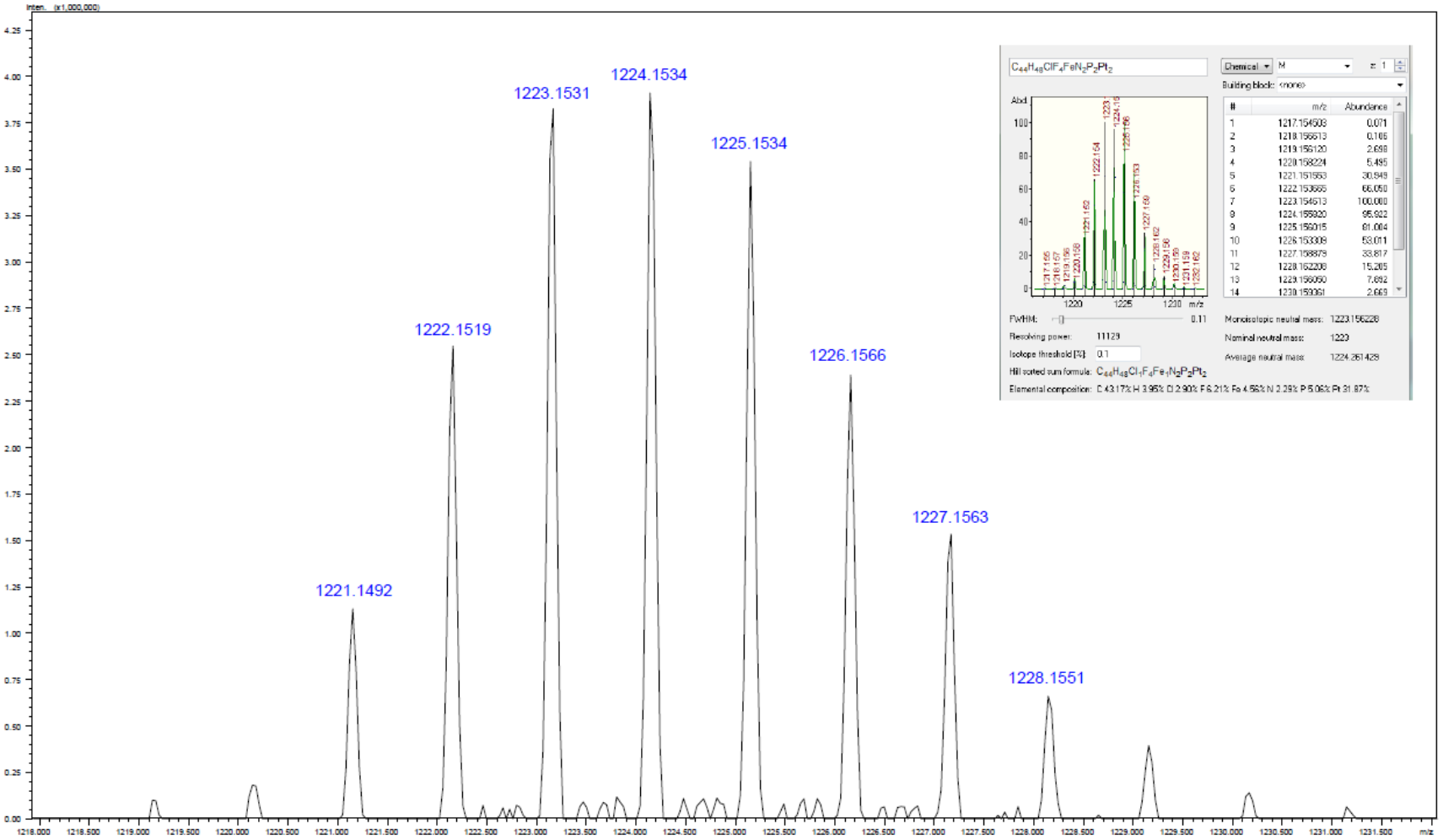

Figure S20. HR ESI Mass spectrum of **3c**. Inset shows the calculated pattern.

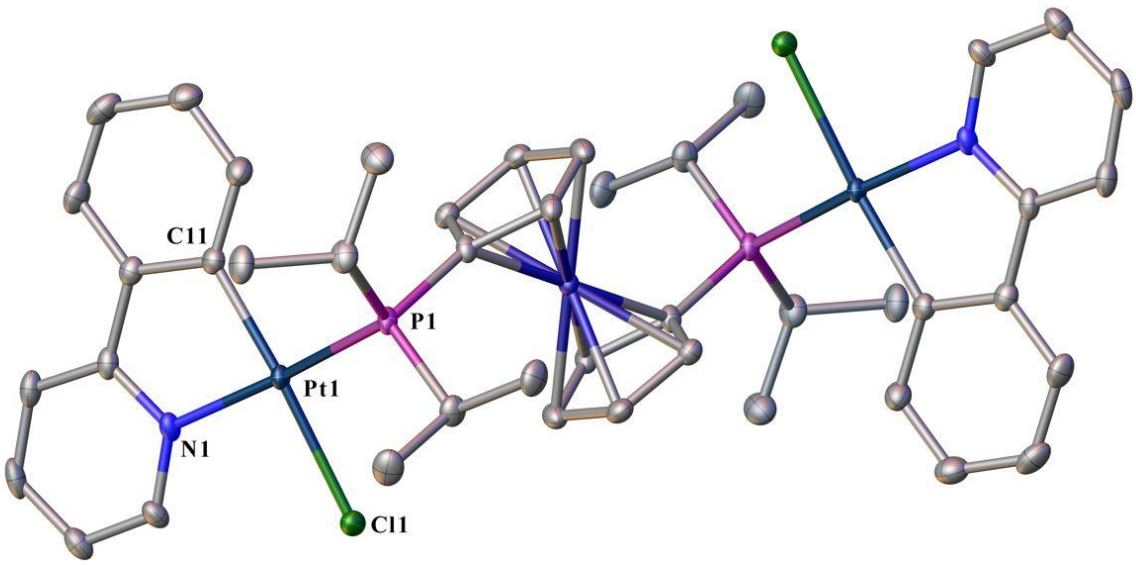

Figure S21. Molecular structure of **2c** in the solid state. Thermal ellipsoids are set at the 50% probability level. Hydrogen atoms have been omitted for clarity. Selected bond lengths [Å]: Pt1–C11=2.007 (3), Pt1–N1=2.096 (2), Pt1–P1=2.2589 (7), Pt1–Cl1=2.4051 (6). Details of crystal data, data collection and structure refinement are given in Table S2.

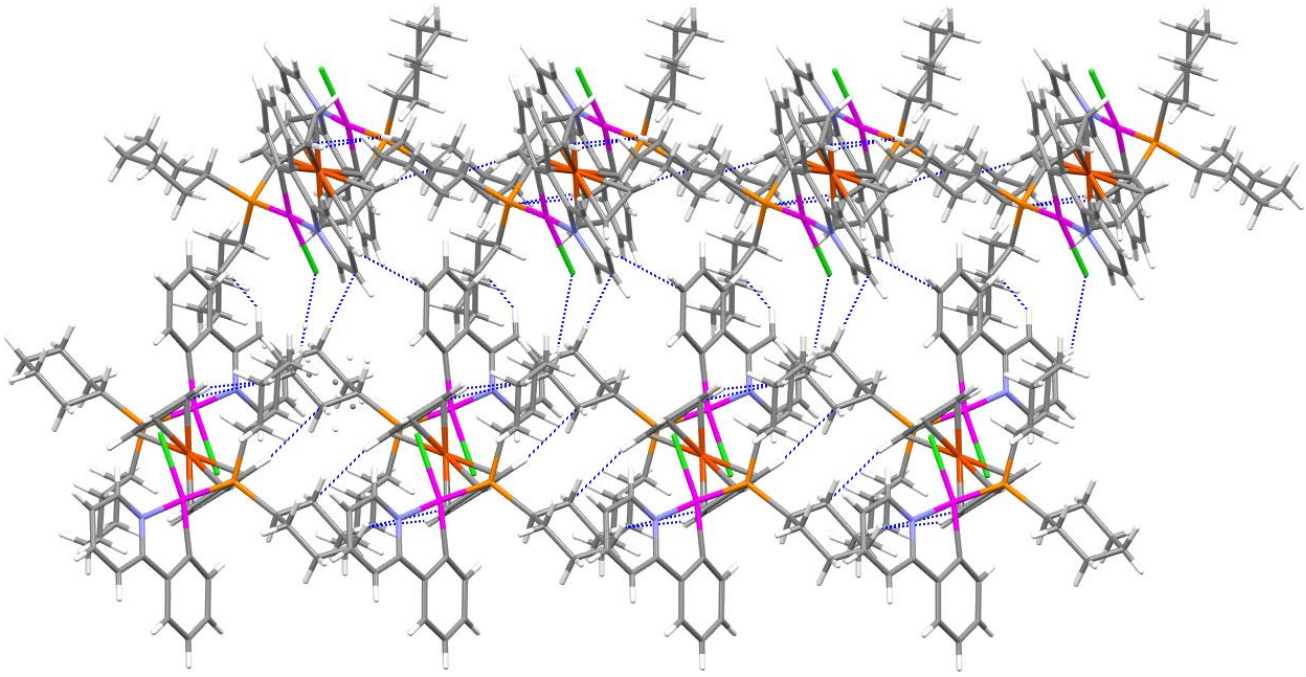

Figure S22. Crystal Packing of **2b**.

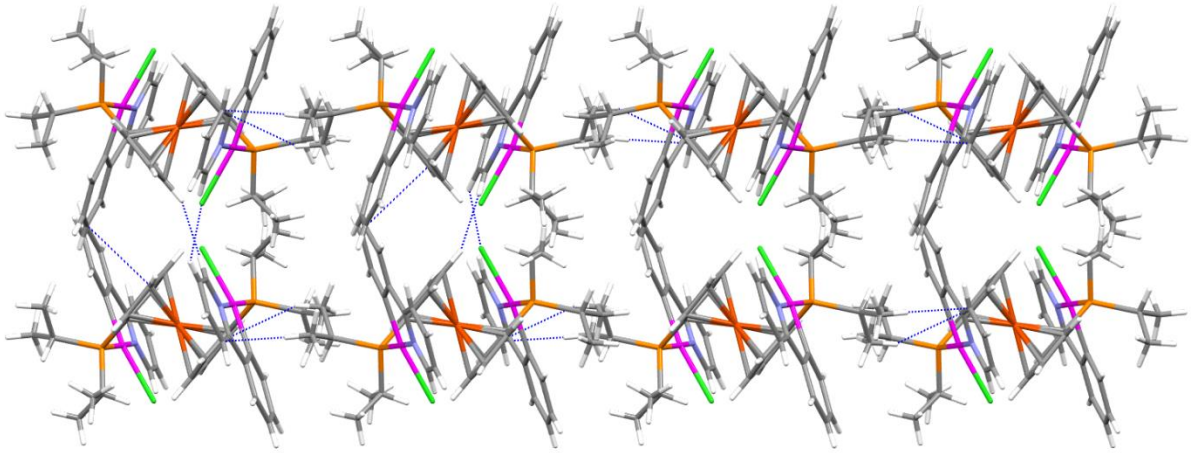

Figure S23. Crystal Packing of **2c**.

Table S1. Crystallographic and structure refinement data for **2b**.

Empirical formula	$C_{56}H_{68}Cl_2FeN_2P_2Pt_2$	
	Formula weight	1348.007
Crystal system	Monoclinic	
Space group	$P2_1/n$	
Unit cell dimensions	a = 9.0061(8) Å	α = 90°
	b = 30.535(3) Å	β = 109.756(3)°
	c = 10.3235(9) Å	γ = 90°
Volume	2671.9(4) Å3	
Z, Z'	2, 0.5	
Density (calculated)	1.764 Mg/m^3	
Wavelength	0.71073 Å	
Temperature	100(2) K	
F(000)	1396	
Absorption coefficient	5.790 mm^{-1}	
Absorption correction	semi-empirical from equivalents	
Max. and min. transmission	0.5699 and 0.3317	
Theta range for data collection	2.485 to 28.282°	
Reflections collected	45950	
Independent reflections	6599 [R(int) = 0.0501]	
Data / restraints / parameters	6599 / 87 / 344	
$wR(F^2$ all data)	$wR2$ = 0.0639	
$R(F$ obsd data)	$R1$ = 0.0248	
Goodness-of-fit on F^2	1.007	
Observed data [I > 2σ(I)]	6295	
Largest and mean shift / s.u.	0.004 and 0.000	
Largest diff. peak and hole	1.236 and -1.286 e/Å3	

$wR2 = \{ \Sigma [w(F_o^2 - F_c^2)^2] / \Sigma [w(F_o^2)^2] \}^{1/2}$

$R1 = \Sigma ||F_o| - |F_c|| / \Sigma |F_o|$

Table S2. Crystallographic and structure refinement data for **2c**.

Empirical formula	$C_{44}H_{52}Cl_2FeN_2P_2Pt_2$	
Formula weight	1187.74	
Crystal system	orthorhombic	
Space group	*Pbca*	
Unit cell dimensions	a = 14.8443(4) Å	α = 90°
	b = 12.8796(4) Å	β = 90°
	c = 20.9625(7) Å	γ = 90°
Volume	4007.8(2) Å^3	
Z	4	
Density (calculated)	1.968 Mg/m^3	
Wavelength	0.71073 Å	
Temperature	100(2) K	
F(000)	2304	
Absorption coefficient	7.570 mm^{-1}	
Absorption correction	semi-empirical from equivalents	
Max. and min. transmission	0.713 and 0.297	
Theta range for data collection	2.308 to 28.694°	
Reflections collected	33429	
Independent reflections	5176 [R(int) = 0.0361]	
Data / restraints / parameters	5176 / 0 / 241	
wR(F^2 all data)	$wR2$ = 0.0601	
R(F obsd data)	$R1$ = 0.0213	
Goodness-of-fit on F^2	1.005	
Observed data [I > 2σ(I)]	4998	
Largest and mean shift / s.u.	0.002 and 0.000	
Largest diff. peak and hole	1.330 and -1.374 e/Å^3	

$wR2 = \{ \Sigma [w(F_o^2 - F_c^2)^2] / \Sigma [w(F_o^2)^2] \}^{1/2}$

$R1 = \Sigma ||F_o| - |F_c|| / \Sigma |F_o|$

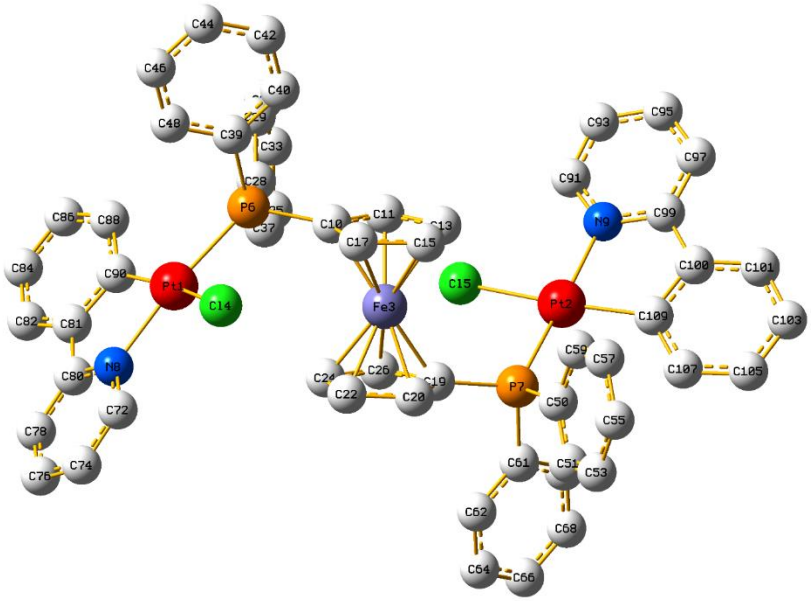

Figure S24. View of the optimized structure of **2a** in gas phase (S_0) with the atom numbering.

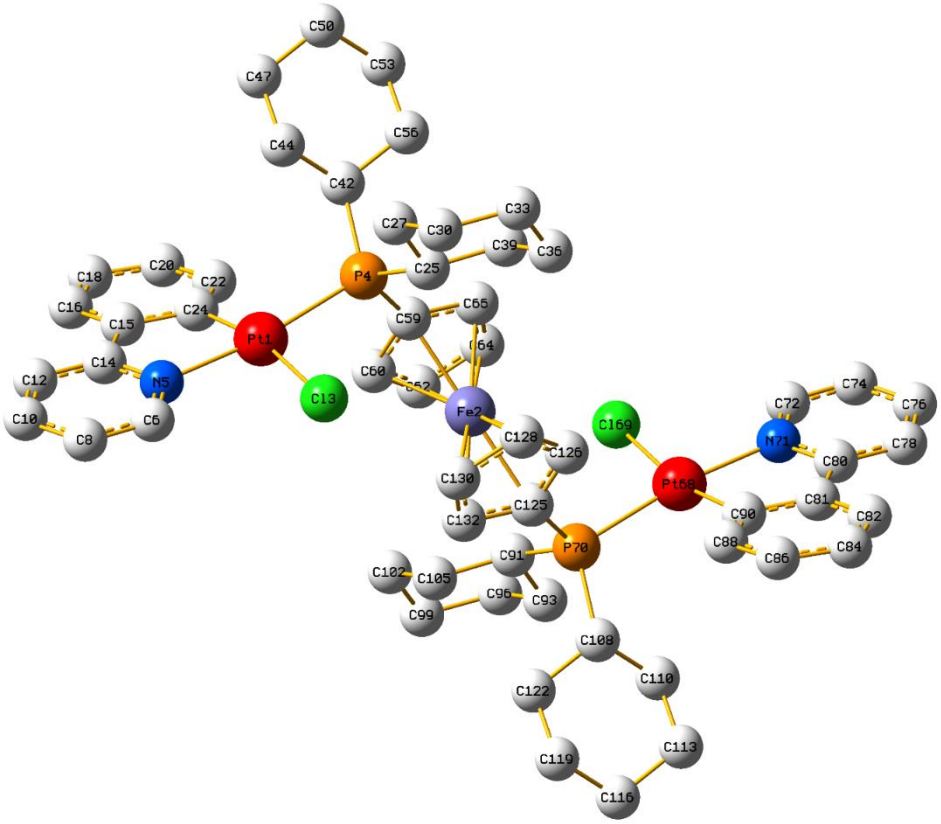

Figure S25. View of the optimized structure of **2b** in gas phase (S_0) with the atom numbering.

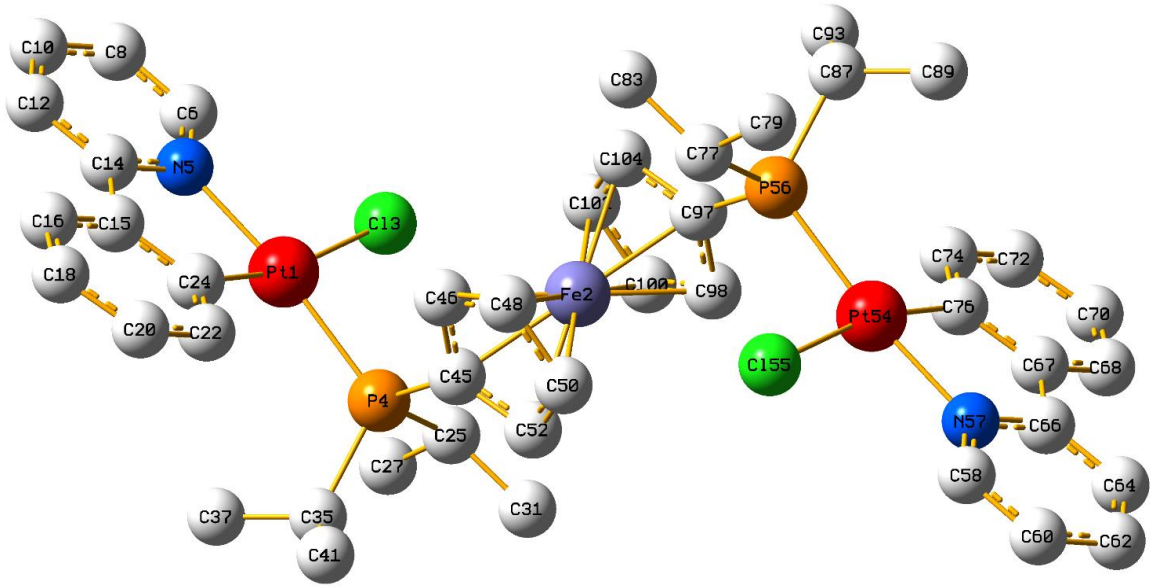

Figure S26. View of the optimized structure of **2c** in gas phase (S_0) with the atom numbering.

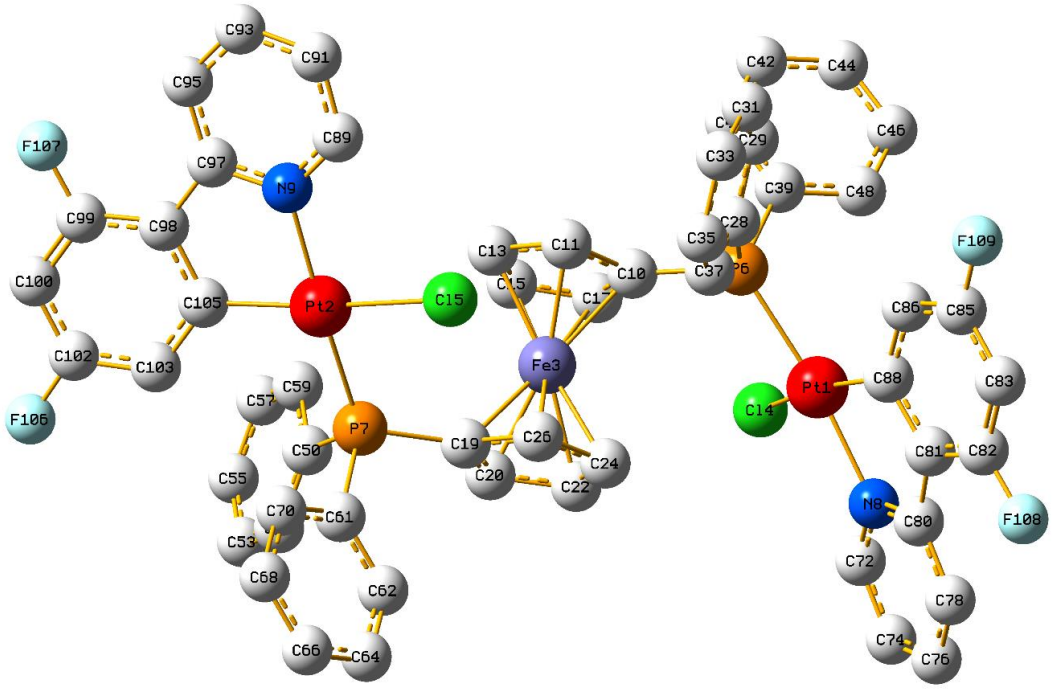

Figure S27. View of the optimized structure of **3a** in gas phase (S_0) with the atom numbering.

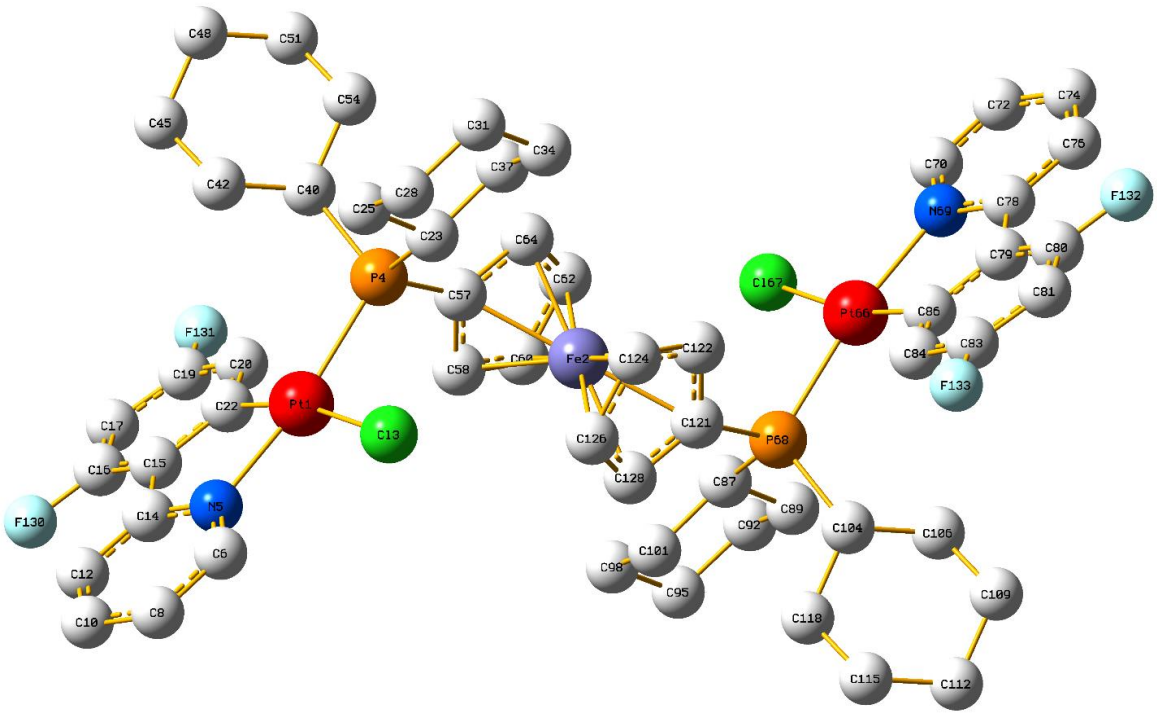

Figure S28. View of the optimized structure of **3b** in gas phase (S_0) with the atom numbering.

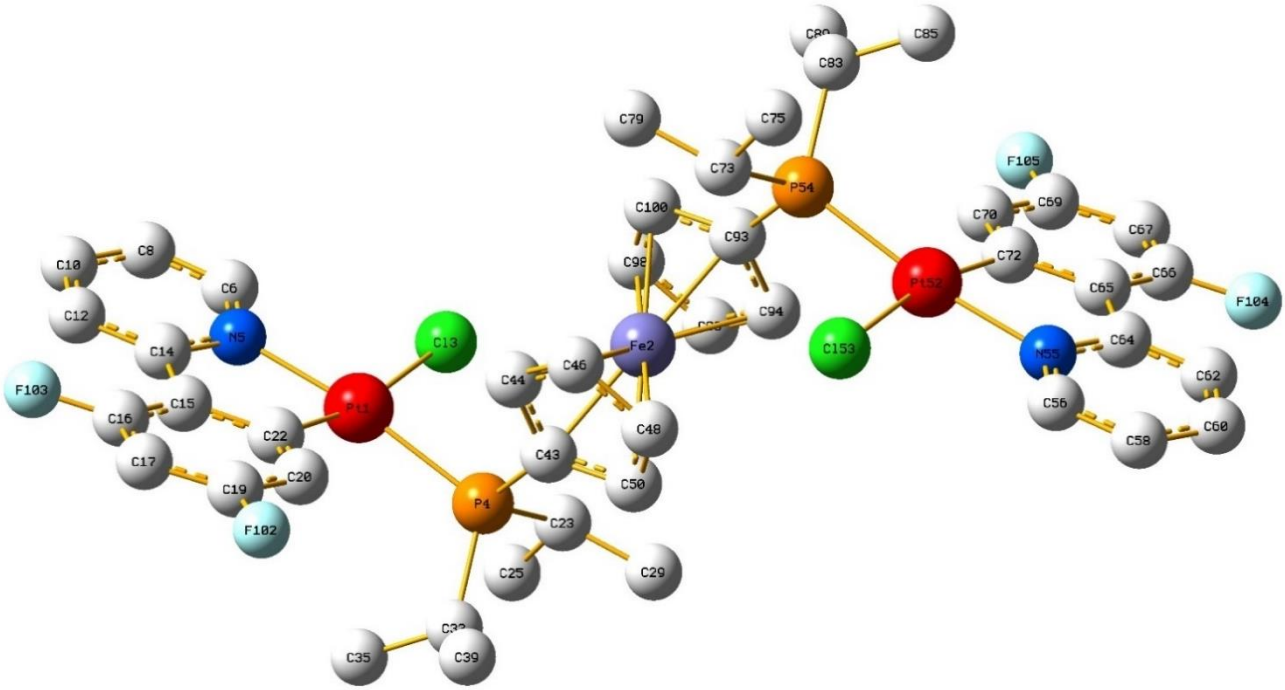

Figure S29. View of the optimized structure of **3c** in gas phase (S_0) with the atom numbering.

Table S3. Selected bond distances (A°) and angles (deg) for the calculated (S_0 and T_1 in gas phase and S_0 in CH_2Cl_2) and crystal structures of **2a.**

Bond length and angles	X-ray	S_0 (gas phase)	S_0 (CH_2Cl_2)	T_1 (gas phase)
Pt1—C45	2.011 (7)	2.0293	2.0221	2.0267
Pt1—N1	2.087 (5)	2.1262	2.1279	2.1281
Pt1—P1	2.2286 (18)	2.3190	2.3259	2.3208
Pt1—Cl1	2.3946 (19)	2.4818	2.5337	2.4899
Pt2—C56	2.009 (7)	2.0273	2.0237	2.0302
Pt2—N2	2.075 (5)	2.1258	2.1300	2.1278
Pt2—P2	2.2377 (17)	2.3212	2.3280	2.3200
Pt2—Cl2	2.3797 (19)	2.4902	2.5325	2.4806
C45—Pt1—N1	81.0 (2)	79.76	79.78	79.72
C45—Pt1—P1	97.87 (19)	98.71	100.11	99.75
N1—Pt1—P1	168.12 (16)	172.80	169.91	172.49
C45—Pt1—Cl1	159.7 (2)	166.48	163.77	166.37
N1—Pt1—Cl1	90.28 (17)	90.77	91.61	91.05
P1—Pt1—Cl1	94.36 (6)	91.85	90.76	90.71
C56—Pt2—N2	80.4 (3)	79.71	79.78	79.80
C56—Pt2—P2	98.4 (2)	100.31	99.15	98.10
N2—Pt2—P2	172.06 (17)	172.22	171.38	173.86
C56—Pt2—Cl2	161.4 (2)	166.28	164.41	167.87
N2—Pt2—Cl2	90.73 (17)	91.19	91.09	90.66
P2—Pt2—Cl2	92.56 (7)	90.18	91.73	92.13

Table S4. Selected bond distances (A°) and angles (deg) for the calculated (S_0 in gas phase and S_0 in CH_2Cl_2) and crystal structures of **2b** (The molecule was located on an inversion center, thus only ½ of the atoms were unique).

Bond length and angles	X-ray	S_0 (gas phase)	S_0 (CH_2Cl_2)
Pt1—C11	2.000 (3)	2.0280	2.0260
Pt1—N1	2.096 (2)	2.1321	2.1389
Pt1—P1	2.2646 (6)	2.3415	2.3518
Pt1—Cl1	2.3999 (7)	2.4961	2.5309
C11—Pt1—N1	80.35 (10)	79.73	79.71
C11—Pt1—P1	98.01 (8)	99.00	98.52
N1—Pt1—P1	172.70 (7)	171.64	171.27
C11—Pt1—Cl1	167.05 (7)	167.92	167.29
N1—Pt1—Cl1	89.81 (7)	90.36	90.43
P1—Pt1—Cl1	92.79 (2)	91.80	92.42

Table S5. Selected bond distances (A°) and angles (deg) for the calculated (S_0 in gas phase and S_0 in CH_2Cl_2) and crystal structures of **2c** (The molecule was located on an inversion center, thus only ½ of the atoms were unique).

Bond length and angles	X-ray	S_0 (gas phase)	S_0 (CH_2Cl_2)
Pt1—C11	2.007(3)	2.0211	2.0186
Pt1—N1	2.096(2)	2.1307	2.1389
Pt1—P1	2.2589(7)	2.3376	2.3503
Pt1—Cl1	2.4051(6)	2.4974	2.5392
C11—Pt1—N1	80.30(10)	79.76	79.73
C11—Pt1—P1	97.33(8)	98.94	98.48
N1—Pt1—P1	173.19(7)	172.95	173.00
C11—Pt1—Cl1	167.45(8)	167.73	167.06
N1—Pt1—Cl1	90.42(6)	90.45	90.48
P1—Pt1—Cl1	92.81(2)	91.66	92.22

Table S6. Selected bond distances (A°) and angles (deg) for the calculated (S_0 and T_1 in gas phase and S_0 in CH_2Cl_2) and crystal structures of **3a.**

Bond length and angles	X-ray	S_0 (gas phase)	S_0 (CH_2Cl_2)	T_1 (gas phase)
Pt1—C88	-	2.0237	2.0190	2.0229
Pt1—N8	-	2.1210	2.1242	2.1234
Pt1—P6	-	2.3283	2.3330	2.3238
Pt1—Cl4	-	2.4799	2.5175	2.4804
Pt2—C105	-	2.0249	2.0204	2.0252
Pt2—N9	-	2.1213	2.1257	2.1228
Pt2—P7	-	2.3258	2.3348	2.3266
Pt2—Cl5	-	2.4731	2.5148	2.4725
C88—Pt1—N8	-	79.67	79.70	79.68
C88—Pt1—P6	-	101.02	99.76	100.55
N8—Pt1—P6	-	172.11	170.69	172.24
C88—Pt1—Cl4	-	166.67	164.85	166.65
N8—Pt1—Cl4	-	91.67	91.85	91.65
P6—Pt1—Cl4	-	88.95	90.60	89.42
C105—Pt2—N9	-	79.73	79.66	79.77
C105—Pt2—P7	-	99.24	99.65	98.68
N9—Pt2—P7	-	172.62	171.26	173.44
C105—Pt2—Cl5	-	166.58	164.68	167.77
N9—Pt2—Cl5	-	91.37	91.84	91.27
P7—Pt2—Cl5	-	90.86	90.66	91.14

Table S7. Selected bond distances (A°) and angles (deg) for the calculated (S_0 in gas phase and S_0 in CH_2Cl_2) and crystal structures of **3b** (The molecule was located on an inversion center, thus only ½ of the atoms were unique).

Bond length and angles	X-ray	S_0 (gas phase)	S_0 (CH_2Cl_2)
Pt1—C22	-	2.0233	2.0205
Pt1—N5	-	2.1277	2.1333
Pt1—P4	-	2.3489	2.3595
Pt1—Cl3	-	2.4849	2.5168
C22—Pt1—N5	-	79.66	79.61
C22—Pt1—P4	-	99.10	98.65
N5—Pt1—P4	-	171.37	171.93
C22—Pt1—Cl3	-	168.14	168.48
N5—Pt1—Cl3	-	90.84	90.87
P4—Pt1—Cl3	-	91.34	91.66

Table S8. Selected bond distances (A°) and angles (deg) for the calculated (S_0 in gas phase and S_0 in CH_2Cl_2) and crystal structures of **3c** (The molecule was located on an inversion center, thus only ½ of the atoms were unique).

Bond length and angles	**X-ray**	**S_0 (gas phase)**	**S_0 (CH_2Cl_2)**
Pt1—C22	-	2.0149	2.0115
Pt1—N5	-	2.1264	2.1345
Pt1—P4	-	2.3441	2.3530
Pt1—Cl3	-	2.4857	2.5222
C22—Pt1—N5	-	79.68	79.63
C22—Pt1—P4	-	98.76	98.22
N5—Pt1—P4	-	172.72	171.36
C22—Pt1—Cl3	-	168.25	167.45
N5—Pt1—Cl3	-	91.07	91.35
P4—Pt1—Cl3	-	91.31	91.96

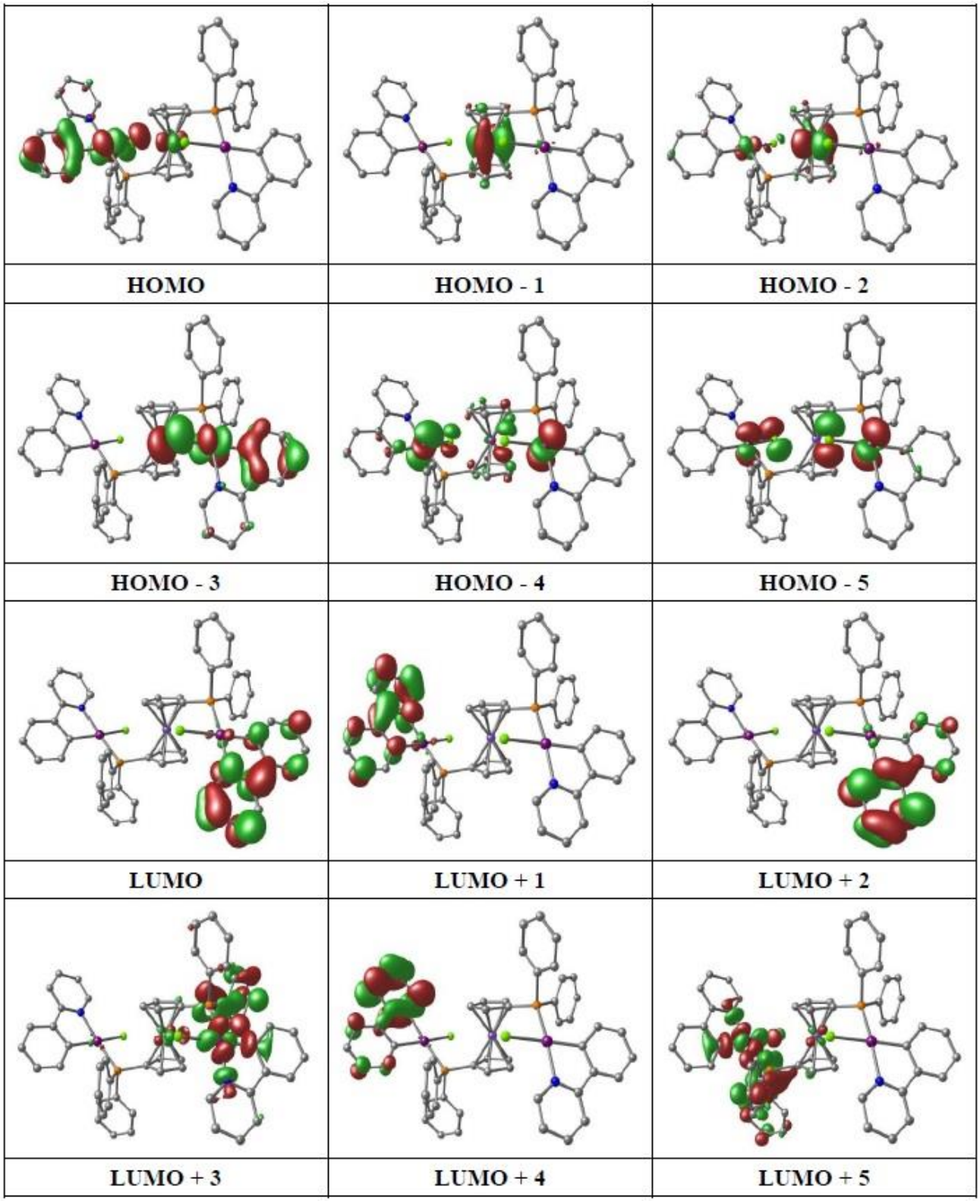

Figure S30. Molecular orbital plots for the optimized structure of **2a** in CH_2Cl_2 solution.

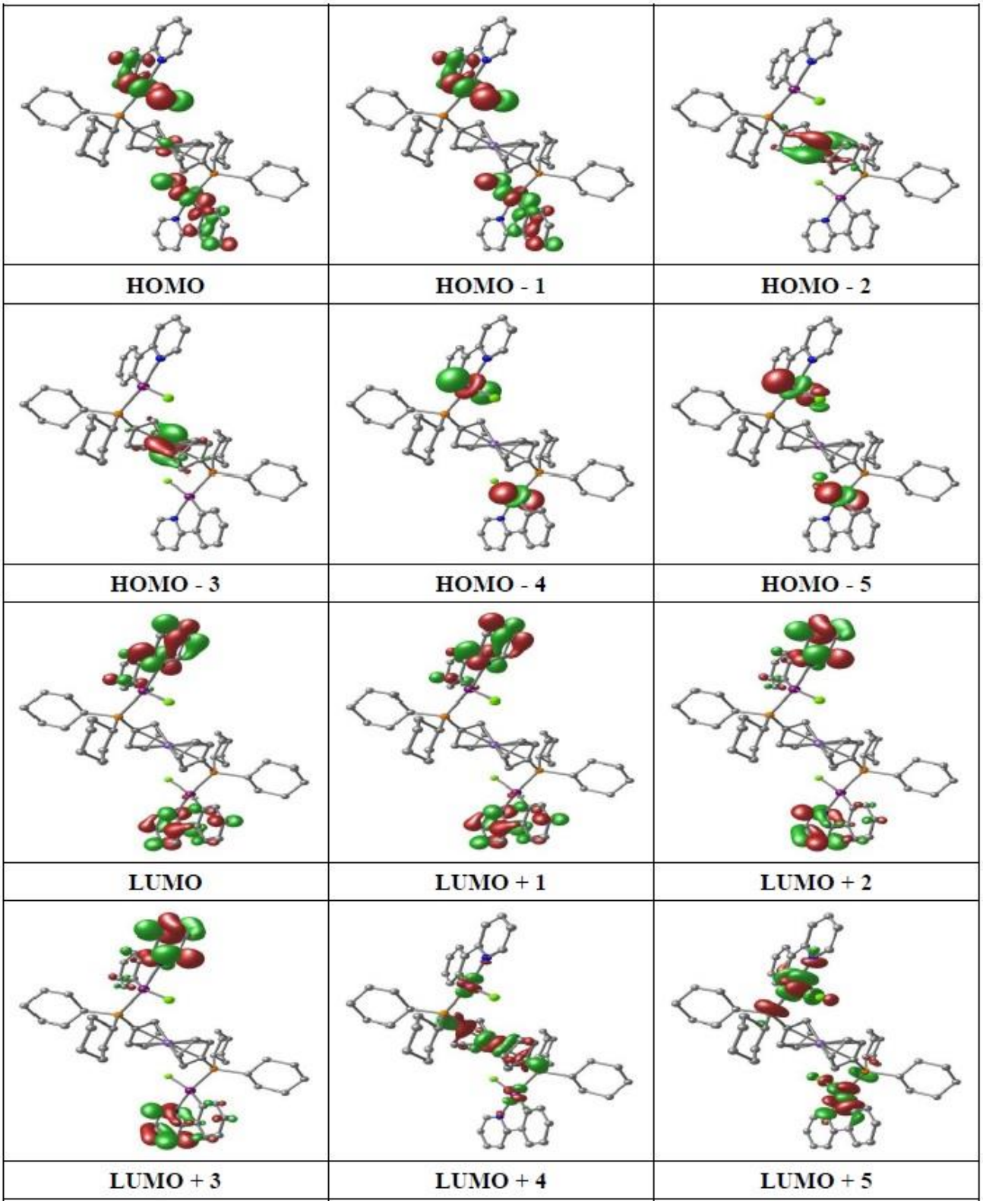

Figure S31. Molecular orbital plots for the optimized structure of **2b** in CH_2Cl_2 solution.

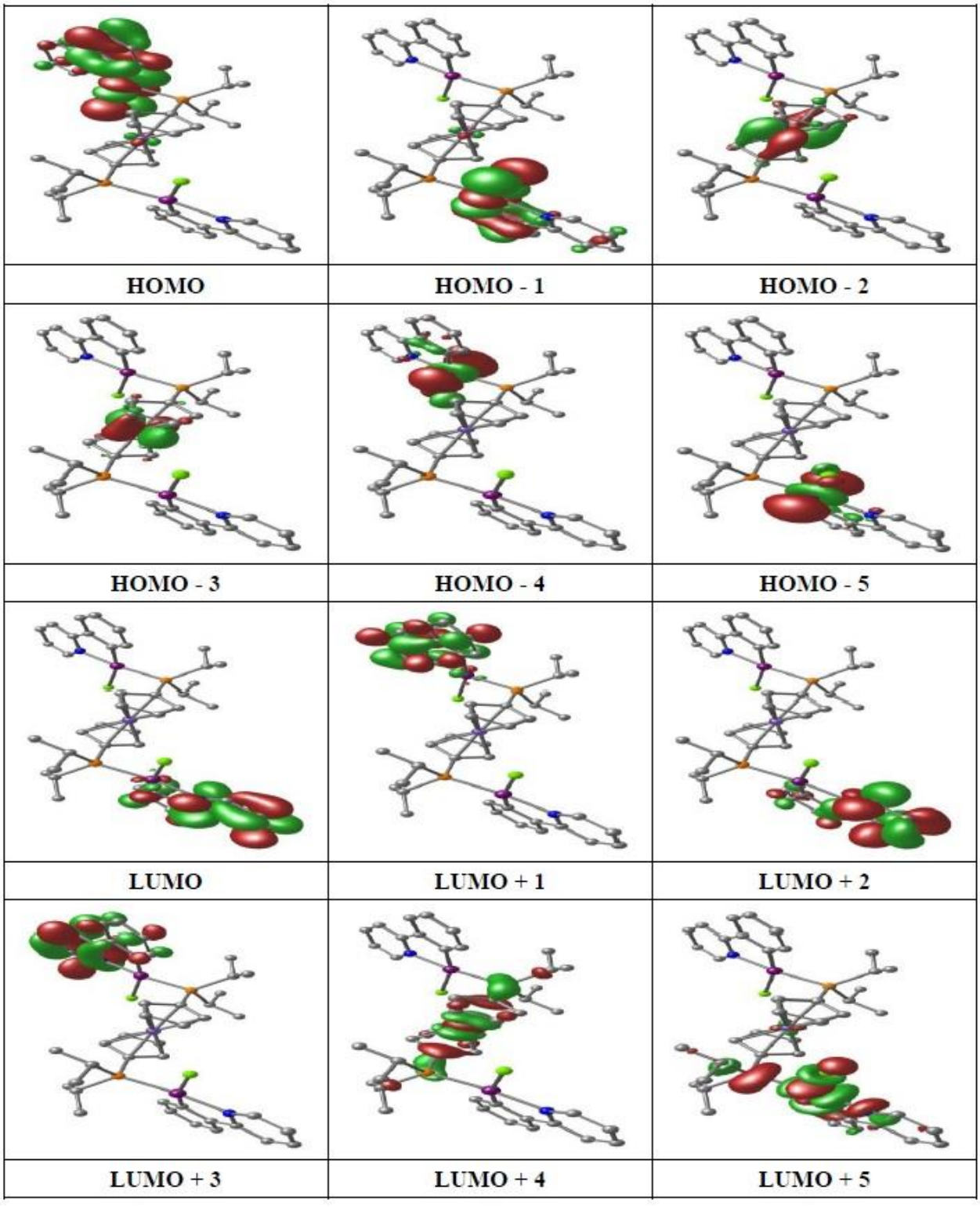

Figure S32. Molecular orbital plots for the optimized structure of **2c** in CH_2Cl_2 solution.

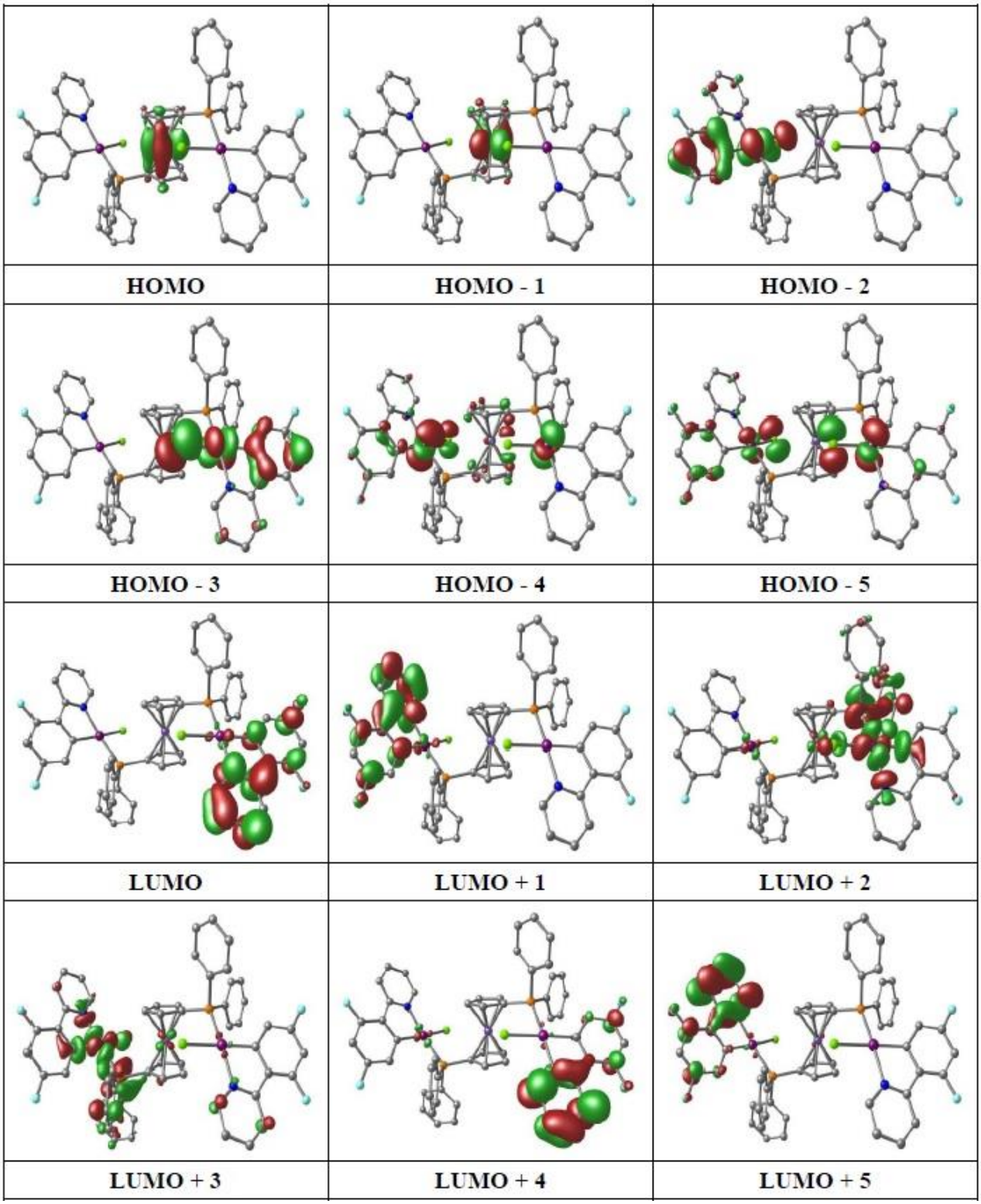

Figure S33. Molecular orbital plots for the optimized structure of **3a** in CH_2Cl_2 solution.

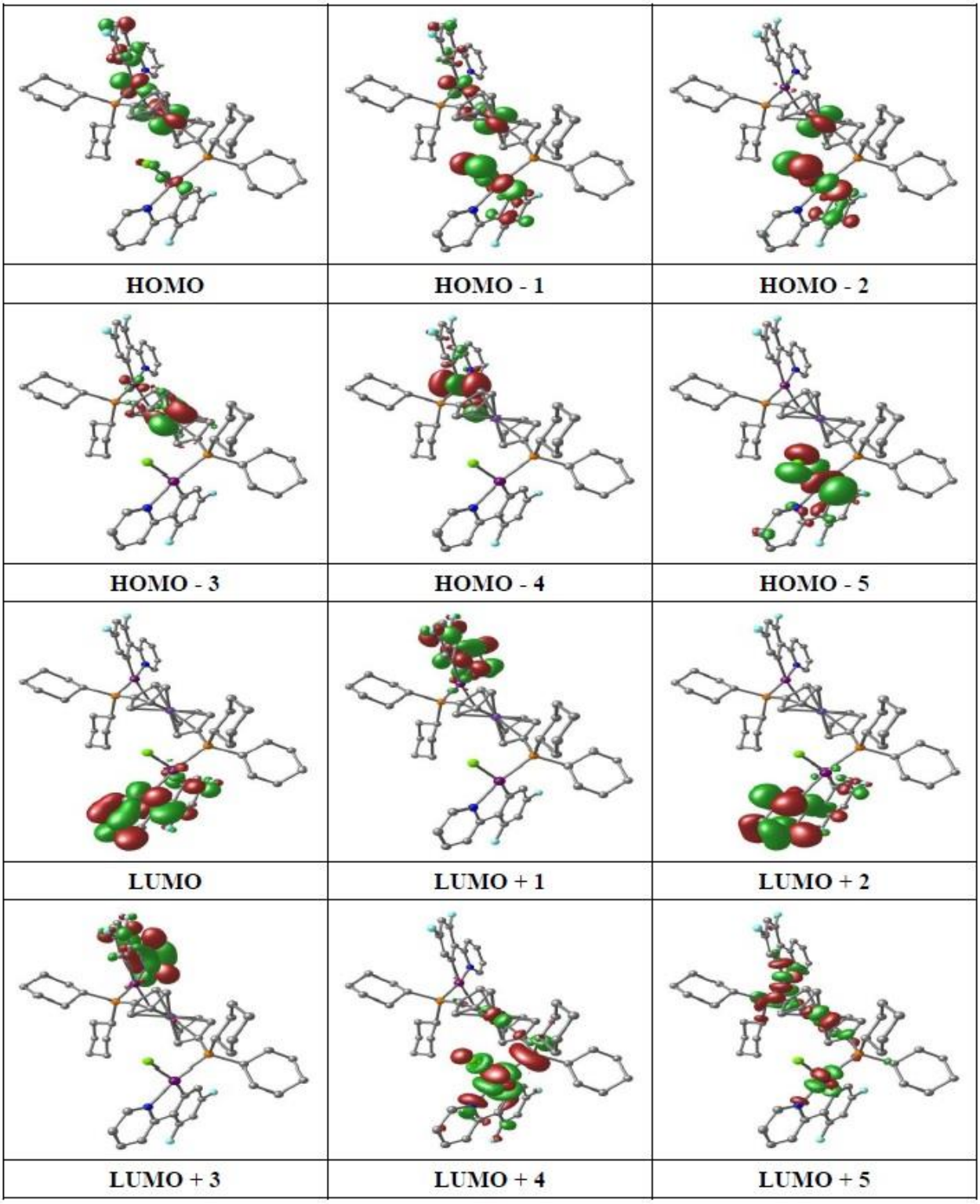

Figure S34. Molecular orbital plots for the optimized structure of **3b** in CH_2Cl_2 solution.

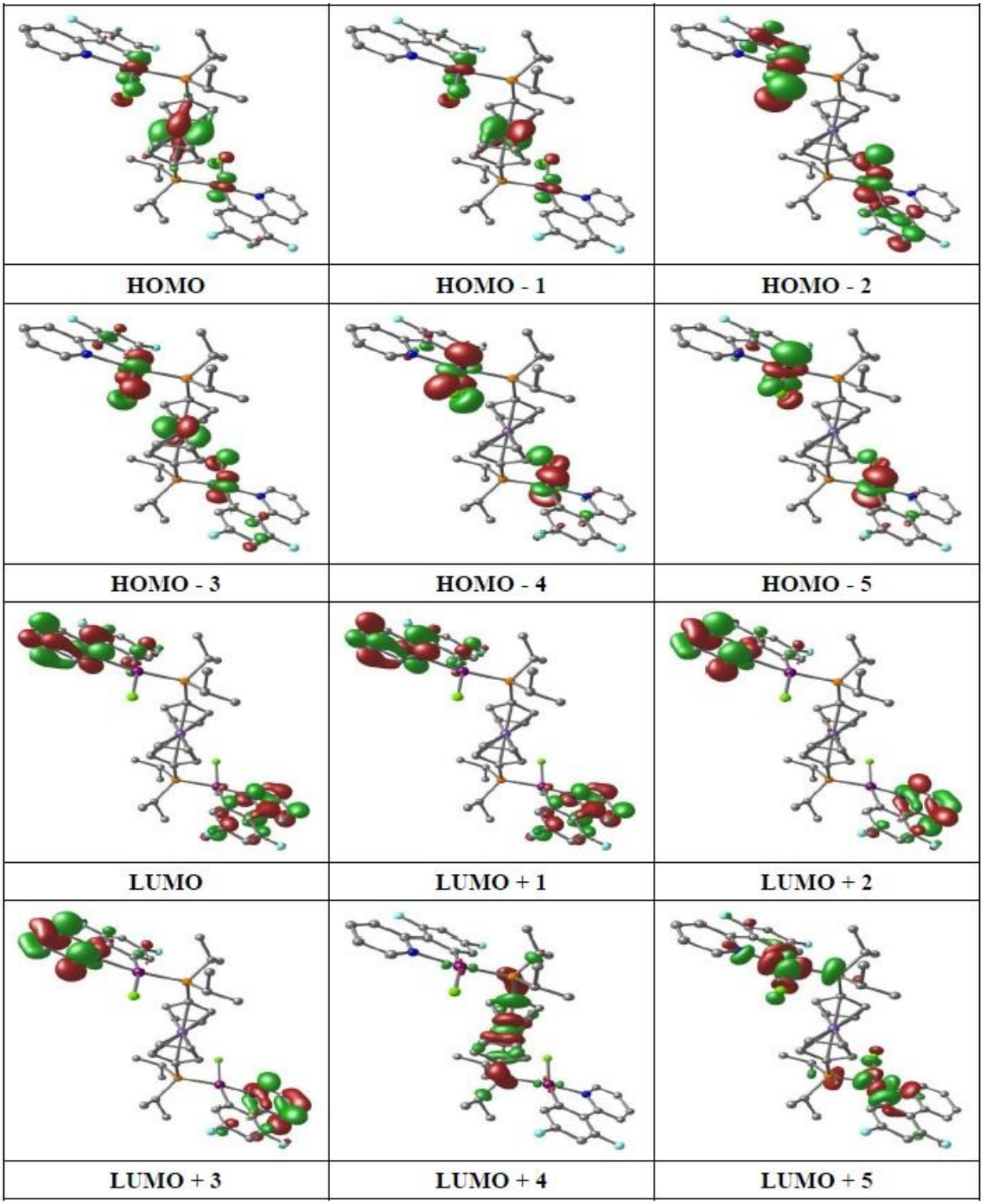

Figure S35. Molecular orbital plots for the optimized structure of **3c** in CH_2Cl_2 solution.

Table S9. The energies of the selected molecular orbitals of **2a** with their compositions in CH_2Cl_2 where M_1 = Pt_1, M_2 = Pt_2, L_1 = ppy_1, L_2 = ppy_2 L_3 = Cl_1, L_4 = Cl_2 and L_f =dppf.

MO	# of MO	Energy (ev)	Complex 2a (solution phase singlet)						
			Components (%)						
			Pt (1) (M_1)	Pt (2) (M_2)	ppy (1) (L_1)	ppy (2) (L_2)	Cl_1 (L_3)	Cl_2 (L_4)	dppf (L_f)
LUMO+5	261	-0.785	30	1	18	1	3	0	47
LUMO+4	260	-0.870	1	0	94	0	0	0	5
LUMO+3	259	-0.901	1	29	1	17	0	2	50
LUMO+2	258	-0.940	0	2	0	92	0	0	6
LUMO+1	257	-1.539	5	0	89	0	1	0	5
LUMO	256	-1.607	0	5	0	89	0	1	5
HOMO	255	-5.369	37	0	24	0	21	0	18
HOMO-1	254	-5.386	1	1	1	1	1	1	94
HOMO-2	253	-5.398	6	1	4	1	3	0	85
HOMO-3	252	-5.420	0	41	0	26	0	26	7
HOMO-4	251	-5.903	39	24	7	4	6	5	15
HOMO-5	250	-5.971	21	24	5	6	23	14	7

Table S10. The energies of the selected molecular orbitals of **2b** with their compositions in CH_2Cl_2 where M_1 = Pt_1, M_2 = Pt_2, L_1 = ppy_1, L_2 = ppy_2 L_3 = Cl_1, L_4 = Cl_2 and L_f =dcpf.

MO	# of MO	Energy (ev)	Complex 2b (solution phase singlet)						
			Components (%)						
			Pt (1) (M_1)	Pt (2) (M_2)	ppy (1) (L_1)	ppy (2) (L_2)	Cl_1 (L_3)	Cl_2 (L_4)	dcpf (L_f)
LUMO+5	273	-0.516	18	18	13	13	3	3	32
LUMO+4	272	-0.586	4	4	3	3	1	1	84
LUMO+3	271	-0.910	1	1	48	48	0	0	2
LUMO+2	270	-0.913	1	1	48	48	0	0	2
LUMO+1	269	-1.578	3	2	47	44	0	0	4
LUMO	268	-1.578	2	3	44	47	0	0	4
HOMO	267	-5.453	22	22	13	13	11	11	8
HOMO-1	266	-5.459	24	24	14	14	11	11	2
HOMO-2	265	-5.521	1	1	1	1	1	1	94
HOMO-3	264	-5.540	1	1	0	0	0	0	98
HOMO-4	263	-5.986	42	42	4	4	1	1	6
HOMO-5	262	-5.991	40	40	4	4	3	3	6

Table S11. The energies of the selected molecular orbitals of **2c** with their compositions in CH_2Cl_2 where M_1 = Pt_1, M_2 = Pt_2, L_1 = ppy_1, L_2 = ppy_2 L_3 = Cl_1, L_4 = Cl_2 and L_f =dippf.

MO	# of MO	Energy (ev)	Complex 2c (solution phase singlet)						
			Components (%)						
			Pt (1) (M_1)	Pt (2) (M_2)	ppy (1) (L_1)	ppy (2) ($L_{2)}$	Cl_1 (L_3)	Cl_2 (L_4)	dippf (L_f)
LUMO+5	229	-0.523	35	0	1	26	0	6	32
LUMO+4	228	-0.680	1	1	1	2	0	0	95
LUMO+3	227	-0.929	0	1	2	95	0	0	2
LUMO+2	226	-0.940	1	0	95	2	0	0	2
LUMO+1	225	-1.602	0	5	0	90	0	1	4
LUMO	224	-1.614	5	0	90	0	1	0	4
HOMO	223	-5.464	1	45	0	28	0	23	3
HOMO-1	222	-5.485	45	1	28	0	22	0	4
HOMO-2	221	-5.575	1	0	1	0	1	0	97
HOMO-3	220	-5.595	1	1	0	0	0	0	98
HOMO-4	219	-6.016	0	75	0	10	1	9	5
HOMO-5	218	-6.033	81	1	9	0	3	1	5

Table S12. The energies of the selected molecular orbitals of **3a** with their compositions in CH_2Cl_2 where M_1 = Pt_1, M_2 = Pt_2, L_1 = $dfppy_1$, L_2 = $dfppy_2$ L_3 = Cl_1, L_4 = Cl_2 and L_f =dppf.

MO	# of MO	Energy (ev)	Complex 3a (solution phase singlet)						
			Components (%)						
			Pt (1) (M_1)	Pt (2) (M_2)	dfppy (1) (L_1)	dfppy (2) ($L_{2)}$	Cl_1 (L_3)	Cl_2 (L_4)	dppf (L_f)
LUMO+5	277	-0.891	4	0	86	0	0	0	10
LUMO+4	276	-0.950	3	4	3	78	0	0	12
LUMO+3	275	-0.991	28	1	20	5	4	0	42
LUMO+2	274	-1.078	2	29	1	20	0	4	44
LUMO+1	273	-1.661	6	0	88	0	1	0	5
LUMO	272	-1.724	0	5	0	89	0	1	5
HOMO	271	-5.516	1	1	0	0	0	0	98
HOMO-1	270	-5.530	1	0	0	0	0	0	99
HOMO-2	269	-5.647	42	0	26	0	29	0	3
HOMO-3	268	-5.690	0	42	0	25	0	30	3
HOMO-4	267	-6.112	43	16	11	2	9	3	16
HOMO-5	266	-6.175	10	23	14	8	23	15	7

Table S13. The energies of the selected molecular orbitals of **3b** with their compositions in CH_2Cl_2 where M_1 = Pt_1, M_2 = Pt_2, L_1 = $dfppy_1$, L_2 = $dfppy_2$ L_3 = Cl_1, L_4 = Cl_2 and L_f =dcpf.

MO	# of MO	Energy (ev)	Complex 3b (solution phase singlet)						
			Components (%)						
			Pt (1) (M_1)	Pt (2) (M_2)	dfppy (1) (L_1)	dfppy (2) ($L_{2)}$	Cl_1 (L_3)	Cl_2 (L_4)	dcpf (L_f)
LUMO+5	289	-0.739	16	8	13	7	4	1	51
LUMO+4	288	-0.760	1	28	1	25	0	6	39
LUMO+3	287	-0.912	2	0	95	0	0	0	3
LUMO+2	286	-0.931	0	2	0	95	0	0	3
LUMO+1	285	-1.681	5	0	90	0	1	0	4
LUMO	284	-1.697	0	6	0	89	0	1	4
HOMO	283	-5.695	26	4	15	2	16	2	35
HOMO-1	282	-5.707	13	18	8	10	8	10	33
HOMO-2	281	-5.726	2	22	1	13	1	14	47
HOMO-3	280	-5.733	4	0	2	0	2	0	92
HOMO-4	279	-6.191	72	0	10	0	11	1	6
HOMO-5	278	-6.200	0	68	0	13	0	14	5

Table S14. The energies of the selected molecular orbitals of **3c** with their compositions in CH_2Cl_2 where M_1 = Pt_1, M_2 = Pt_2, L_1 = $dfppy_1$, L_2 = $dfppy_2$ L_3 = Cl_1, L_4 = Cl_2 and L_f =dippf.

MO	# of MO	Energy (ev)	Complex 3c (solution phase singlet)						
			Components (%)						
			Pt (1) (M_1)	Pt (2) (M_2)	dfppy (1) (L_1)	dfppy (2) ($L_{2)}$	Cl_1 (L_3)	Cl_2 (L_4)	dippf (L_f)
LUMO+5	245	-0.752	17	17	15	15	3	3	30
LUMO+4	244	-0.839	2	2	3	3	0	0	90
LUMO+3	243	-0.956	1	1	48	48	0	0	2
LUMO+2	242	-0.960	1	1	47	47	0	0	4
LUMO+1	241	-1.731	3	3	46	44	0	0	4
LUMO	240	-1.732	3	3	45	44	0	0	5
HOMO	239	-5.719	7	7	3	3	3	3	74
HOMO-1	238	-5.746	5	5	4	3	3	3	77
HOMO-2	237	-5.746	22	23	13	13	13	14	2
HOMO-3	236	-5.760	11	11	6	6	6	6	54
HOMO-4	235	-6.235	27	27	8	8	12	12	6
HOMO-5	234	-6.248	35	35	8	8	5	5	4

Table S15. Wavelengths and the nature of transitions for **2a** where M_1 = Pt_1, M_2 = Pt_2, L_1 = ppy_1, L_2 = ppy_2 L_3 = Cl_1, L_4 = Cl_2 and L_f =dppf.

Excited state	Oscillator strength	Calculated λ (nm)	Transitions (Major Contribution)	Assignment
$S_0 \rightarrow S_3$	0.0	491.9	H-10 → L+8 (15%) H-1 → L+9 (12%)	L_fL_fCT
$S_0 \rightarrow S_5$	0.0623	377.7	H-3 → LUMO (47%) H-1 → LUMO (23%) H-2 → LUMO (10%)	$L_fL_2CT/M_2L_2CT/L_2L_2CT/L_4L_2CT$
$S_0 \rightarrow S_{11}$	0.0069	348.4	HOMO → LUMO (41%) H-1 → LUMO (19%)	$M_1L_2CT/L_1L_2CT/L_3L_2CT/L_fL_2CT$
$S_0 \rightarrow S_{18}$	0.0166	326.8	H-4 → L+2 (32%) H-5 → L+2 (14%) H-5 → L+3 (11%)	$M_1L_2CT/M_2L_2CT/L_3L_2CT/L_4L_2CT$ $M_1L_fCT/L_3L_fCT/L_4L_fCT$
$S_0 \rightarrow S_{21}$	0.0619	308.0	H-3 → L+4 (29%) H-7 → LUMO (21%) H-1 → L+4 (14%)	$M_2L_1CT/L_2L_1CT/L_4L_1CT$ M_2L_2CT/L_4L_2CT L_fL_1CT
$S_0 \rightarrow S_{27}$	0.0901	300.6	H-7 → LUMO (32%) H-9 → LUMO (20%) H-3 → L+4 (11%)	$M_2L_2CT/L_4L_2CT/M_2L_1CT/L_2L_1CT/L_4L_1CT$

Table S16. Wavelengths and the nature of transitions for **2b** where M_1 = Pt_1, M_2 = Pt_2, L_1 = ppy_1, L_2 = ppy_2 L_3 = Cl_1, L_4 = Cl_2 and L_f =dcpf.

Excited state	Oscillator strength	Calculated λ (nm)	Transitions (Major Contribution)	Assignment
$S_0 \rightarrow S_3$	0.0	503.6	H-10 → L+4 (20%) H-3 → L+7 (15%) H-2 → L+7 (15%) H-12 → L+4 (12%)	$L_fL_fCT/M_1L_fCT/M_2L_fCT$ $L_1L_fCT/L_2L_fCT/L_3L_fCT/L_4L_fCT$
$S_0 \rightarrow S_5$	0.1107	376.1	H-1 → LUMO (48%) HOMO → L+1 (32%) H-2 → L+1 (11%)	$M_1L_1CT/M_1L_2CT/M_2L_1CT/M_2L_2CT/$ $L_3L_1CT/L_3L_2CT/L_4L_1CT/L_4L_2CT$ L_fL_1CT/L_fL_2CT
$S_0 \rightarrow S_{15}$	0.0047	333.7	H-1 → L+6 (24%) HOMO → L+5 (24%) H-1 → L+4 (15%)	$M_1L_fCT/M_2L_fCT/L_3L_fCT/L_4L_fCT$ L_1L_fCT/L_2L_fCT
$S_0 \rightarrow S_{17}$	0.0001	324.0	H-1 → L+1 (34%) HOMO → LUMO (16%) H-1 → LUMO (15%) H-2 → LUMO (10%)	$M_1L_1CT/M_1L_2CT/M_2L_1CT/M_2L_2CT/$ $L_3L_1CT/L_3L_2CT/L_4L_1CT/L_4L_2CT/$ L_fL_1CT/L_fL_2CT
$S_0 \rightarrow S_{26}$	0.2387	295.1	H-7 → LUMO (25%) H-6 → L+1 (25%)	$L_3L_1CT/L_3L_2CT/L_4L_1CT/L_4L_2CT/$ L_fL_1CT/L_fL_2CT
$S_0 \rightarrow S_{29}$	0.2631	286.6	H-11 → LUMO (27%) H-10 → L+1 (25%) H-12 → L+1 (11%)	$M_1L_1CT/M_1L_2CT/M_2L_1CT/M_2L_2CT/$ $L_3L_1CT/L_3L_2CT/L_4L_1CT/L_4L_2CT/L_fL_1CT/$ L_fL_2CT

Table S17. Wavelengths and the nature of transitions for **2c** where M_1 = Pt_1, M_2 = Pt_2, L_1 = ppy_1, L_2 = ppy_2 L_3 = Cl_1, L_4 = Cl_2 and L_f =dippf.

Excited state	Oscillator strength	Calculated λ (nm)	Transitions (Major Contribution)	Assignment
$S_0 \rightarrow S_3$	0.0	506.8	H-10 → L+4 (30%) H-3 → L+7 (28%) H-12 → L+4 (12%) H-2 → L+4 (10%)	$M_2L_fCT/L_2L_fCT/L_4L_fCT$ L_fL_fCT $M_1L_fCT/M_2L_fCT/L_1L_fCT/L_2L_fCT/L_3$ L_fCT/L_4L_fCT L_fL_fCT
$S_0 \rightarrow S_5$	0.0713	377.5	HOMO → L+1 (66%) H-1 → L+1 (23%)	M_2L_2CT/L_4L_2CT $M_1L_2CT/L_1L_2CT/L_3L_2CT$
$S_0 \rightarrow S_{15}$	0.0027	332.2	HOMO → L+6 (53%) H-1 → L+6 (19%)	$M_2L_fCT/L_4L_fCT/L_2L_2CT$ $M_1M_2CT/M_1L_2CT/M_1L_fCT/L_1M_2CT/$ $L_1L_2CT/L_1L_fCT/L_3M_2CT/L_3L_2CT/L_3$ L_fCT
$S_0 \rightarrow S_{21}$	0.0282	307.3	HOMO → L+3 (45%) H-6 → L+1 (15%) H-1 → L+3 (14%)	M_2L_2CT/L_4L_2CT M_2L_2CT/L_4L_2CT $M_1L_2CT/L_1L_2CT/L_3L_2CT$
$S_0 \rightarrow S_{26}$	0.2317	294.1	H-6 → L+1 (30%) H-8 → L+1 (20%) H-7 → LUMO (11%)	M_2L_2CT/L_4L_2CT $L_1L_2CT/L_2L_2CT/L_4L_2CT$ M_1L_1CT/L_3L_1CT
$S_0 \rightarrow S_{29}$	0.1304	286.0	H-11 → L+1 (23%) H-10 → L+1 (23%)	$M_1L_2CT/L_1L_2CT/L_3L_2CT/L_4L_2CT/L_f$ L_2CT $M_2L_2CT/L_4L_2CT/L_fL_2CT$

Table S18. Wavelengths and the nature of transitions for **3a** where M_1 = Pt_1, M_2 = Pt_2, L_1 = $dfppy_1$, L_2 = $dfppy_2$ L_3 = Cl_1, L_4 = Cl_2 and L_f =dppf.

Excited state	Oscillator strength	Calculated λ (nm)	Transitions (Major Contribution)	Assignment
$S_0 \rightarrow S_3$	0.0	491.5	H-1 → L+9 (15%) H-1 → L+13 (10%) H-8 → L+8 (10%)	$L_fL_fCT/M_1L_fCT/M_2L_fCT/L_3L_fCT/L_4L_fCT$
$S_0 \rightarrow S_6$	0.0964	364.3	H-2 → L+1 (51%) H-3 → LUMO (30%)	M_1L_1CT/L_3L_1CT M_2L_2CT/L_4L_2CT
$S_0 \rightarrow S_{10}$	0.0135	350.4	HOMO → L+1 (56%) H-1 → LUMO (19%)	L_fL_1CT L_fL_2CT
$S_0 \rightarrow S_{17}$	0.0133	327.7	H-4 → L+2 (26%) H-5 → L+3 (16%) H-4 → LUMO (12%)	$M_1M_2CT/M_1L_2CT/M_1L_fCT$ $M_2M_1CT/M_2L_1CT/M_2L_fCT$ $M_1L_2CT/M_2L_2CT/L_1L_2CT/L_fL_2CT$
$S_0 \rightarrow S_{25}$	0.2384	307.6	H-6 → L+1 (48%) H-7 → LUMO (13%) H-6 → LUMO (12%)	M_1L_1CT/L_4L_1CT $M_1L_2CT/L_1L_2CT/L_3L_2CT/L_4L_2CT$ $M_1L_2CT/L_1L_2CT/L_4L_2CT$

Table S19. Wavelengths and the nature of transitions for **3b** where M_1 = Pt_1, M_2 = Pt_2, L_1 = $dfppy_1$, L_2 = $dfppy_2$ L_3 = Cl_1, L_4 = Cl_2 and L_f =dcpf.

Excited state	Oscillator strength	Calculated λ (nm)	Transitions (Major Contribution)	Assignment
$S_0 \rightarrow S_3$	0.000	496.3	H-1 → L+7 (29%) H-10 → L+6 (25%) HOMO → L+6 (12%)	$M_1L_fCT/M_2L_fCT/L_2L_fCT/L_4L_fCT$ $M_2M_1CT/M_2L_1CT/M_2L_fCT/L_2M_1CT/L_2L_1$ $CT/L_2L_fCT/L_4M_1CT/L_4L_1CT/L_4L_fCT$ L_1L_fCT
$S_0 \rightarrow S_6$	0.061	363.7	H-2 → L+1 (82%)	$M_2L_1CT/L_2L_1CT/L_4L_1CT/L_fL_1CT$
$S_0 \rightarrow S_9$	0.015	340.9	H-4 → L+1 (59%)	M_1L_1CT/L_3L_1CT
$S_0 \rightarrow S_{22}$	0.1624	304.3	H-6 → LUMO (58%	M_2L_2CT/L_4L_2CT
$S_0 \rightarrow S_{35}$	0.1508	281.9	H-8 → L+4 (24%)	L_2L_fCT

Table S20. Wavelengths and the nature of transitions for **3c** where M_1 = Pt_1, M_2 = Pt_2, L_1 = $dfppy_1$, L_2 = $dfppy_2$ L_3 = Cl_1, L_4 = Cl_2 and L_f =dippf.

Excited state	Oscillator strength	Calculated λ (nm)	Transitions (Major Contribution)	Assignment
$S_0 \rightarrow S_3$	0.0	506.3	H-10 → L+4 (30%) H-1 → L+7 (30%) HOMO → L+4 (13%)	L_fL_fCT L_fL_fCT L_fL_fCT
$S_0 \rightarrow S_6$	0.1075	364.2	H-2 → L+1 (48%) H-3 → LUMO (45%)	$M_1L_1CT/M_1L_2CT/M_2L_1CT/M_2L_2CT/$ $L_3L_1CT/L_3L_2CT/L_4L_1CT/L_4L_2CT$ L_fL_1CT/L_fL_2CT
$S_0 \rightarrow S_{11}$	0.014	340.5	H-1 → LUMO (60%) H-4 → L+1 (17%) H-5 → LUMO (16%)	L_fL_1CT/L_fL_2CT $M_1L_1CT/M_1L_2CT/M_2L_1CT/M_2L_2CT/$ $L_3L_1CT/L_3L_2CT/L_4L_1CT/L_4L_2CT$
$S_0 \rightarrow S_{26}$	0.0524	289.4	H-2 → L+2 (28%) H-3 → L+3 (27%)	$M_1L_1CT/M_1L_2CT/M_2L_1CT/M_2L_2CT/$ $L_3L_1CT/L_3L_2CT/L_4L_1CT/L_4L_2CT/L_fL_1C$ T/L_fL_2CT
$S_0 \rightarrow S_{33}$	0.2095	283.8	H-11 → L+1 (15%) H-10 → LUMO (14%)	$M_1L_1CT/M_1L_2CT/M_2L_1CT/M_2L_2CT/$ $L_3L_1CT/L_3L_2CT/L_4L_1CT/L_4L_2CT/L_fL_1C$ T/L_fL_2CT

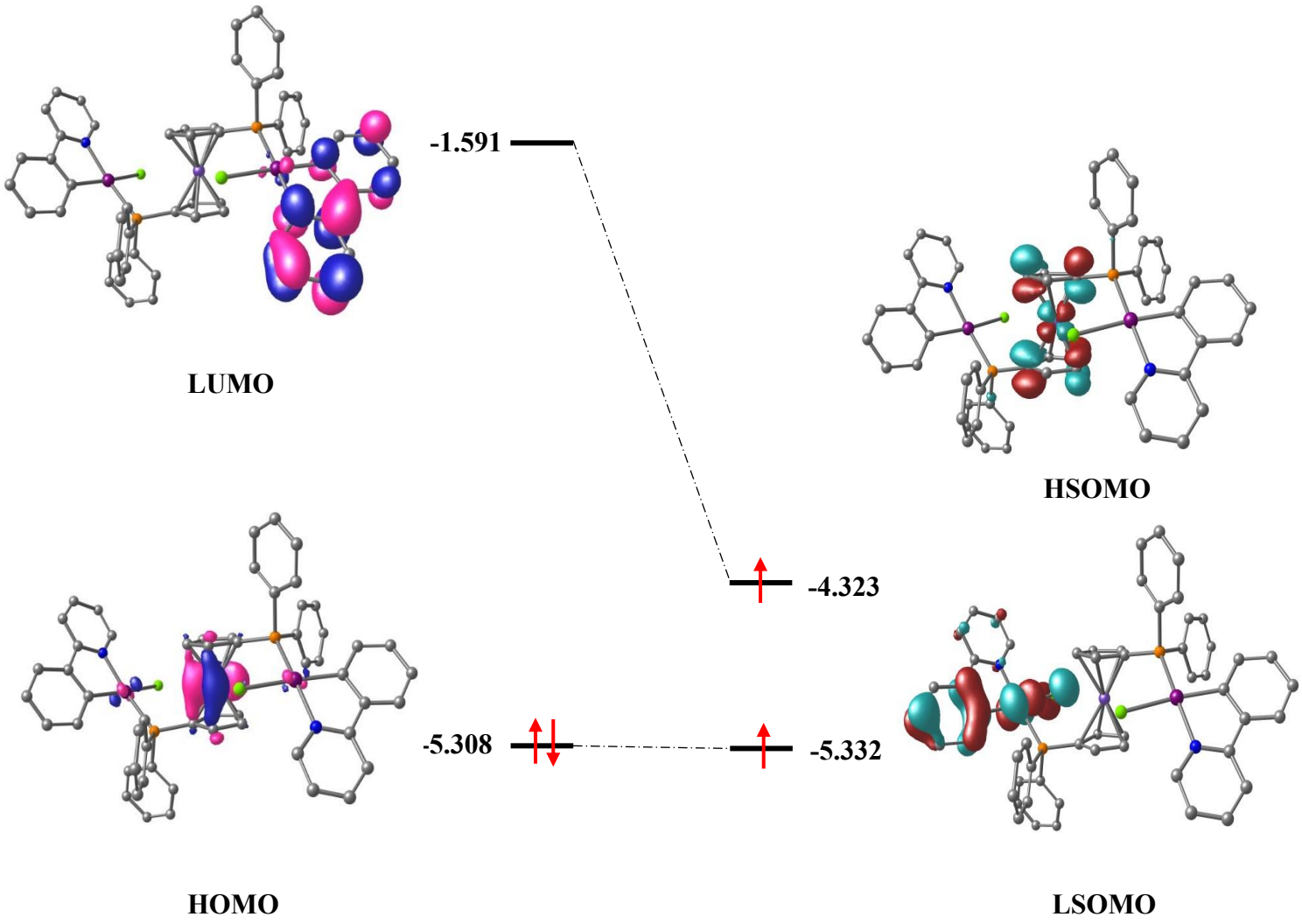

Figure S36. Comparative MO diagram for computed S_0 (Left) and T_1 (Right) states of the **2a** in gas phase.

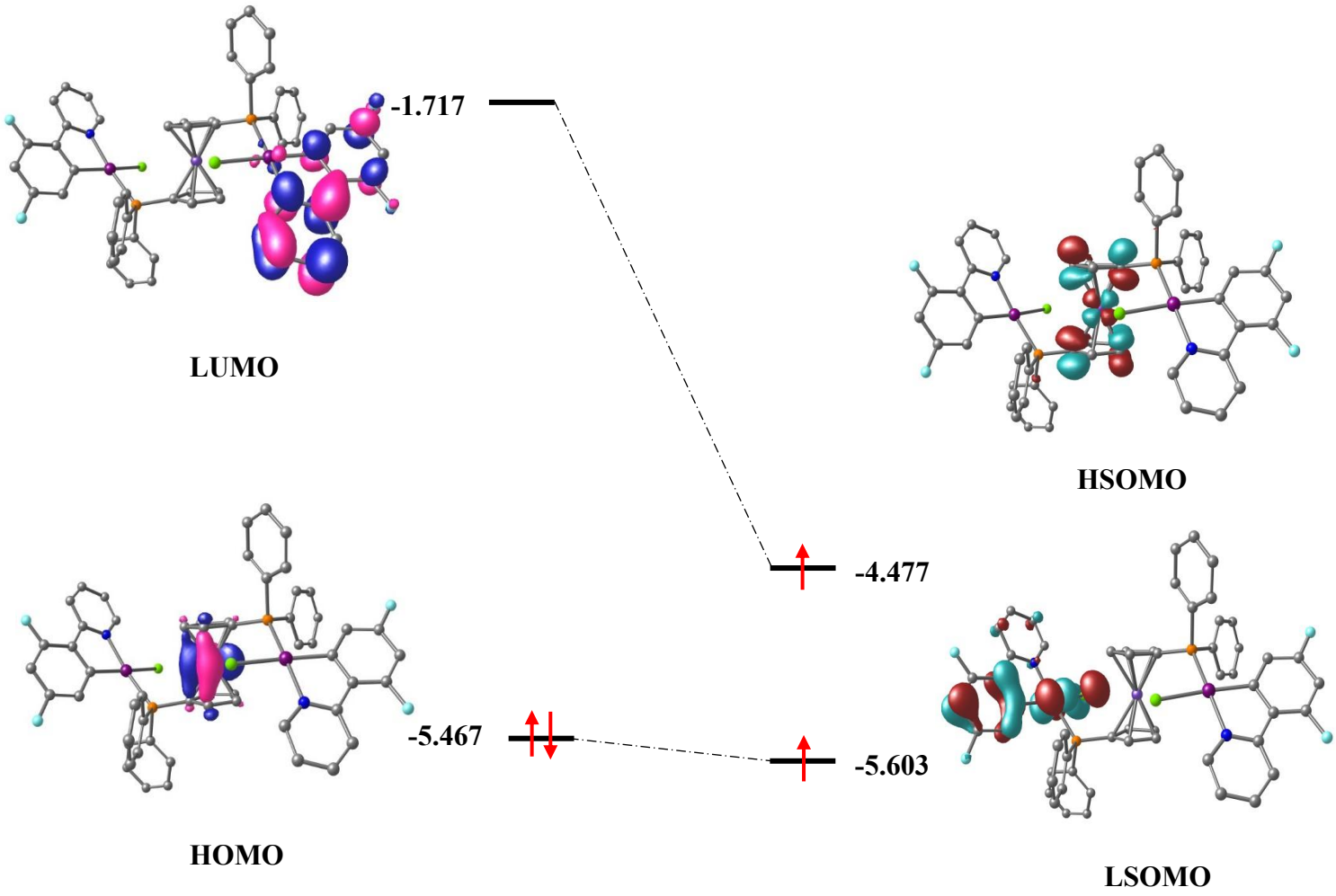

Figure S37. Comparative MO diagram for computed S_0 (Left) and T_1 (Right) states of the **3a** in gas phase.

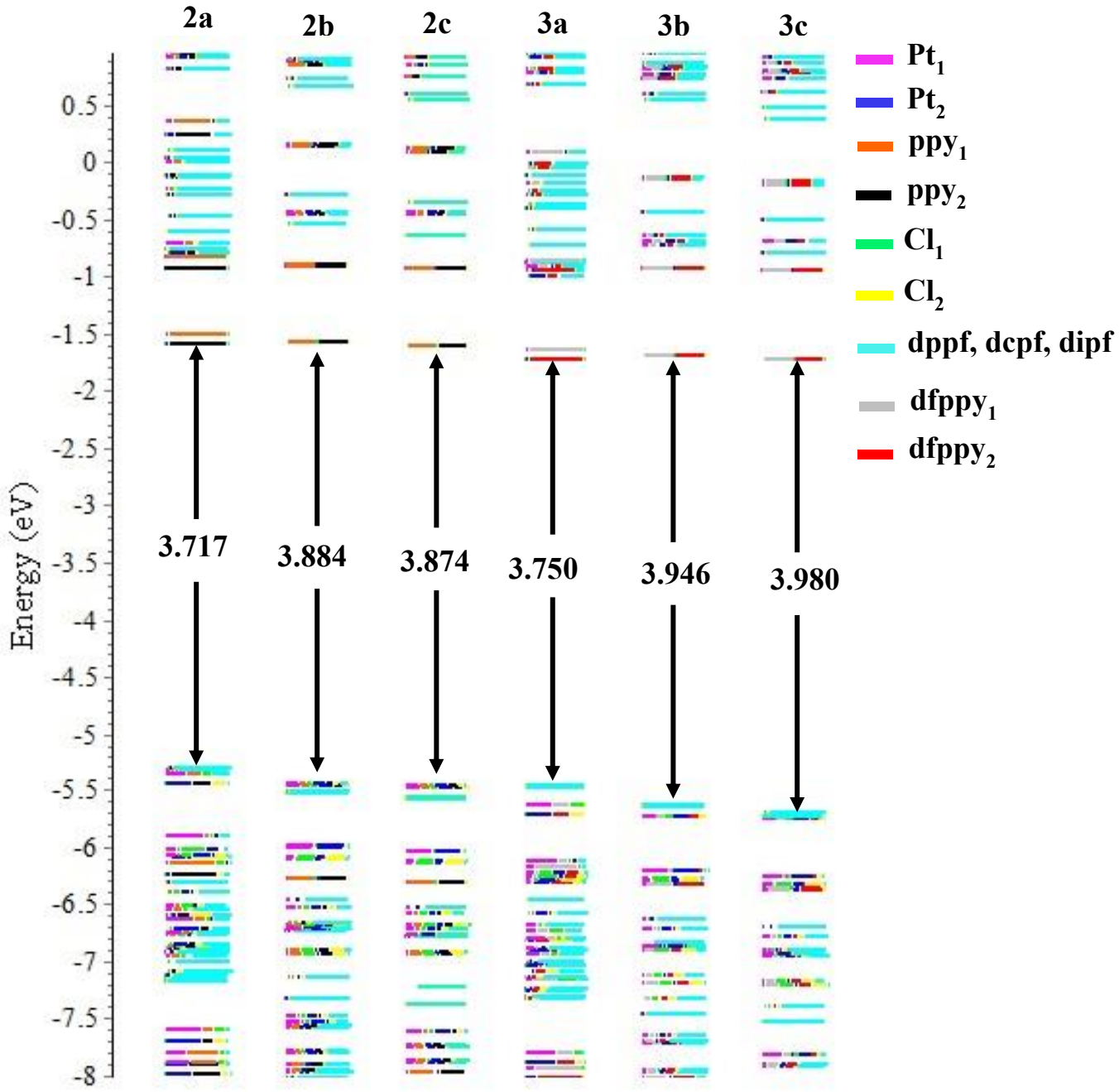

Figure S38. Comparative energy diagram of the complexes **2a–3c** in gas phase.

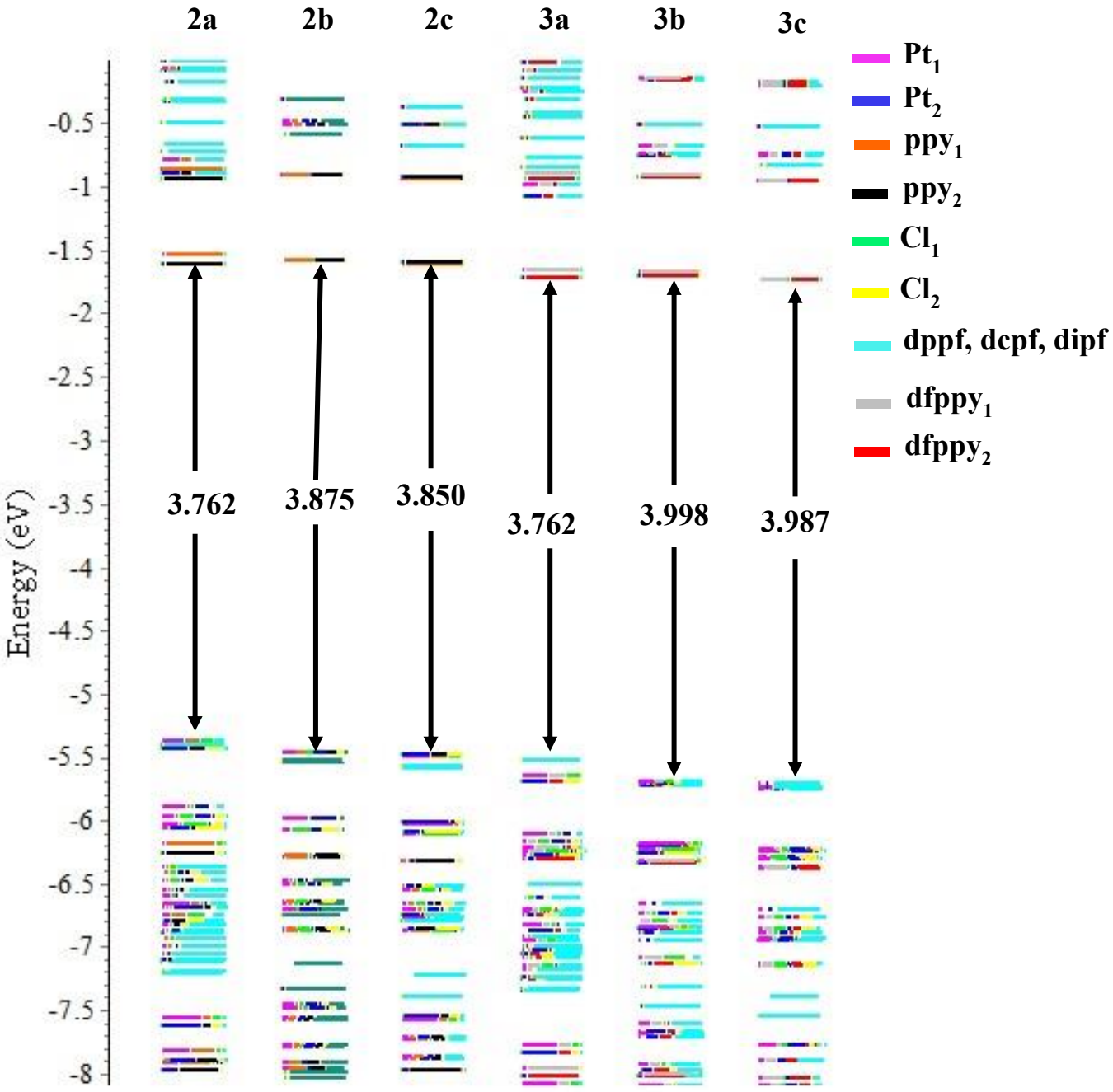

Figure S39. Comparative energy diagram of the complexes **2a–3c** in solution phase.

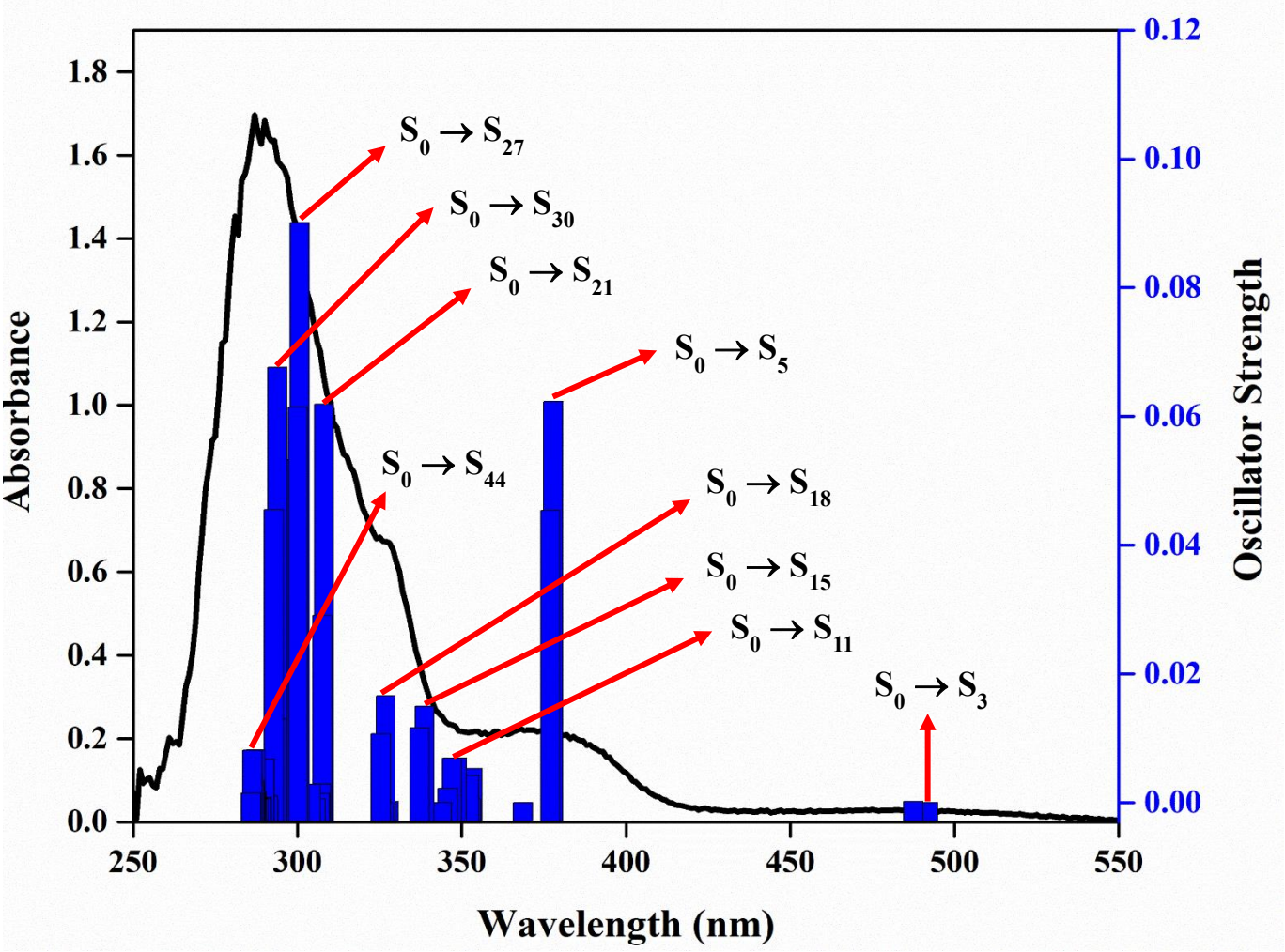

Figure S40. Overlaid experimental (spectra) and theoretical (bars) absorbance for **2a**.

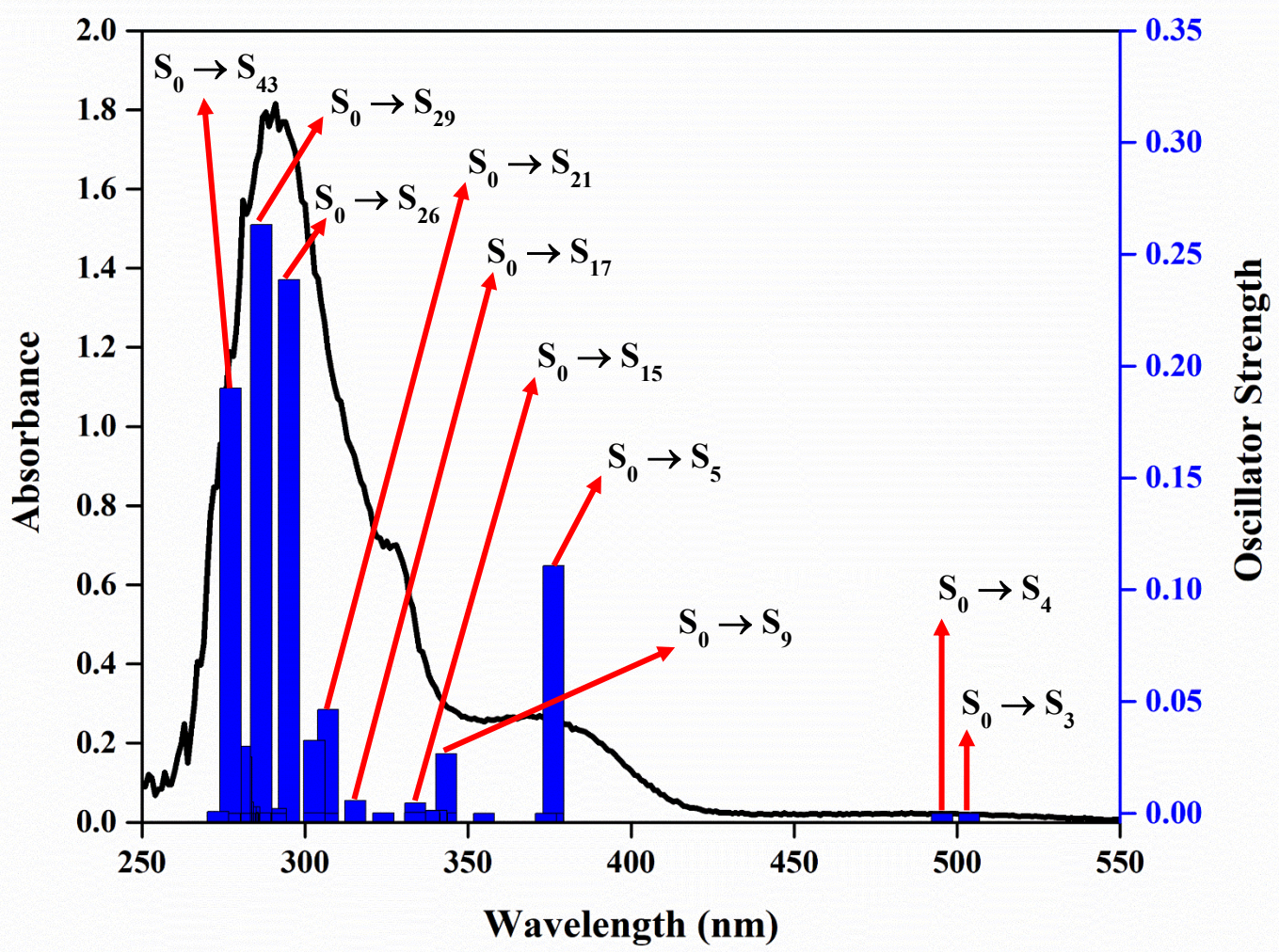

Figure S41. Overlaid experimental (spectra) and theoretical (bars) absorbance for **2b**.

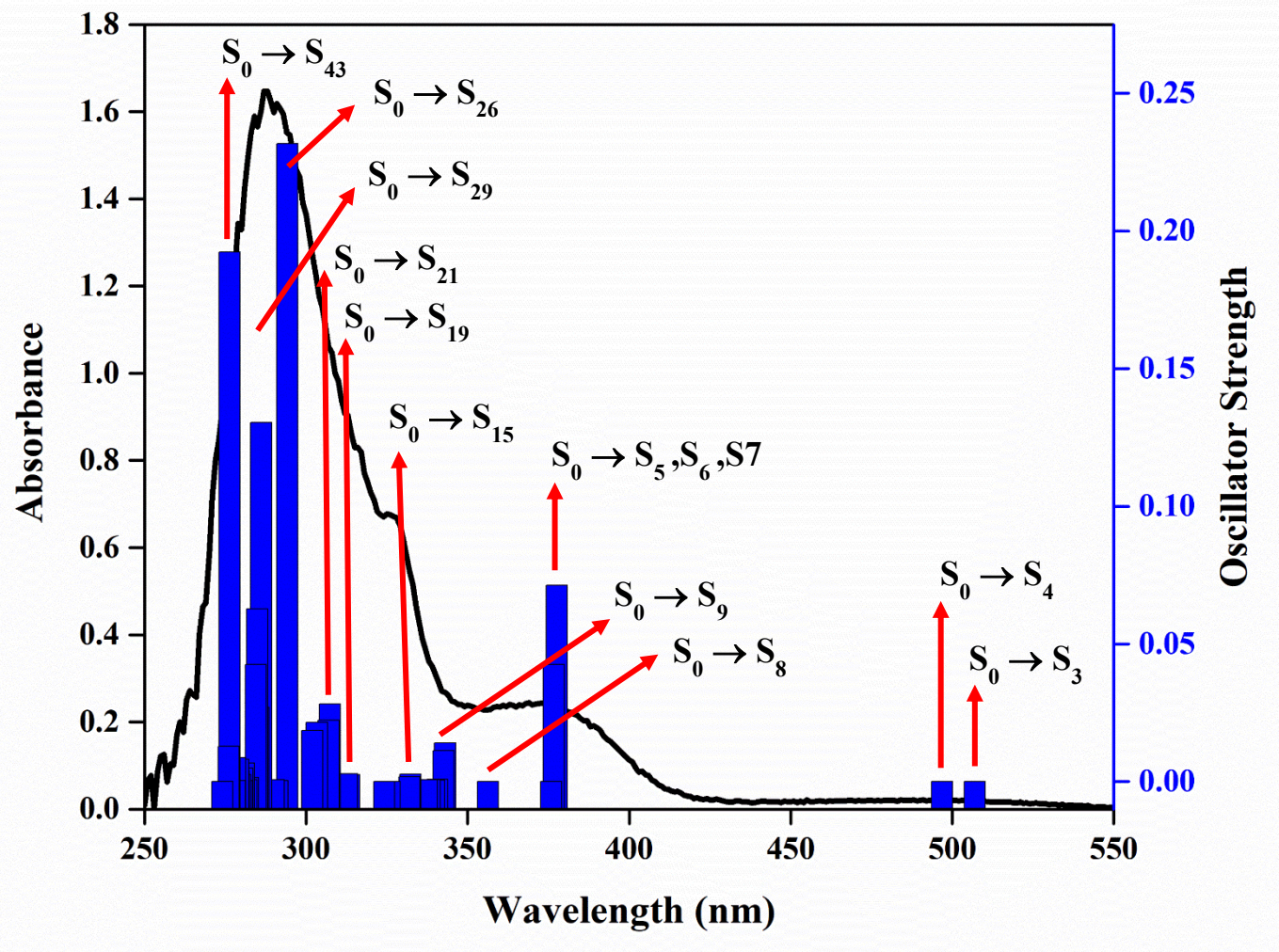

Figure S42. Overlaid experimental (spectra) and theoretical (bars) absorbance for **2c**.

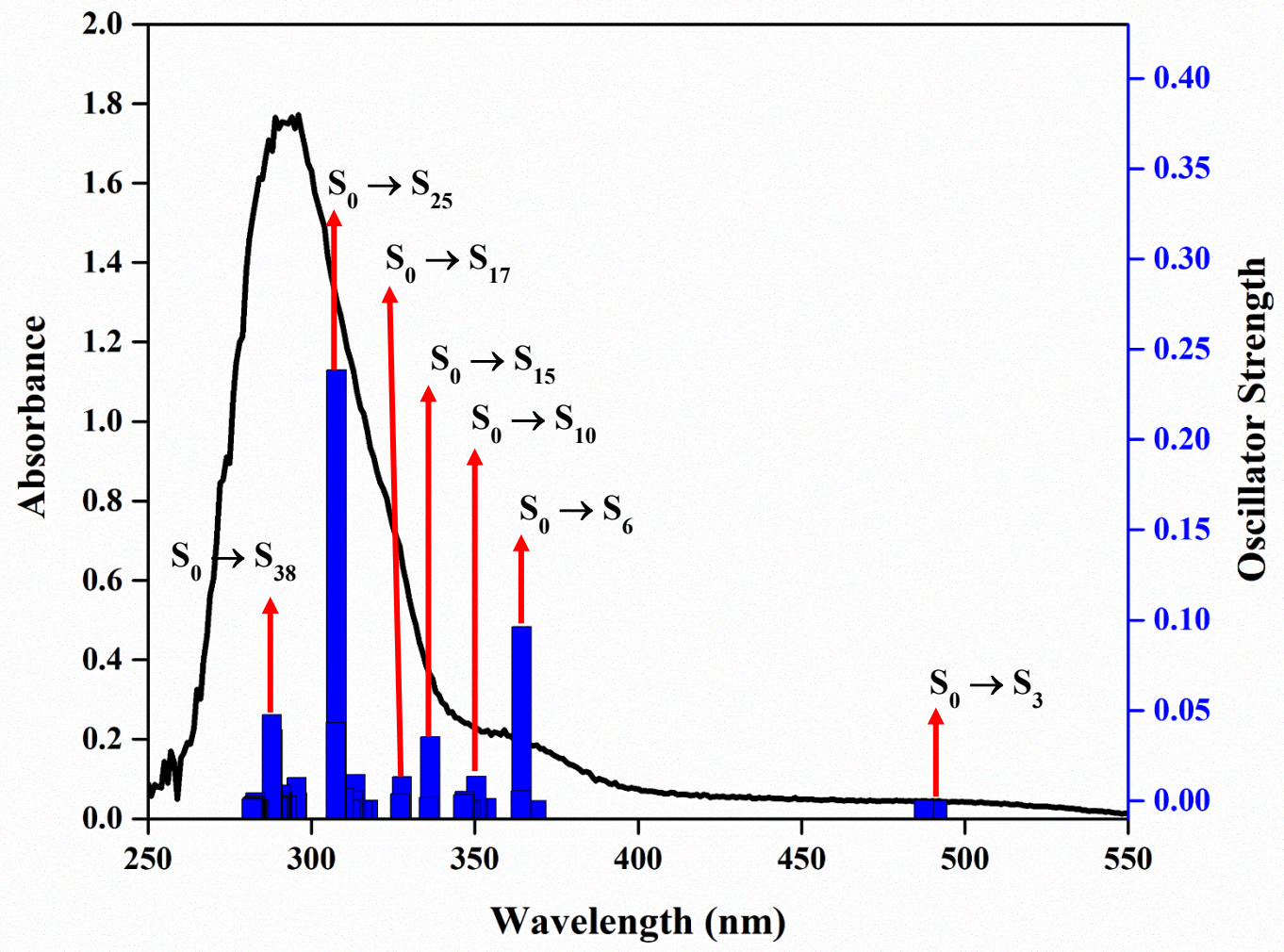

Figure S43. Overlaid experimental (spectra) and theoretical (bars) absorbance for **3a**.

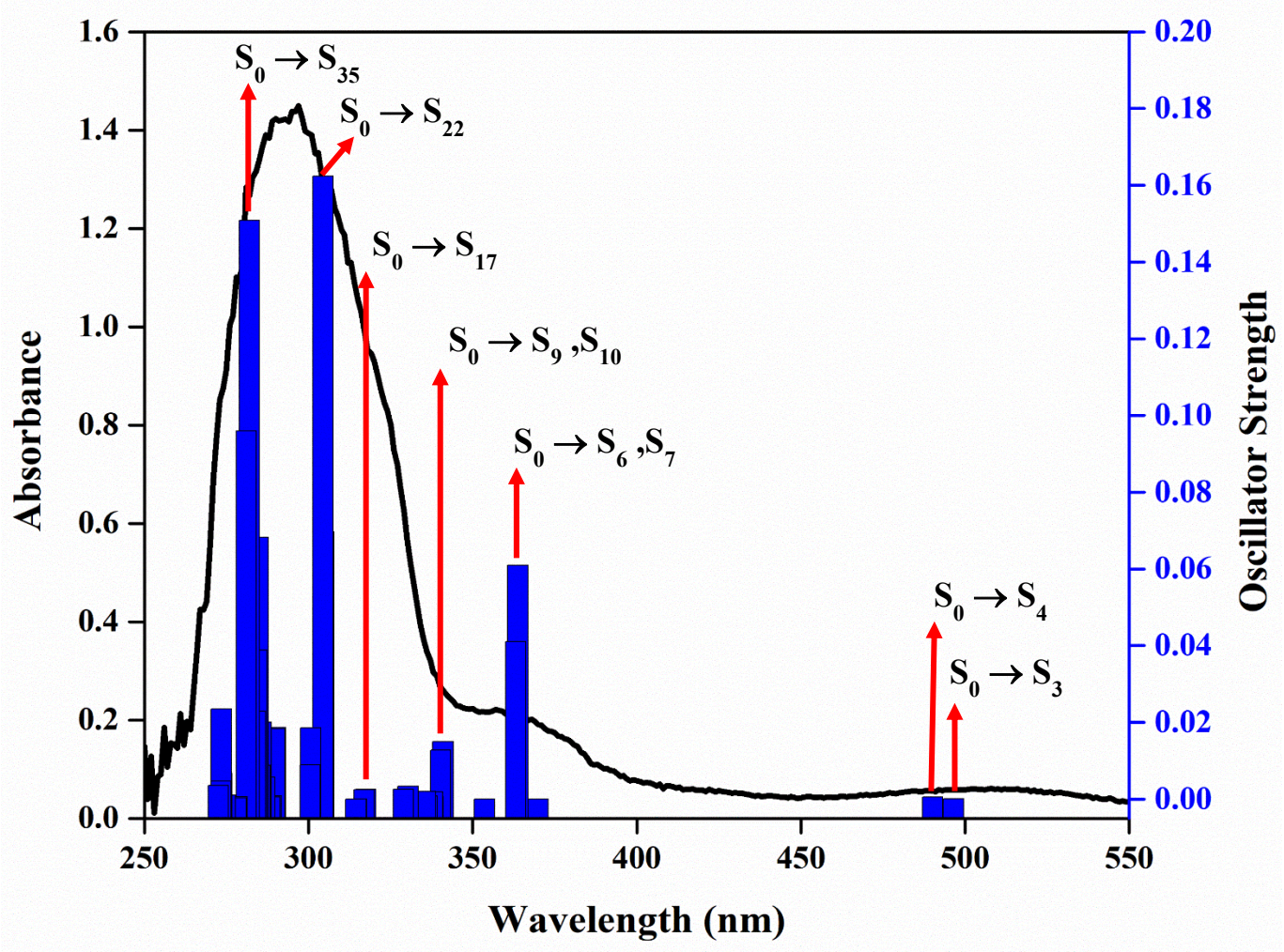

Figure S44. Overlaid experimental (spectra) and theoretical (bars) absorbance for **3b**.

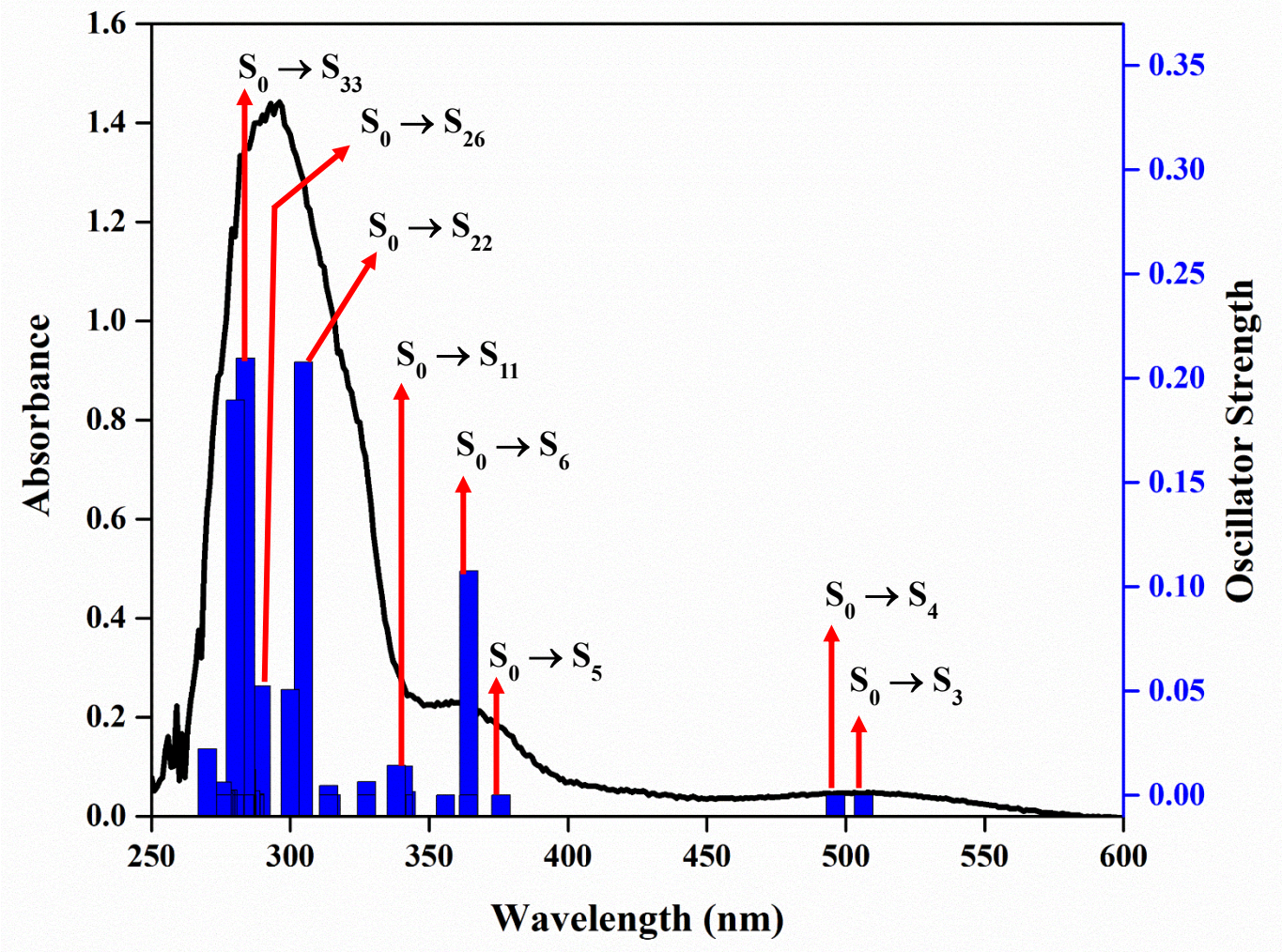

Figure S45. Overlaid experimental (spectra) and theoretical (bars) absorbance for **3c**.

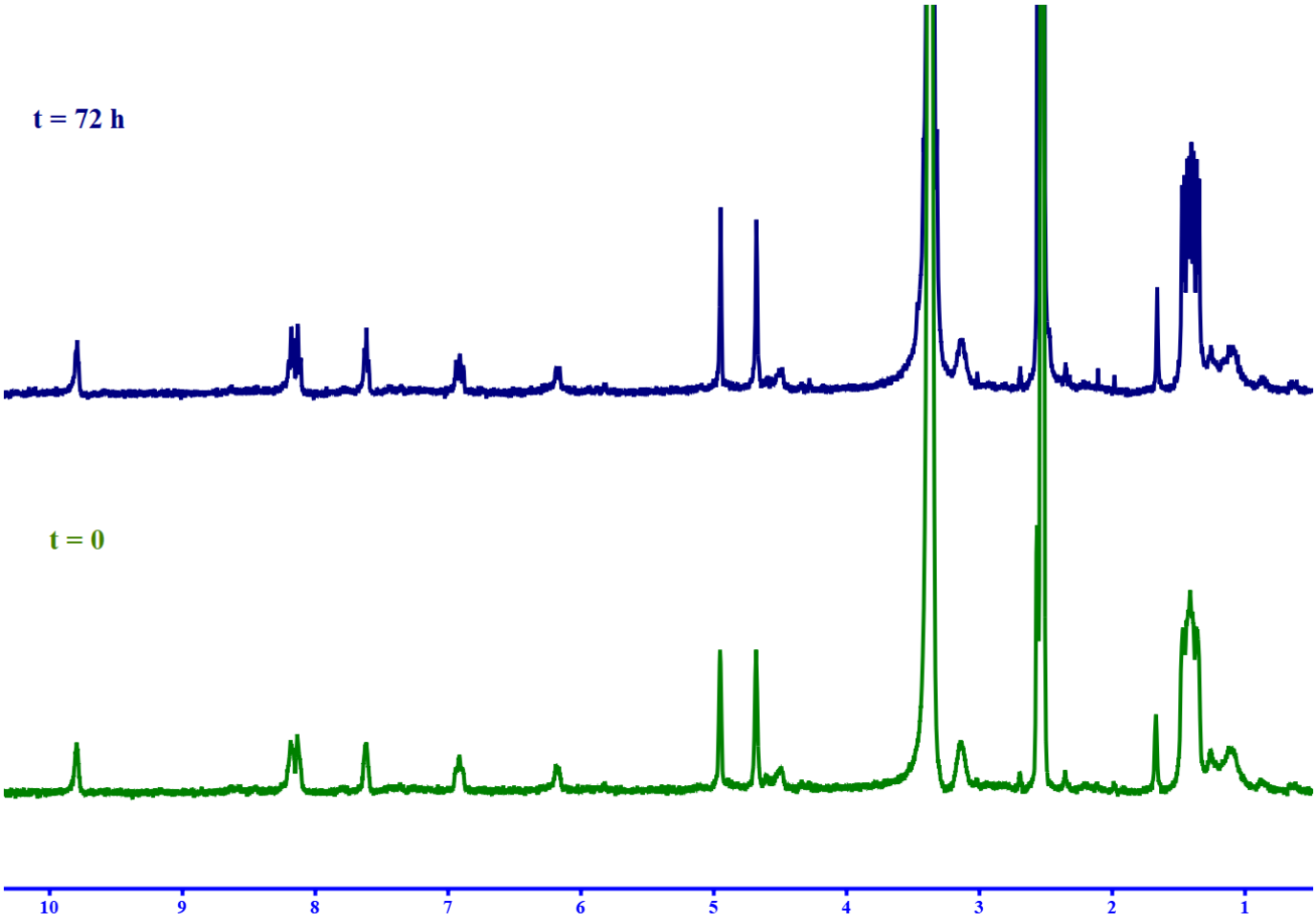

Figure S46. Time course ^{1}H NMR spectrum of **3c** in dmso-d_6 at room temperature.

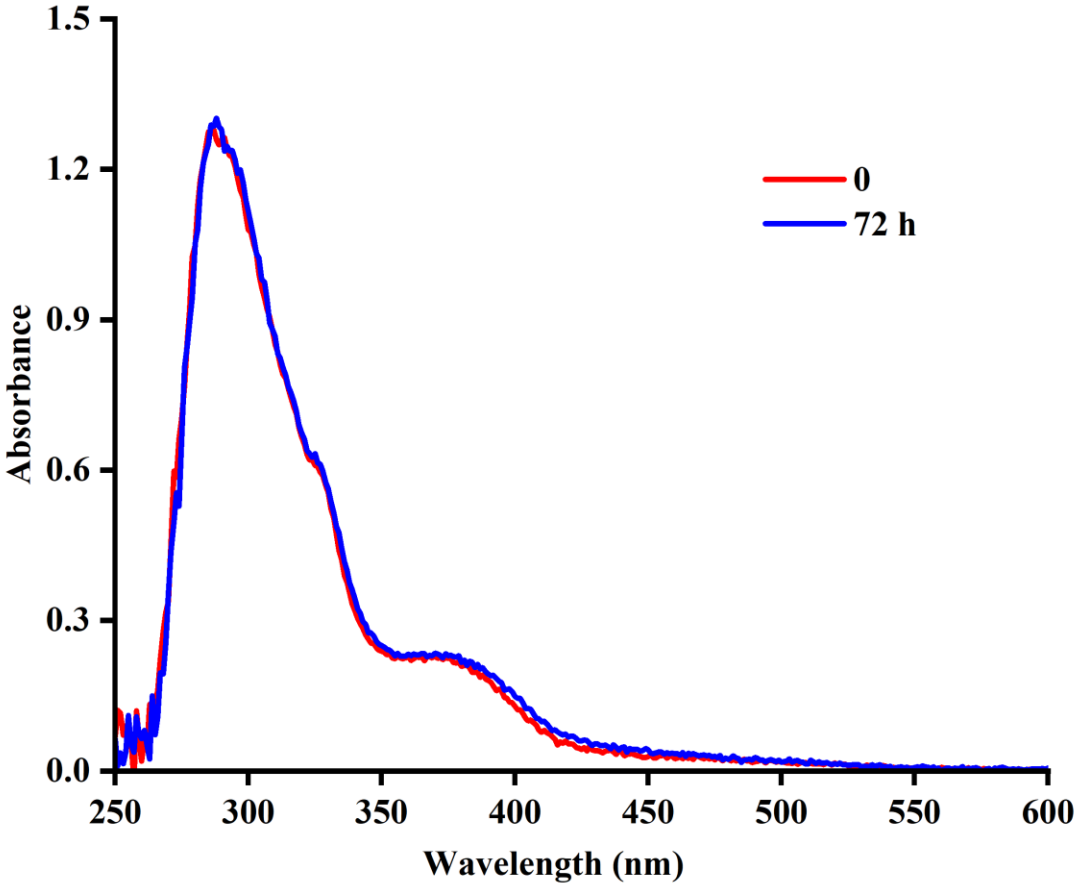

Figure S47. Time course UV-vis spectra of **3c** (5×10^{-5} M) dissolved in dmso. The spectra were recorded over 72 hours at room temperature.

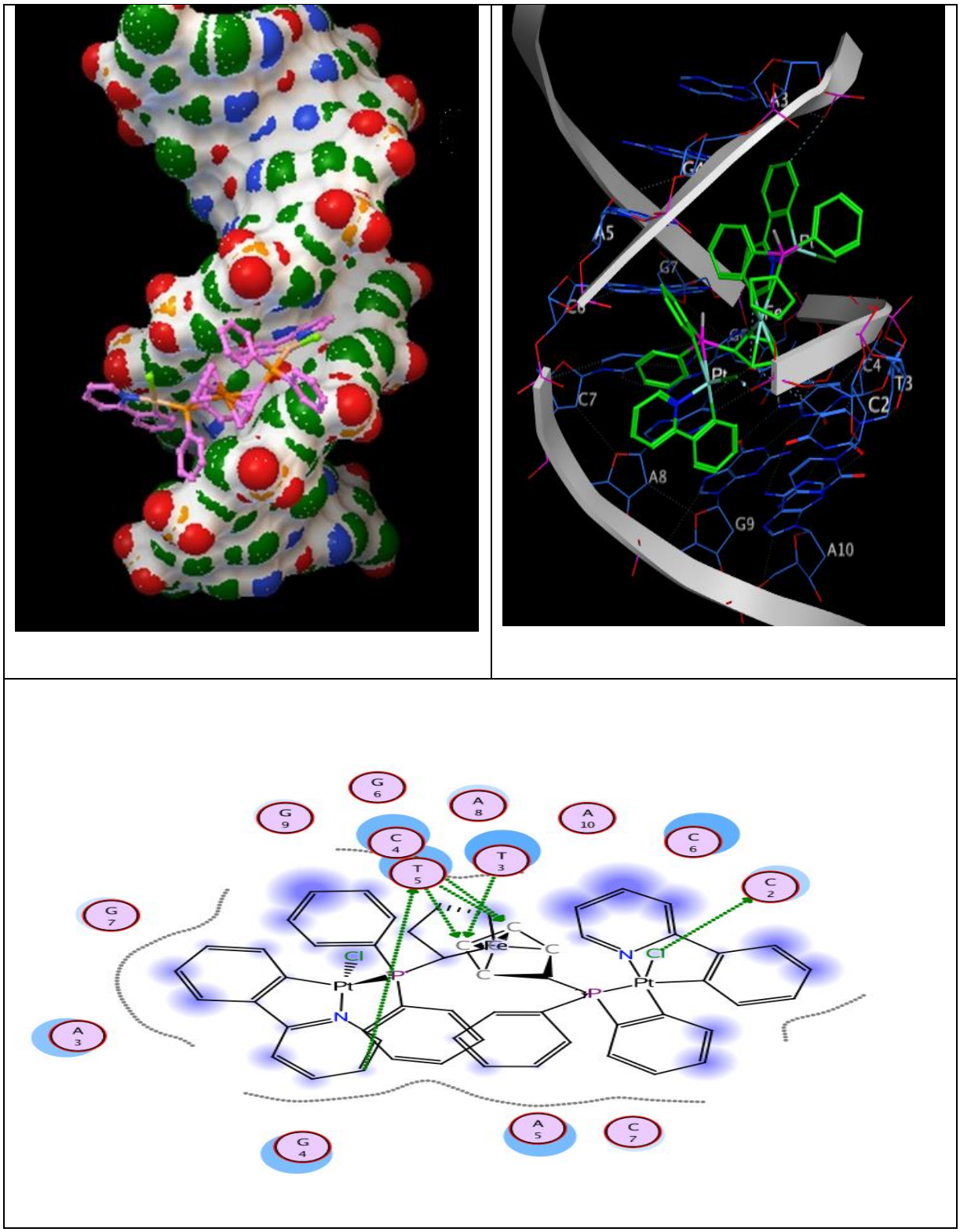

Figure S48. The best docked conformation of **2a**, in the best binding sites with 1LU5 structure.

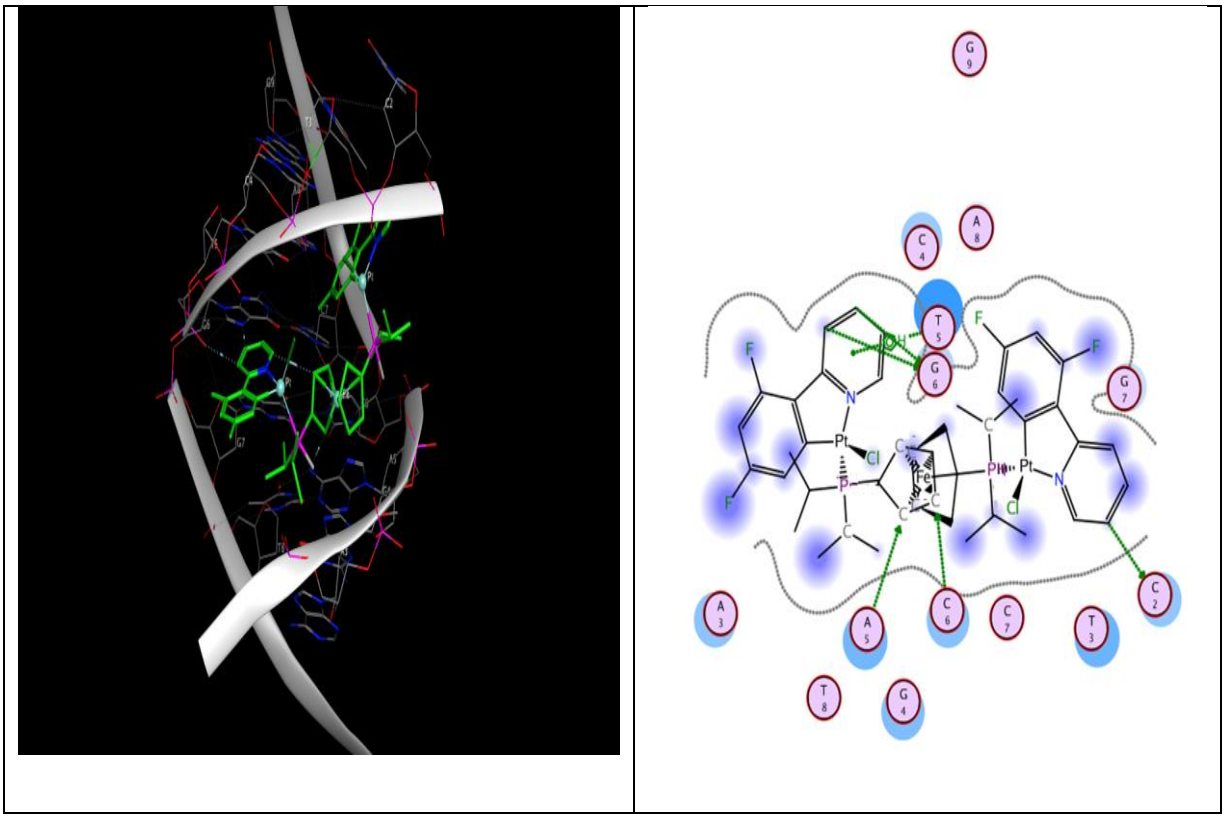

Figure S49. The best docked conformation of **3c**, in the best binding sites with 1LU5 structure.

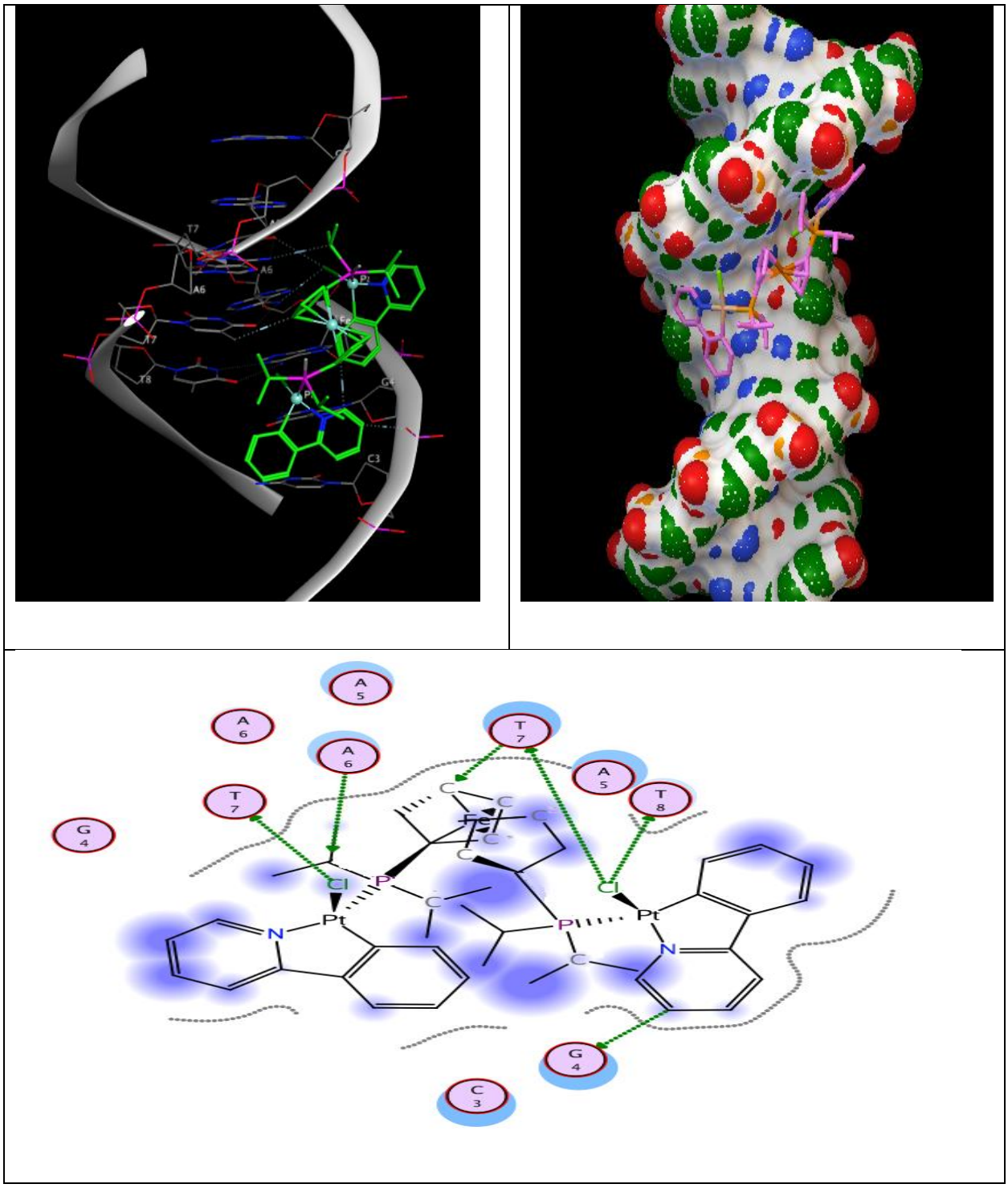

Figure S50. The best docked conformation of **2c**, in the best binding sites with 1BNA structure.

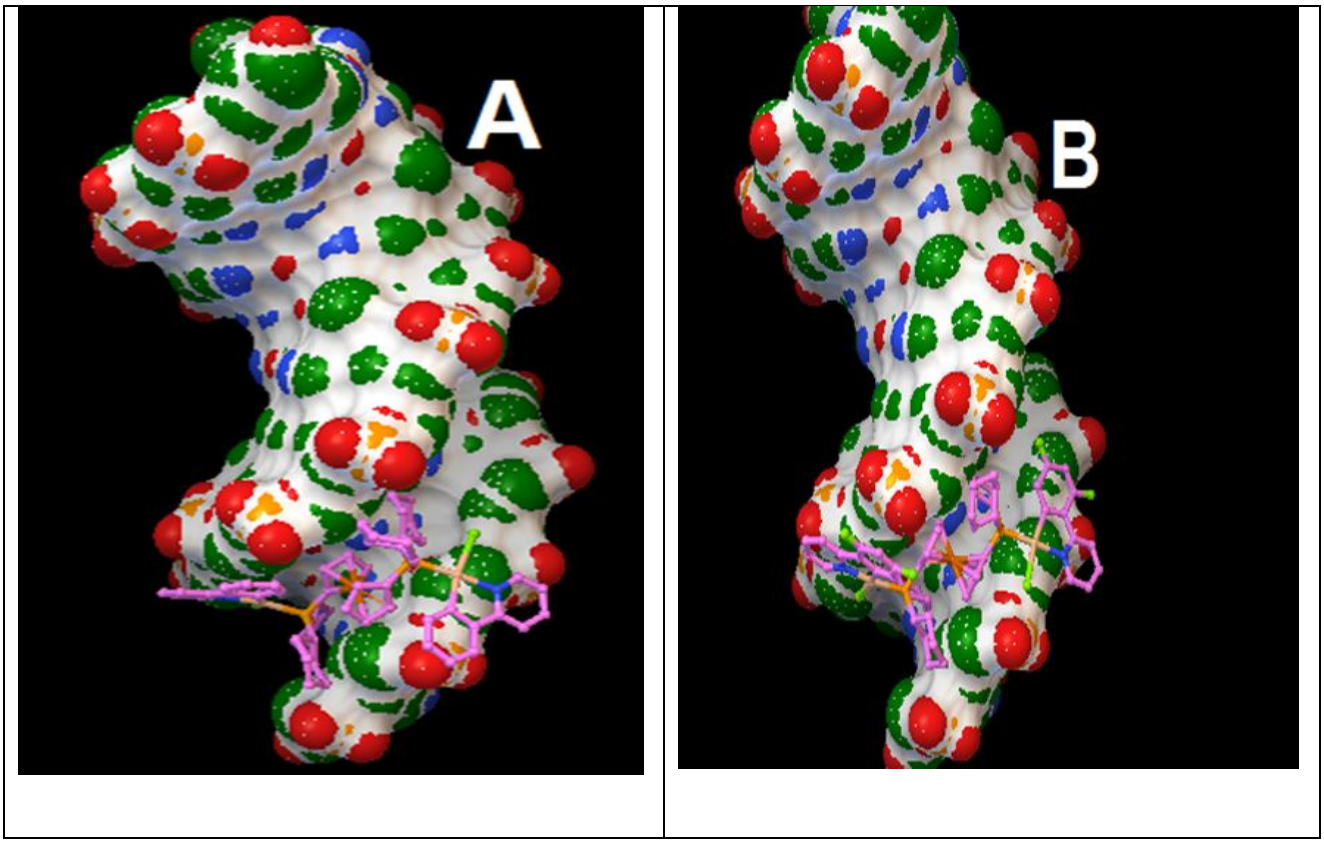

Figure S51. Molecular docking simulation studies of the interaction between **2b** with 3CO3 (A) and **3b** in the best binding sites of 3CO3 (B).

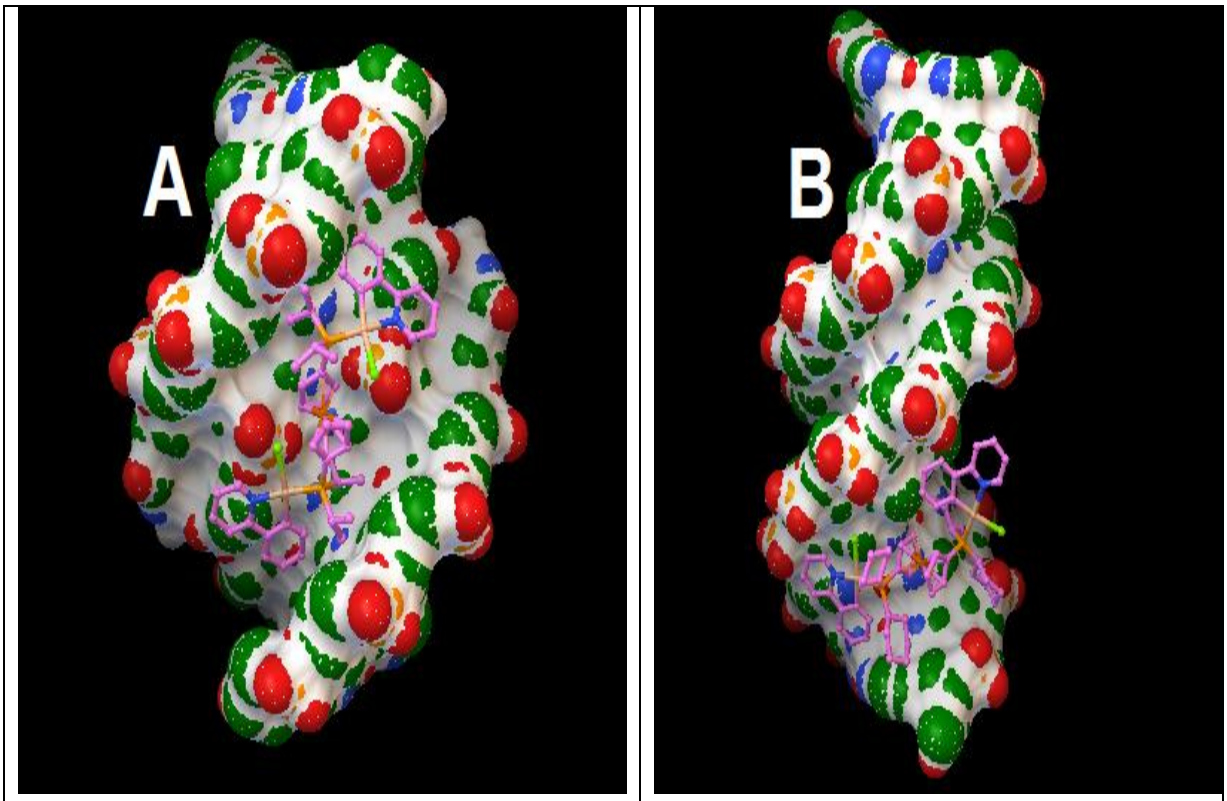

Figure S52. The best docked conformation of **2c**, in the best binding sites with 1DDP (A) and **2b** in the 1BNA structure (B).

Table S21. One-way ANOVA statistical analysis on the IC_{50} data of A549 cell line.

Tukey's multiple comparisons test	Mean Diff.	95.00% CI of diff.	Significant?	Summary	Adjusted P Value	
2a vs. 2b	-7.000	-8.692 to -5.308	Yes	****	<0.0001	A-B
2a vs. 2c	25.40	23.71 to 27.09	Yes	****	<0.0001	A-C
2a vs. 3a	4.960	3.268 to 6.652	Yes	****	<0.0001	A-D
2a vs. 3b	0.2600	-1.432 to 1.952	No	ns	0.9980	A-E
2a vs. 3c	41.85	40.16 to 43.54	Yes	****	<0.0001	A-F
2a vs. cisplatin	32.60	30.91 to 34.29	Yes	****	<0.0001	A-G
2b vs. 2c	32.40	30.71 to 34.09	Yes	****	<0.0001	B-C
2b vs. 3a	11.96	10.27 to 13.65	Yes	****	<0.0001	B-D
2b vs. 3b	7.260	5.568 to 8.952	Yes	****	<0.0001	B-E
2b vs. 3c	48.85	47.16 to 50.54	Yes	****	<0.0001	B-F
2b vs. cisplatin	39.60	37.91 to 41.29	Yes	****	<0.0001	B-G
2c vs. 3a	-20.44	-22.13 to -18.75	Yes	****	<0.0001	C-D
2c vs. 3b	-25.14	-26.83 to -23.45	Yes	****	<0.0001	C-E
2c vs. 3c	16.45	14.76 to 18.14	Yes	****	<0.0001	C-F
2c vs. cisplatin	7.200	5.508 to 8.892	Yes	****	<0.0001	C-G
3a vs. 3b	-4.700	-6.392 to -3.008	Yes	****	<0.0001	D-E
3a vs. 3c	36.89	35.20 to 38.58	Yes	****	<0.0001	D-F
3a vs. cisplatin	27.64	25.95 to 29.33	Yes	****	<0.0001	D-G
3b vs. 3c	41.59	39.90 to 43.28	Yes	****	<0.0001	E-F
3b vs. cisplatin	32.34	30.65 to 34.03	Yes	****	<0.0001	E-G
3c vs. cisplatin	-9.250	-10.94 to -7.558	Yes	****	<0.0001	F-G

Table S22. One-way ANOVA statistical analysis on the IC_{50} data of MCF-7 cell line.

Ordinary one-way ANOVA
Multiple comparisons

Tukey's multiple comparisons test	Mean Diff.	95.00% CI of diff.	Significant?	Summary	Adjusted P Value	
2a vs. 2b	1.520	-1.306 to 4.346	No	ns	0.5470	A-B
2a vs. 2c	16.59	13.76 to 19.42	Yes	****	<0.0001	A-C
2a vs. 3a	7.250	4.424 to 10.08	Yes	****	<0.0001	A-D
2a vs. 3b	3.670	0.8442 to 6.496	Yes	**	0.0079	A-E
2a vs. 3c	20.97	18.14 to 23.80	Yes	****	<0.0001	A-F
2a vs. cisplatin	29.25	26.42 to 32.08	Yes	****	<0.0001	A-G
2b vs. 2c	15.07	12.24 to 17.90	Yes	****	<0.0001	B-C
2b vs. 3a	5.730	2.904 to 8.556	Yes	***	0.0001	B-D
2b vs. 3b	2.150	-0.6758 to 4.976	No	ns	0.1984	B-E
2b vs. 3c	19.45	16.62 to 22.28	Yes	****	<0.0001	B-F
2b vs. cisplatin	27.73	24.90 to 30.56	Yes	****	<0.0001	B-G
2c vs. 3a	-9.340	-12.17 to -6.514	Yes	****	<0.0001	C-D
2c vs. 3b	-12.92	-15.75 to -10.09	Yes	****	<0.0001	C-E
2c vs. 3c	4.380	1.554 to 7.206	Yes	**	0.0017	C-F
2c vs. cisplatin	12.66	9.834 to 15.49	Yes	****	<0.0001	C-G
3a vs. 3b	-3.580	-6.406 to -0.7542	Yes	**	0.0096	D-E
3a vs. 3c	13.72	10.89 to 16.55	Yes	****	<0.0001	D-F
3a vs. cisplatin	22.00	19.17 to 24.83	Yes	****	<0.0001	D-G
3b vs. 3c	17.30	14.47 to 20.13	Yes	****	<0.0001	E-F
3b vs. cisplatin	25.58	22.75 to 28.41	Yes	****	<0.0001	E-G
3c vs. cisplatin	8.280	5.454 to 11.11	Yes	****	<0.0001	F-G

Table S23. One-way ANOVA statistical analysis on the IC_{50} data of HeLa cell line.

Ordinary one-way ANOVA
Multiple comparisons

Tukey's multiple comparisons test	Mean Diff.	95.00% CI of diff.	Significant?	Summary	Adjusted P Value	
2a vs. 2b	13.48	9.282 to 17.68	Yes	****	<0.0001	A-B
2a vs. 2c	42.92	38.72 to 47.12	Yes	****	<0.0001	A-C
2a vs. 3a	11.96	7.762 to 16.16	Yes	****	<0.0001	A-D
2a vs. 3b	24.90	20.70 to 29.10	Yes	****	<0.0001	A-E
2a vs. 3c	51.33	47.13 to 55.53	Yes	****	<0.0001	A-F
2a vs. cisplatin	49.98	45.78 to 54.18	Yes	****	<0.0001	A-G
2b vs. 2c	29.44	25.24 to 33.64	Yes	****	<0.0001	B-C
2b vs. 3a	-1.520	-5.718 to 2.678	No	ns	0.8685	B-D
2b vs. 3b	11.42	7.222 to 15.62	Yes	****	<0.0001	B-E
2b vs. 3c	37.85	33.65 to 42.05	Yes	****	<0.0001	B-F
2b vs. cisplatin	36.50	32.30 to 40.70	Yes	****	<0.0001	B-G
2c vs. 3a	-30.96	-35.16 to -26.76	Yes	****	<0.0001	C-D
2c vs. 3b	-18.02	-22.22 to -13.82	Yes	****	<0.0001	C-E
2c vs. 3c	8.410	4.212 to 12.61	Yes	***	0.0001	C-F
2c vs. cisplatin	7.060	2.862 to 11.26	Yes	***	0.0008	C-G
3a vs. 3b	12.94	8.742 to 17.14	Yes	****	<0.0001	D-E
3a vs. 3c	39.37	35.17 to 43.57	Yes	****	<0.0001	D-F
3a vs. cisplatin	38.02	33.82 to 42.22	Yes	****	<0.0001	D-G
3b vs. 3c	26.43	22.23 to 30.63	Yes	****	<0.0001	E-F
3b vs. cisplatin	25.08	20.88 to 29.28	Yes	****	<0.0001	E-G
3c vs. cisplatin	-1.350	-5.548 to 2.848	No	ns	0.9185	F-G

Table S24. Chemical descriptors of the complexes **2a–c** and **3a–c**.

Name	SA(Ap)[a] ($Å^2$)	SA(G)[b] ($Å^2$)	Volume ($Å^3$)	HE[c] (kcal/mol)	$LogP_{o/w}$	Ref[d] ($Å^3$)	Pol[e] ($Å^3$)	Mass (amu)
2a	764.27	1049.48	2165.42	-6.87	8.56	277.39	98.72	1323.82
2b	646.31	995.62	2183.00	-5.91	9.82	263.01	101.02	1348.01
2c	754.23	923.10	1927.07	-3.64	7.59	215.71	82.10	1187.75
3a	776.40	1062.09	2221.77	-5.64	9.02	277.91	98.36	1395.78
3b	727.14	1022.97	2236.93	-4.70	10.96	263.61	100.66	1419.97
3c	787.87	934.39	1981.27	-2.10	8.83	213.17	82.02	1259.71

[a] Surface Area (approx.) $Å^2$
[b] Surface Area (grid) $Å^2$
[c] Hydration Energy $Å^3$
[d] Refractivity
[e] Polarizability

Experimental Section

General Remarks

(^{1}H (400 MHz), ^{19}F (376 MHz), ^{31}P{^{1}H} (162 MHz) and ^{195}Pt{^{1}H} (86 or 64 MHz)) NMR spectra were recorded on a Bruker Avance instrument at 295 K. All chemical shifts (δ) are reported in ppm relative to their corresponding external standards ($SiMe_4$ for ^{1}H, $CFCl_3$ for ^{19}F, 85% H_3PO_4 for ^{31}P, Na_2PtCl_6 for ^{195}Pt) and the coupling constants (*J*) have been expressed in Hz. The instrument for HR ESI-Mass measurement was a Shimadzu IT-TOF with an electrospray ionization source. Microanalyses were performed with a Thermo Finnigan Flash EA-1112 CHNSO rapid elemental analyzer. UV–vis absorption spectra were carried out using an Ultrospec 4000 Pro. The 2-phenylpyridine (ppyH), 2-(2,4-difluorophenyl)pyridine (dfppyH), 1,1'-bis(diphenylphosphino)ferrocene (dppf), 1,1'-bis(dicyclohexylphosphino)ferrocene (dcpf), 1,1'-bis(diisopropylphosphino)ferrocene (dippf) and all other chemicals were purchased from commercial suppliers.

X-ray Crystallography

Single crystals of **2b** (CCDC Number: 2213182) and **2c** (CCDC Number: 2213181) were obtained by slow diffusion of *n*-hexane into its CH_2Cl_2 solution at room temperature. A suitable crystal was selected for structural analysis and intensity data for **2b** and **2c** were collected using a Bruker APEX-II CCD diffractometer. The crystal was kept at 100.0 K during data collection. Using Olex2,[1] the structure was solved with the ShelXT[2] structure solution program using Intrinsic Phasing and refined with the ShelXL[3] refinement package using Least Squares minimization. The crystallographic data and refinement parameters are summarized in Tables S1 and S2.

Computational Details

Density functional calculations were performed with the program suite Gaussian 09[4] using the B3LYP level of theory.[5-7] The LANL2DZ basis set was chosen to describe Fe and Pt[8, 9] and the 6-31G(d) basis set was chosen for other atoms. The geometries of complexes were fully optimized by employing the density functional theory without imposing any symmetry constraints. In order to ensure the optimized geometries, frequency calculations were performed employing analytical second derivatives. Time-dependent DFT (TD-DFT) calculations were carried out at the same level of theory and basis sets. Solvent effects have been considered by the conductor-like polarizable continuum model (CPCM).[10, 11] The calculations for the electronic absorption spectra by TD-DFT were performed at the same level of theory.

Biological Assay

MTT Assay

Human cell lines were examined using the MTT assay according to procedures in the literature and our previous work.[12-14] The comprehensive description of the MTT assay is provided in the following:

Human cancer cell lines such as breast cancer (MCF-7), cervix cancer (HeLa), and non-small cell lung cancer (A549) as well as human breast epithelial cell line (MCF-10A) were purchased from National Cell Bank of Iran (NCBI, Pasteur Institute, Tehran, Iran). The cancer cells were grown in complete culture media containing RPMI 1640 (Biosera, France), 10% fetal bovine serum (FBS; Gibco, USA) and 1% penicillin−streptomycin (Biosera, France) and kept at 37 °C in a humidified CO_2 incubator. MCF-10A and HeLa cells were cultured in DMEM/Ham's F-12 (GIBCO-Invitrogen, Carlsbad, CA) supplemented with 100 ng/ml cholera toxin, 20 ng/ml epidermal growth factor (EGF), 0.01 mg/ml insulin, 500 ng/ml hydrocortisone, and 5% chelex-treated horse serum.

Cytotoxic activities of the synthesized Pt(II) complexes were determined using a standard 3-(4,5-dimethylthiazol-yl)-2,5-diphenyl-tetrazolium bromide (MTT) assay, as previously described.[13] To do this, the cells with a density of 0.8×10^4 cells per well were seeded in 96-well microplates and kept for 24h to recover. The cells were then treated with the Pt(II) complexes in different concentrations from 1 to 100 μM in a triplicate manner and incubated for more 72 hours at 37 °C in humidified CO_2 incubator. Following incubation, the media were completely discarded and replaced with 150 μl of RPMI 1640 containing 0.5 mg/mL MTT solution and incubated at room temperature for 3h. To dissolve the formazan crystals, the media containing MTT was discarded again and 150 μl of DMSO was added to each well and incubated for more 30 min at 37 °C in the dark. It should be mentioned that, cisplatin were applied as reference drug (positive control). The absorbance of individual well was then read at 490 nm with an ELISA reader. The 50% inhibitory concentration of each compound (IC_{50}) was calculated with CurveExpert 1.4. Data are presented as mean ± SD. Additionally, the stability behavior of **2a–c** and **3a–c** in the cell culture media was investigated by NMR and UV-vis spectroscopies, and the resulting data showed the complexes were stable in these conditions.

Docking Procedure

Docking studies of **2a–c** and **3a–c** on four different DNA structures, (PDB ID: 1BNA, 1DDP, 3CO3, and 1LU5) were carried out using Autodock Dock 4.2 according to known methods in the literature and our previous work.[12, 13] The following procedure reports on the entire docking protocol:

The four different 3D crystal structures of DNA (PDB ID: 1BNA, 1DDP, 3CO3, and 1LU5) were retrieved from protein data bank (www.rcsb.org/pdb). Co-crystal ligand molecules were removed from the PDBs structures. Then, MGLtools 1.5.6 was applied to convert these corrected PDB files to PDBQT. For the preparation of ligands, the structure of each Pt(II) complexes was created by HyperChem Professional (Version 8, Hypercube Inc., Gainesville, FL, USA). Each complexes was optimized by molecular mechanic

methods (MM^+) using HyperChem 8, followed by energy minimization calculations at Hartree-Fock (HF) level, using Gaussian 09. The output structures were thereafter converted to PDBQT using MGLtools 1.5.6. After the preparation of ligands and receptors, the ligands, were docked to DNA using AutoDock 4.2, based on Lamarckian genetic algorithm. The grid center on the DNA structures was maintained by centering the grid box on the minor groove, major groove and the intercalation site to cover the full of DNA structure. The grid maps for all DNA structures had a spacing of 0.375 Å. All the other parameters were kept at their default values. Parameters of metal ions for docking were added to the gpf and dpf files. Concerning the AutoDock scoring function, the best binding mode of ligands and receptors was chosen base on the lowest docking binding energy conformation. Visualization of the docked pose has been performed by means of Molecular Operating Environment (MOE) and AutoDock Tools 1.5.6.

Apoptosis Assay

Apoptotic effect of **3c** was carried out with A549 cell by using an Annexin V/7AAD assay according to the previously described method.[12, 13, 15] All details are available in the following:

To assess the apoptotic effect of **3c**, BioLegend's PE Annexin V Apoptosis Detection Kit with 7AAD (Biolegend, USA) was applied according to the previously described method. Briefly, 0.5 x 10^5 cells per 1 ml of complete culture medium were seeded in a 24-well culture plate, treated with different concentrations (10, 20, and 30 µM) of compound **3c** for 48 h. An untreated sample was also included as a negative control. Treated and untreated cells were then harvested and washed twice with cold BioLegend's Cell Staining Buffer, transferred to the polystyrene round-bottom tubes (BD Bioscience, USA) and stained with 2 µl of PE-conjugated Annexin V and 2 µl of 7-AAD solution for 15 min at room temperature in the dark. 300 µl of Binding Buffer was added to each tube and analyzed immediately by four-color FACSCalibur flow cytometer (BD Bioscience, USA) with proper setting. The data were analyzed by FlowJo software packages.

DNA Damage Determination (Comet Assay)

Genotoxic effect was investigated by the comet assay to measure DNA damage potential of **3c** in A549 cells according to known protocols and our previous work.[16, 17] Details of the protocol can be found in the following:

Using comet assay, the genotoxicity (destructive effect on a cell's genetic material) of **3c** was also assessed. At first, 5 x 10^5 A549 cells in 2 mL complete culture medium were prepared and treated with two different concentrations (5 and 15 μM) of compound **3c**. Untreated as well as cisplatin (15 μM) treated cells were also included as negative and positive controls, respectively. The cells were incubated for 20 min at 37 °C in a humidified incubator with 5% CO_2. The cells were then participated, re-suspended in 100 μl 1× PBS, mixed with low melting point agarose (LMPA) and dropped on a slide pre-coated slide with normal melting point agarose (NMPA) layer. A coverslip was placed over the gel and put at 4 °C for 15 min. The coverslip was then removed and 100 μl of LMPA was added onto the agarose gel mixture layer, covered with a new coverslip and placed at 4°C for 15 min. The coverslip was then removed and the slides were immersed into cold lysis solution and refrigerated overnight and then in fresh cold alkaline electrophoresis buffer for 40 min. The slides were electrophoresed with the adjusted voltage (25V) and current (300 mA). Afterward, the slides were flooded with neutralizing Tris buffer (pH=7.5) and distilled water for 5 min, and then in 70%, 90% and 100% Ethanol (Merck, Germany), sequentially. The slides were lastly stained with 100 μl ethidium bromide (20μg/ml) and visualized by a high resolution fluorescent microscopy (BX61, Olympus). The comets were observed at 400 × magnification under a fluorescent microscope. At least 100 comets were randomly recorded for each case, and the percent of DNA in the tail, tail length, and tail moment for each comet was measured using image analysis software (comet score).

Determination of Intracellular Reactive Oxygen Species (ROS)

Intracellular ROS generation was measured in A549 cells using, Dichlorodihydrofluorescein's diacetate (DCFH-DA, a fluorescent probe), adopting published method. Briefly, the cells were treated with varying concentrations of compounds (100-300 µM) for 4 h and then collected by spinning at 3000 rpm for 5 min. Cold PBS was used twice to wash the pellet and re-suspended in PBS (500 µl). At 37 °C, cells were incubated with DCFH-DA (5 µM) in the dark for 1 h. The DCFH-DA marked cells without treating with tested compounds was the control. Upon excitation at 488 nm, the fluorescence has been recorded. The fluorescence (Green color) from 2′,7′-dichlorofluorescein (DCF) through 525 nm band-pass filter was measured using FL1 Log channel. The ROS production qualitative analysis was validated by treating HepG2 cell with tested complexes and then staining with 5 µM of DCFH-DA for 1 h. Images collected from Fluorescence microscope (Nikon Eclipse 80i, Japan).

Statistical Analysis

In this work, Analysis of Variance (ANOVA) and Tukey post-hoc test was used to determine statistical significance on all calculations by Graphpad Prism software. *P*-values ≤ 0.0001 were considered significant. Data are presented as mean ± SD.

References

1. O. V. Dolomanov, L. J. Bourhis, R. J. Gildea, J. A. K. Howard and H. Puschmann, *J. Appl. Cryst.*, 2009, **42**, 339-341.
2. G. Sheldrick, *Acta Cryst.*, 2015, **A71**, 3-8.
3. G. Sheldrick, *Acta Cryst.*, 2015, **C71**, 3-8.
4. M. J. Frisch, G. W. Trucks, H. B. Schlegel, G. E. Scuseria, M. A. Robb, J. R. Cheeseman, G. Scalmani, V. Barone, B. Mennucci, G. A. Petersson, H. Nakatsuji, M. Caricato, X. Li, H. P. Hratchian, A. F. Izmaylov, J. Bloino, G. Zheng, J. L. Sonnenberg, M. Hada, M. Ehara, K. Toyota, R. Fukuda, J. Hasegawa, M. Ishida, T. Nakajima, Y. Honda, O. Kitao, H. Nakai, T. Vreven, J. J. A. Montgomery, J. E. Peralta, F. Ogliaro, M. Bearpark, J. J. Heyd, E. Brothers, K. N. Kudin, V. N. Staroverov, T. Keith, R. Kobayashi, J. Normand, K. Raghavachari, A. Rendell, J. C. Burant, S. S. Iyengar, J. Tomasi, M. Cossi, N. Rega, J. M. Millam, M. Klene, J. E. Knox, J. B. Cross, V. Bakken, C. Adamo, J. Jaramillo, R. Gomperts, R. E. Stratmann, O. Yazyev, A. J. Austin, R. Cammi, C. Pomelli, J. W. Ochterski, R. L. Martin, K. Morokuma, V. G. Zakrzewski, G. A. Voth, P. Salvador, J. J. Dannenberg, S. Dapprich, A. D. Daniels, O. Farkas, J. B. Foresman, J. V. Ortiz, J. Cioslowski and D. J. Fox, *Gaussian 09, Revision A.02*, 2016.
5. A. D. Becke, *J. Chem. Phys.*, 1993, **98**, 5648-5652.
6. B. Miehlich, A. Savin, H. Stoll and H. Preuss, *Chem. Phys. Lett.*, 1989, **157**, 200-206.
7. C. Lee, W. Yang and R. G. Parr, *Phys. Rev. B*, 1988, **37**, 785.
8. W. R. Wadt and P. J. Hay, *J. Chem. Phys.*, 1985, **82**, 284-298.
9. L. E. Roy, P. J. Hay and R. L. Martin, *J. Chem. Theory Comput.*, 2008, **4**, 1029-1031.
10. M. Cossi, G. Scalmani, N. Rega and V. Barone, *J. Chem. Phys.*, 2002, **117**, 43-54.
11. V. Barone, M. Cossi and J. Tomasi, *J. Chem. Phys.*, 1997, **107**, 3210-3221.

12. M. Fereidoonnezhad, Z. Ramezani, M. Nikravesh, J. Zangeneh, M. Golbon Haghighi, Z. Faghih, B. Notash and H. R. Shahsavari, *New J. Chem.*, 2018, **42**, 7177-7187.

13. M. Fereidoonnezhad, H. R. Shahsavari, S. Abedanzadeh, B. Behchenari, M. Hossein-Abadi, Z. Faghih and M. H. Beyzavi, *New J. Chem.*, 2018, **42**, 2385-2392.

14. J. V. Meerloo, G. J. Kaspers and J. Cloos, in *Cancer Cell Culture*, Springer, 2011, pp. 237-245.

15. I. Lakshmanan and S. K. Batra, *Bio-Protocol*, 2013, **3**, e374-e374.

16. P. L. Olive and J. P. Banáth, *Nat. Protoc.*, 2006, **1**, 23-29.

17. N. Ghassemi-Barghi, J. Varshosaz, M. Etebari and A. J. Dehkordi, *Toxicol. In Vitro*, 2016, **36**, 46-52.